An Expression of Interest

to Construct

a Major SSC Detector

July 8, 1991

Contact Persons::

Barry Barish
Caltech
HEP 256-48
Pasadena, CA 91125
(818) 356-6684
Barish@Cithex.Bitnet

William Willis
Nevis Laboratory
Columbia University
P. O. Box 137
Irvington, NY 10533
(212) 932-3169
Willis@Nevis.Bitnet

TABLE OF CONTENTS

MEMBERS OF THE COLLABORATION iii

1.0 INTRODUCTION AND DETECTOR OVERVIEW 1-1
- 1.1 Physics Goals 1-1
- 1.2 Design Philosophy and Detector Parameters 1-2
- 1.3 Detector Architecture 1-3
- 1.4 Preliminary Cost Estimate 1-4
- 1.5 Expected Time and Design Milestones 1-7
- 1.6 Management of the Collaboration 1-8
- 1.7 R & D Funds Requested 1-8

2.0 PHYSICS WITH THE PROPOSED DETECTOR 2-1
- 2.1 Introduction 2-1
  - 2.1.1. Physics at the 1 TeV Energy Scale 2-1
  - 2.1.2 The Need for Two Complementary Detectors 2-3
  - 2.1.3. Physics Goals of the Detector 2-4
- 2.2 Selected Physics Processes 2-6
- 2.3 Search for the Standard Higgs Boson 2-8
- 2.4 Search for a Heavy Top Quark 2-16
- 2.5 Discovery and Properties of a Heavy Z' 2-19
- 2.6 Supersymmetry 2-21
- 2.7. Technicolor 2-23
- 2.8. Quark and Lepton Substructure 2-26

3.0 DETECTOR SUBSYSTEMS 3-1
- 3.1 Magnet 3-1
  - 3.1.1 Introduction 3-1
  - 3.1.2 Design Considerations 3-1
  - 3.1.3 Design Description 3-1
  - 3.1.4 Magnet Manufacturer and Schedule 3-10
  - 3.1.5 Fringe Field Effects - Safety and Interface Issues 3-10
  - 3.1.6 Research and Development 3-10
- 3.2 Muon System 3-15
- 3.3 Calorimetry 3-18
- 3.4 Tracking 3-31
  - 3.4.1 Physics Performance 3-31
  - 3.4.2 Additional Options 3-32
  - 3.4.3 Baseline R&D Issues 3-32
- 3.5. Triggering and Data Acquisition 3-38

4.0 DETECTOR HALL AND SURFACE FACILITIES 4-1

5.0 DESIGNING TO COST AND SCHEDULE 5-1

6.0 COLLABORATION ORGANIZATION 6-1

7.0 PROPOSED PLAN AND FUNDING REQUESTS 7-1

7.1 Preparing the LOI (July–November 1991) 7-1

7.2 Preparation of Engineering Design Report (Nov 91 - Nov 92) 7-2

APPENDIX A THE HIGH FIELD OPTION A-1

MEMBERS OF THE COLLABORATION

Adelphi University: R. V. Steiner

University of Arizona: G. Forden, J. Rutherfoord, M. Shupe

Boston University: S. Ahlen, E. Booth, R. Carey, S. Dye, E. Hazen, D. Higby, T. Johnson, S. Klein, K. Lane, A. Marin, J. Miller, B. L. Roberts, J. T. Shank, J. Stone, L. Sulak, J. S. Whitaker, R. J. Wilson, W. Worstell, B. Zhou

Brookhaven National Laboratory: M. Atiya, I. Chiang, B. Gibbard, H. Gordon, J. Haggerty, S. Kahn, H. Kraner, P. Kroon, T. Kycia, L. Littenberg, H. Ma, D. Makowiecki, M. J. Murtagh, L. Paffrath, F. Paige, V. Polychronakos, S. Protopopescu, V. Radeka, D. C. Rahm, S. Rankowitz, P. Rehak, S. Rescia, N. Samios, D. Stephani, I. Stumer, M. Tannenbaum, C. L. Woody, S. P. Yamin

Brown University: M. Widgoff

University of California, San Diego: J. Branson, H. Kobrak, R. Masek, H. Paar, M. Sivertz, B. Swanson

California Institute of Technology: B. Barish, G. Gratta, D. Kirkby, W. Lu, R. Mount, H. Newman, X. Shi, R. Zhu

Carnegie Mellon University: M. Clemen, J. Russ

Columbia University: E. Aprile, T. Bolton, M. Moulsen, R. Mukherjee, J. Parsons, P. Rowson, M. Shaevitz, M. Seman, W. Sippach, W. Willis, Yin Au

University of Delhi, India: V. Kapoor, R. K. Shivpuri

Draper Laboratories: F. Ayer, F. Nimblett, E. Womble

Drexel University: C. Lane

Fairfield University: D. Winn

Universität Hamburg, Germany: E. Fretwurst, G. Lindström, V. Riech

University of Houston: K. Lau, B. Mayes, L. Pinsky, J. Pyrlik, R. Weinstein

Indiana University: D. Alyea, C. Bower, M. Gephart, R. Heinz, S. Mufson, J. Musser, J. Pitts

Institute of Atomic Physics, Romania: A. Aculai, C. Blaj, H. Bozdog, L. Butacu, M. Ciobanu, D. Ighigeanu, D. Lazarovici, S. Miron, G. Pascovici, M. Pentia, D. Pop, V. Popa, G. Radulescu, D. Spanu, V. Valeanu

Institute of High Energy Physics, China: W. Gu, Y. Gu, Y. Guo, Y. Huang, J. Li, C. Mao, H. Sheng, R. Xu, D. Zhang, B. Zhuang

Institute of High Energy Physics, USSR: N. N. Fedyakin, R. N. Krasnokutsky, R. S. Shuvalov, V. V. Sushkov

Institute of Theoretical and Experimental Physics, USSR: A. Bolozdynya, P. Goritchev, L. Gusev, V. Khovansky, A. Koutchenkov, A. Kovalenko, V. Lebedenko, V. Tchernyshev, V. A. Vinogradov

University of Iowa: N. Akchurin, D. Kadrmas, K. Langland, E. R. McCliment, Y. Meurice, F. Olchowski, Y. Onel, M. Reno, V. Rodgers

Lawrence Livermore National Laboratory: R. Ables, R. Bionta, C. Britt, H. Britt, M. Capell, A. Chargin, G. Deis, O. Fackler, C. Johnson, M. Lowry, M. Mugge, W. Stoffel, T. J. Wenaus, C. Wuest

Leningrad Nuclear Physics Institute, USSR: V. M. Samsonov, V. A. Schegelsky, N. K. Terentyev

Los Alamos National Laboratory: J. Boissevain, M. Brooks, D. Brown, T. Coan, R. Farber, S. Hahn, J. Kapustinsky, W. Kinnison, K. Lackner, D. Lee, A. Lapedes, W. B. Maier, G. Mills, G. Sanders, D. Sharp, W. Sommer, W. Sondheim, B. Smith

Martin Marietta Astronautics: N. J. DiGiacomo, B. Easom, K. Killian, L. Mason

Massachusetts Institute of Technology: P. Burrows, W. Busza, M. Chen, H. Ding, J. Friedman, M. P. J. Gaudreau, E. Hafen, P. Haridas, H. Kendall, V. Lebedenko, D. Montgomery, L. Osborne, I. Pless, L. Rosenson, S. Shotkin, R. Shuvalov, J. Sullivan, K. Sumorok, F. Taylor, R. Verdier, B. Wadsworth, X. J. Yan, X. Zhang

University of Michigan: D. Levin, G. Tarle

Michigan State University: M. Abolins, C. Bromberg, B. Pope

University of Mississippi: L. Cremaldi, B. Moore, J. Reidy

Oak Ridge National Laboratory: M. L. Bauer, H. O. Cohn, F. Plasil, K. Read, M. Rennich, T. Shannon

University of Oregon: J. Brau, R. E. Frey, K. Furuno, D. M. Strom, C. J. Zeitlin

Princeton University: P. Denes, M. Ito, D. Marlow

University of Rochester: G. Fanourakis, T. Ferbel, M. Zielinski

Riken, Saitama, Japan : M. Suzuki, T. Takahashi

Rutgers University: P. Jacques, M. Kalelkar, R. Plano, P. Stamer, G. Word

Superconducting Super Collider Laboratory: L. Cormell, J. Kuzminski, A. Maschke, R. Meinke, K. Morgan, B. Parker, L. A. Roberts, R. Soundranayagam, F. Stocker, L. Villasenor†, G. P. Yost, J. Yarba

University of Sao Paulo, Brazil: O. P. Eboli, C. O. Escobar, P. Gouffon, M. Luksys, S. F. Novaes

Saitama College of Health, Japan: K. Masuda, E. Shibamura

Southern Methodist University: R. Stroynowski, V. Teplitz

SUNY at Stonybrook: C. K. Jung, M. Marx, R. L. McCarthy, M. M. Mohammadi, M. Rijsenbeek, C. Yanagisawa

Tbilisi State University, USSR: N. S. Amaglobeli, W. P. Dzhordzhadze, A. J. Mchedlishvili, D. A. Mzavia, R. G. Shanidze, F. G. Tkebuchava

Temple University: S. Kettell, K. McFarlane

Texas A&M: R. C. Webb

Texas Tech University: R. Wigmans

University of Tennessee: S. Berridge, W. M. Bugg, Y. C. Du, R. Kroeger, I. Tsveybak

University of Texas, Austin: G. W. Hoffmann, K. Lang, J. Ritchie

Vanderbilt University: R. Panvini, J. Venuti

Vassar College: C. Schwarz
Waseda University, Japan: T. Doke, A. Hitachi, N. Ishida, T. Kashiwagi, J. Kikuchi
Washington University: J. Beatty, D. Ficenec
University of Washington: V. Cook, J. Eisenberg, D. Forbush, P. Mockett, S. Sutlief, F. Toeus
Yale University: R. Adair, C. Baltay, R. David, W. Emmett, H. Kasha, S. Manly, J. Turk

† On leave of absence from University of Michoacan, Mexico

1.0 INTRODUCTION AND DETECTOR OVERVIEW

A new international collaboration has been formed to propose the design and construction of a large detector for the SSC. Building on the previous work of the L* and EMPACT/TEXAS collaborations we were able to form a strong core for a new collaboration, which intends to propose a major detector combining precision measurements of leptons and photons, and robust muon detection for the SSC. This collaboration includes almost the entire set of U.S. groups from both the L* and EMPACT/TEXAS Letters of Intent as well as several important new groups who have not been previously involved in SSC proposals. This represents a strong core around which to build the plans for this detector. We intend to have an open policy both with respect to individuals and new groups being added, at least through the period of preparation of the LOI. At the time of this submission, our collaboration contains over 300 collaborators from over 50 institutions. Each individual collaborator has made a specific commitment to devote a significant fraction of time to this project.

It is our full intention to form a broad international collaboration, and we already have collaborating groups from Brazil, China, Germany, India, Japan, Romania, and the Soviet Union, and are carrying on preliminary discussions with several other groups.

We will negotiate major responsibilities within the collaboration, and define the commitments from non-US groups once this experiment has received preliminary approvals to proceed towards a Technical Proposal. The process of obtaining and expanding foreign participation will be facilitated by (1) the preliminary approvals and (2) a clearly established framework in which this experiment may move forward on an equal basis with SDC. Despite the extremely short time for formation of the collaboration, even prior to these steps, the clear physics principles which are at the basis of our new collaboration have enabled us to attract a number of non-U.S. groups, despite the present asymmetric status of this experiment vis a vis SDC, and the series of previous rejections of proposals.

This new collaboration was formed in June of 1991, with the first collaboration meeting on June 18, 1991. Therefore this document, submitted in early July of 1991 is very preliminary. The fact that we are able to submit an EOI at this early stage is due both to the quick convergence and dedication of the new group, and to the fact that we were able to build on the hard work and expertise developed in preparing the the L* , Texas and EMPACT EoI's, the reports to the PAC in response to detailed physics questions in mid-1990, and the L* and EMPACT/TEXAS LoI's. We note that the collaboration is so new that we have not yet faced what may be the most difficult decision, i.e., naming the detector, but we hope to make some progress on this issue in the near future.

1.1 Physics Goals

The physics goals of a large high p_T detector for the SSC are centered on the topics that form the main justification of the construction of the SSC–namely the elucidation of the physics behind the electroweak symmetry breaking that is expected to explain the mass spectrum of the physically observed gauge bosons and fermions. This implies the search for the Higgs boson, technicolor, supersymmetry, as well as the search for new quarks, leptons, Z's and W's, as discussed in more detail in Chapter 2 of this EOI. In addition to these topics one has always to prepare for the unpredicted or unknown new phenomena that nature might have in store for us. These

considerations, as well as the realization that some of these searches might necessitate the highest luminosities attainable at the SSC, lead to the desirability of two large high p_T 4π detectors with complementary capabilities.

1.2 Design Philosophy and Detector Parameters

The SDC collaboration has received encouragement from the SSC to develop a design for a large general purpose detector for the SSC. It is our intent to design a complementary detector, with a compact tracker, precision calorimeters and an extensive muon system, to cover new physics ground necessarily left uncovered by SDC. This implies several things. First, the design of the detector will emphasize the precision measurement of electrons, muons and gammas. Second, there should be a substantial overlap in the capabilities of the two detectors at the SSC design luminosity of 10^{33} cm^{-2} sec^{-1} to provide competition and crosschecks on the hopefully numerous new discoveries at the SSC. To achieve these goals, we believe the detector should have hermetic electromagnetic and hadronic calorimetry and central tracking in a magnetic field. Another important design consideration is to preserve as much of these capabilities as possible up to the highest luminosities eventually attainable at the SSC.

The above considerations lead to the following detector parameters:

1. *Precision muon momentum measurement outside of the calorimeter.* The main reason for this is that making the muon momentum measurements outside of 10 to 12 interaction lengths of absorber gives us robustness to the highest luminosities. Our design goal is a precision of ~ 5% for 0.5 TeV muons at a luminosity of 10^{34} or higher. We believe that the most economical way to achieve this goal is to have high precision muon chambers in a large magnetic field free of iron.

2. High precision electromagnetic calorimeters without a magnet coil in front of them. The design goal is a resolution of $\Delta E/E = (1.5 \text{ or } 7)\%/\sqrt{E} \oplus 0.5\%$. The high precision of $1.5\%/\sqrt{E}$ is characteristic of totally absorbing crystal calorimeters while $7\%/\sqrt{E}$ is about the best that one can achieve with sampling calorimeters such as lead-liquid argon or lead-scintillator calorimeters. We are presently studying the performance vs. cost of these two basic design goals and plan to make the choice between them in the near future.

3. Hermetic, projective tower geometry hadron calorimetry with energy resolution of the order of $\Delta E/E = 50\%/\sqrt{E} \oplus 2\%$. The total thickness of the EM and hadronic calorimeters should be 10 to 12 interaction lengths. We are considering performance vs. cost optimization both with respect to different technologies and other possibilities such as a finely segmented front end, where most of the energy is deposited, with a more coarsely segmented tail end, whose main purpose is to detect large fluctuations in the depth of energy deposition.

4. Central tracking in a magnetic field. The goals of our tracker are more modest than for SDC, and we expect the radius of the central tracking to be 1 meter or less. The detailed goals and technologies will be defined by studies in the coming months.

1.3 Detector Architecture

An illustrative example of how the above parameters can be realized in a self-consistent detector architecture is shown in Figs. 1-1 and 1-2. In this example, an 8 to 10 Kg magnetic field for both the muon momentum measurement and the central tracking is provided by a large superconducting solenoid. This baseline magnet has been the basis of our initial cost and technical considerations. The coil has iron poles at the two ends but no flux return (coils or iron) in the barrel region. Preliminary studies of the effect of such fringe fields, from the standpoint of the accelerator, safety, and logistics of the experiment, are encouraging. Further study is clearly necessary; however, this possibility represents a substantial savings ($50M) in iron or coil costs.

The length of the magnet is driven by the desire to keep good muon momentum resolution in the small angle region (in the rapidity range of ~ 1.5 to 2.5). Possible ways of reducing the length of the magnet by either shaping the field in the forward region or by the use of external muon chambers are under study.

The outside dimensions of this magnet are the largest we envision. Further optimization studies will possibly reduce the size somewhat but not increase it significantly. Such a magnet will fit conveniently into the hall that has been designed at interaction region IR1, where this detector will presumably be located. Thus the detailed design and construction of the experimental hall can proceed as presently envisioned. This is an important consideration since a redesign of the hall would cause an unacceptable delay in its timely completion.

Our general strategy is to evolve the final magnet from this base-line magnet, after doing an integrated optimization with the various subsystems performance and costs. The magnet and structure will be a framework for building the detector, in which we plan to include some possible staging of detector system as well as the ability to add capability in response to early SSC physics.

1.4 Preliminary Cost Estimate

In the short time available, a detailed engineering design and an accompanying bottoms-up cost estimate, especially of some new ideas, were not possible. However, a lot is known about the costs for both L* and E/T proposed subsystems; therefore to get an indication of the cost of a detector with the parameters discussed above, we have used the L* and EMPACT/TEXAS engineering designs and detailed cost estimates with a "straw-man" detector using a configuration that can be reliably costed from that work. Both the L* and SDC cost estimates have been reviewed by an SSC cost review panel (the Theriot panel). They found the basic cost estimates generally sound, but increased the EDIA costs and contingency estimates. The increase amounted to an overall increase of ~ 40% of the base costs estimated by L* (see Chapter 5.0 for more detail). We have therefore multiplied the costs scaled from L* and E/T by this factor of 1.4 to bring our estimates to the level suggested by the Theriot panel. We have also included an amount for R&D costs scaled from the L* R&D numbers estimated by the Theriot panel.

Figure 1-1 Quadrant View of the Detector Concept

Figure 1-2 End View of the Detector Concept

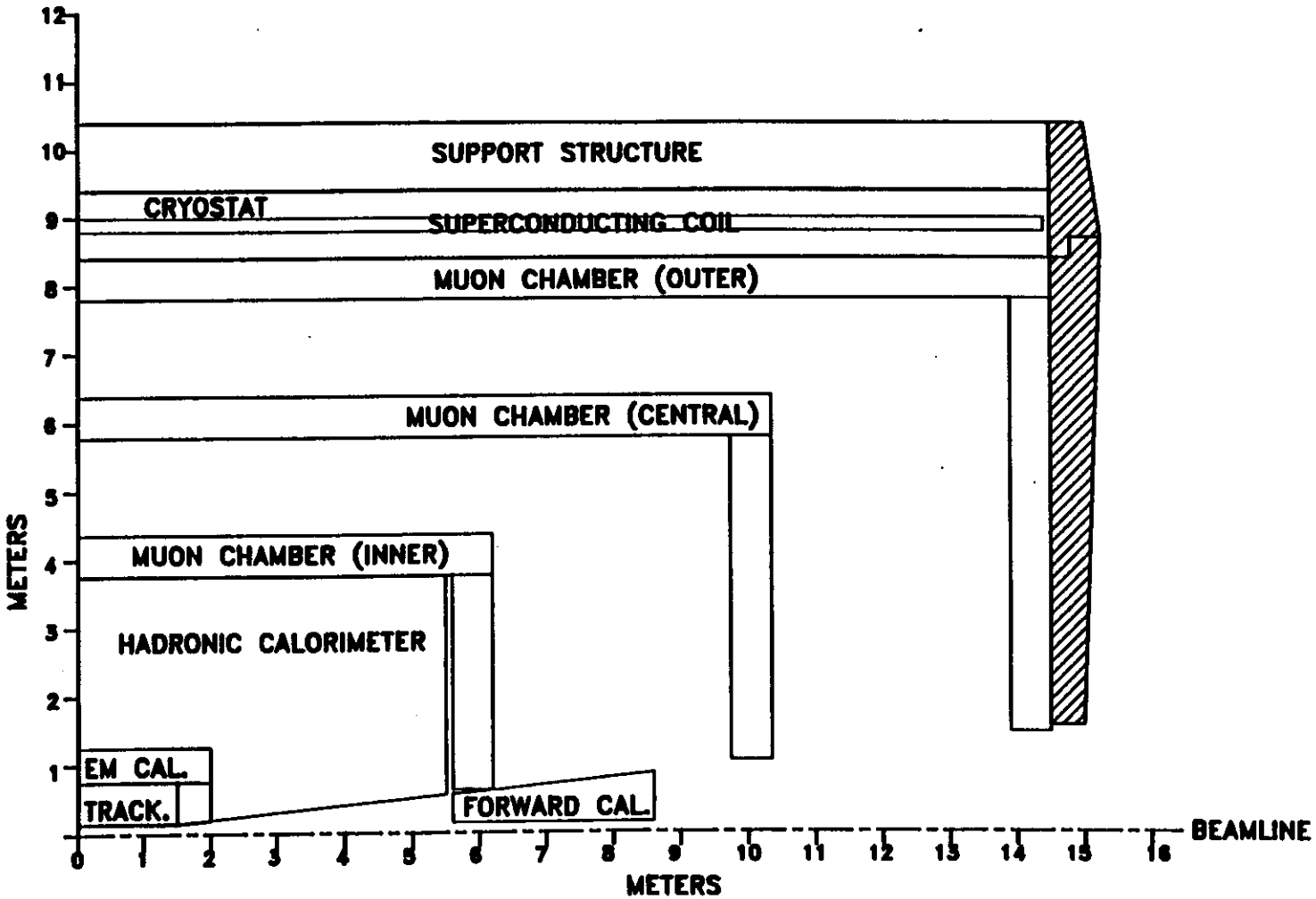

QUADRANT VIEW OF THE DETECTOR CONCEPT

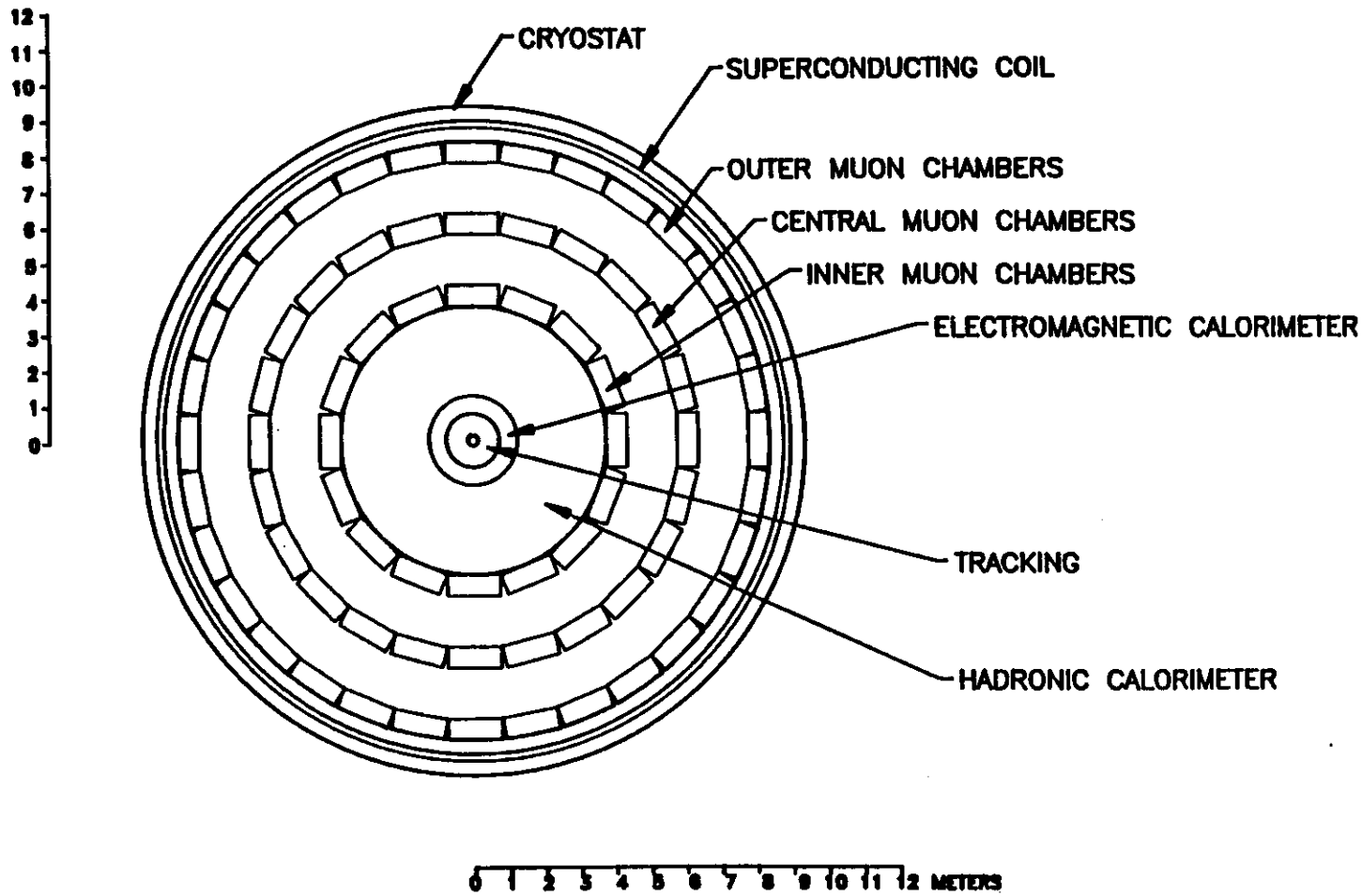

END VIEW OF THE DETECTOR CONCEPT

In this way we arrive at the following range of estimates for two calorimeter options discussed above.

1. Option with precision homogeneous EM calorimetry using Barium Fluoride crystals followed by a sampling hadronic calorimeter.

(EM resolution $\Delta E/E \sim 1.5\%/\sqrt{E} \oplus 0.5\ \%$)

($M dollars)	
Base estimate	332
Increase for Theriot panel estimate	133
Total	465
R&D costs	33
Total detector cost	498

2. Option with lead-fiber scintillator readout EM and hadronic calorimeter.

(EM resolution $\Delta E/E \sim 7\%/\sqrt{E} \oplus 0.5\ \%$)

($M dollars)	
Base estimate	290
Increase for Theriot panel estimate	120
Total	410
R&D costs	29
Total detector cost	439

These estimates are discussed in more detail in Chapter 5.0 of this document.

For the purpose of obtaining these cost estimates, we have assumed the L* and E/T technologies for the various subsystems and scaled them to our parameters. This should not be taken as a decision to use these technologies. This exercise has been done in the spirit of establishing a "proof of principle" that a detector with our parameters can be built for between $400M and $500M. Over the next year or two we will pursue a vigorous R&D program to find the most desirable and cost-effective technologies to achieve the desired detector parameters discussed above, designing to (or below) the costs presented here.

1.5 Expected Time and Design Milestones

If this Expression of Interest is favorably received and appropriate R&D funds are made available to this collaboration, we expect to submit a Letter of Intent by late 1991 and an Engineering Design Report by late 1992. Our present plan is to make the choice between precision homogeneous EM calorimetry (Barium Fluoride or Liquid Xenon) or a sampling type calorimeter (Lead scintillator or Lead-Liquid Argon) by the time of writing of the Letter of Intent. For the Letter of Intent we plan to have narrowed the basic choice of technologies to at most two options for each of the major subsystems. We expect that by the time of writing of the Engineering Design

Report most of the subsystems will have been narrowed down to a single option, although, depending on the availability of test beams, some final choices may have to be delayed to 1993.

1.6 Management of the Collaboration

An interim organization for the collaboration, consisting of a Collaboration Council led by two co-chairmen, has been set up for the purpose of generating this Expression of Interest (EOI). If this EOI is favorably received we envision a more elaborate organization, consisting of a Collaboration Council, a Steering Committee, an International Finance Committee, and a Project Manager. Our present thinking on such an organization is described in Chapter 6.0 of this document. This management structure will be discussed in detail with the SSC Laboratory management and will be modified and evolved to take into account the needs of the laboratory. We hope that the evolution from the interim organization to the final management structure will be achieved by the time of writing of the Letter of Intent or soon after.

1.7 R & D Funds Requested

In order to be able to carry out the R&D and the engineering design needed for writing the Letter of Intent and later the Engineering Design Report, approximately $10M for R&D and $4M for Engineering will be required. for Fiscal Year 1992. Our present expectation for these needs are discussed in Chapter 7.0 of this document. Special care and planning will have to be exercised to reorient some of the previously funded R&D which was motivated by the L* and E/T Letters of Intent toward those problems which are the most crucial for our current vision for the detector. Early reduction of the number of technologies pursued will be required.

2.0 PHYSICS WITH THE PROPOSED DETECTOR

2.1 Introduction

2.1.1. Physics at the 1 TeV Energy Scale

Over twenty years ago, the basic structure of the standard model of electroweak interactions was formulated and given a firm theoretical foundation. This model is based on the gauge symmetry $SU(2) \otimes U(1)$ with gauge bosons that we identify as the photon, $W^{\pm}$ and Z^0. The model provides a phenomenological description of electroweak symmetry breaking, manifested by M_W and $M_Z \neq 0$; accommodates an arbitrary number of quark and lepton flavors, which we now believe to be six; and incorporates their flavor symmetry breaking, manifested by the generation of *different* quark and lepton masses and mixing angles. These four are the fundamental ingredients of electroweak interactions – the gauge symmetry, its spontaneous breakdown, quark and lepton flavors, and the breaking of flavor symmetry. Despite twenty years of the most probing experiments and theoretical effort, we really understand only the first. Thus, there is widespread conviction that the standard model is not the whole story.

In the standard model, electroweak symmetry breaking and fermion mass generation (but *not* flavor symmetry breaking) are implemented with a complex doublet of elementary scalar bosons. Three of these scalars appear as the longitudinal components of the massive $W^{\pm}$ and Z^0. The fourth scalar—the Higgs boson, H^0—remains undiscovered. Its couplings to ordinary matter are completely specified, but its mass cannot be predicted by the model. Experiments at LEP indicate that $M_H \gtrsim 40$ GeV. Either $M_H \lesssim 1$ TeV or the interactions of weak bosons become strong at subprocess energies exceeding about 1 TeV.

The standard model provides no clue to the underlying dynamics of electroweak symmetry breaking. Its description of this phenomenon in terms of the Higgs doublet is incomplete, if not seriously flawed. Furthermore, there is no reason for M_H to be much less than the Planck scale, 10^{19} GeV; this is the famous "naturalness" problem. What the standard model does tell us about electroweak breaking is that its energy scale is *known* to be less than about 1 TeV. This scale is set in the model by the vacuum expectation value of the Higgs field, $v = 2^{-1/4} G_F^{-1/2} = 246$ GeV the analog of the pion decay constant of QCD, $f_\pi = 93$ MeV. Whatever may be the origin of electroweak symmetry breaking, this fact will survive, and precise experimentation at or below the 1 TeV scale is bound to uncover its nature.

The meaning of flavors and the origin of their symmetry breaking are not addressed in the standard model. These essential elements are put in by hand: an arbitrary number of quark/lepton generations and arbitrary couplings of the Higgs boson to the fermions. In particular, the model says nothing about the energy scale of flavor breaking. In some scenarios that attempt to address the flavor problem – e.g., technicolor and compositeness – hints to the answer may come from experiments near the 1 TeV scale. In others – e.g., the standard model and its supersymmetric extensions – the answer may not become apparent without ultra-high energies. Nevertheless, it is important to search for clues to the mystery of flavor in the 1 TeV region.

Until the mysteries of electroweak and flavor symmetry breaking are resolved, progress in understanding physics at still higher energy scales is impossible. Thus, the primary scientific mission of the SSC is to seek, discover and study this physics. The most basic design parameters of the SSC – its energy and luminosity – have been chosen to meet these fundamental physics goals. It is crucial now to design the experimental program to exploit fully the SSC's potential and to do this physics.

Table 2-1 lists most of the popular proposals for new physics in the TeV energy region as well as their principal signatures. This table demonstrates several key points:

- While we are confident of new physics in this region, much of it beyond the standard model, *we do not know what that physics is!* The SSC experimental program must cover this full range of ideas, with the flexibility to go beyond them as the science dictates.

- All proposed new physics signatures involve photons, electrons, muons, jets, heavy flavors and/or missing energy. The SSC experimental program must measure *all* these signatures with precision and good background rejection.

- Last, we note that *all* the physics possibilities in the table were proposed ten or more years ago. There have been no really new ideas since then. Despite the great experimental achievements in W, Z and heavy flavor physics of the past decade, they have given no insight to the fundamental mysteries of the standard model nor any hints how to proceed beyond it. The next big step in particle physics requires the high energy and luminosity of the SSC.

Table 2-1 New Physics Possibilities and Signatures at O (1Tev)

Physics	Signatures
Standard H^0	$\gamma\gamma$, $ZZ^* \rightarrow l^+l^-l^+l^-$ $ZZ \rightarrow l^+l^-l^+l^-$, l^+l^-jj, $l^+l^-\bar{\nu}\nu$
Extended $H^0, h^0, H^\pm$	Same as above Heavy $f\bar{f} \Rightarrow$ flavor tags, isolated $l^\pm$, $W^\pm \rightarrow jj$, etc.
Heavy $Q\bar{Q}$	$W^\pm q \rightarrow$ jets + isolated $l^\pm$
W', Z' (mass, width, asymmetry)	$l^\pm + \not{E}_T$, l^+l^-, dijets
Strong VV scattering	WW, WZ, $ZZ \rightarrow l^\pm$ + jets
Technicolor	$\rho_T \rightarrow$ dijets, WZ ($\rightarrow l^\pm$ jets), $\pi_T\pi_T$ $\pi_T \rightarrow$ heavy $f\bar{f}$, dijets
Supersymmetry	multi-isolated $l^\pm$, jets, $\not{E}_T$
q Substructure	high-mass dijets
qll Substructure	high-mass dileptons, $\not{E}_T$
None of the Above!	All of the Above!

2.1.2 The Need for Two Complementary Detectors

In 1990 three large detector collaborations submitted Letters of Intent to the SSC Laboratory and its Program Advisory Committee. These three LOIs represented many thousands of man- and CPU-hours of research and development, physics simulations, and design work and choices. The performance of the three detectors was measured against a wide range of "standard benchmarks" as well as more specific tests proposed by the PAC. The three LOIs demonstrate that, despite the detectors' enormous size and cost, none alone can cover with precision *all* the physics possibilities and *realities* in the TeV energy region. While each detector has its areas of strength, it is also true that each has weaknesses, including: degraded EM energy measurement at lower energies and much reduced capability at $\mathcal{L} > 10^{33}\,cm^{-2}\,s^{-1}$ for SDC, limited inner tracking at higher momenta for L*,

and lack of magnetic tracking for EMPACT/TEXAS. These deficiencies are a direct consequence of a particular detector's design emphasis. SDC's are due to its large tracking volume and surrounding solenoid with intervening material. Our proposed detector, emphasizing an open geometry and precision lepton and photon measurement, has reduced central tracking abilities. In view of our almost complete ignorance of the dynamics of electroweak and flavor symmetry breakings, it is entirely possible that any single detector could be blind to the signals of new physics.

A second danger arises from the likelihood that new physics signals will be only marginally significant and difficult to extract. The ability to verify discoveries has always been essential to progress in physics. A look back at the physics of the past decade – the discoveries of the W and Z, the false indications of monojet signals for supersymmetry, the discovery of B–$\bar{B}$ mixing, and now the tantalizing prospects for neutrino mass and mixing – all show the importance of being able to check and confirm measurements.

As the SSCL Director and the PAC have emphasized repeatedly, two detectors are necessary for the initial experimental program of the SSC. Given the scope of the potential physics, the complexity of the detectors, and the limited range of a single experiment, the two must be *complementary*. For the other SSC detector, this implies:

- It must be *significantly better* than SDC in certain areas, allowing a broader range of discoveries;
- It must have *significant overlap* with SDC in other areas, to provide cross-checks.

Two complementary detectors have additional advantages over one very large one. Two collaborations promote a variety of styles and approaches to technical problems. Two detectors have different systematic errors. Two collaborations provide a healthy spirit of competitiveness that will help obtain the physics in a timely fashion. Finally, as illustrated in this document, it is entirely feasible to build a detector with the desired complementarity to SDC and correspondingly increased physics coverage that is within the guidelines established by the Laboratory and the PAC.

2.1.3. Physics Goals of the Detector

The detector described in this document will emphasize very precise measurement of photons, electrons and muons at all energies, coupled with excellent hadronic jet energy measurements as well as heavy flavor tagging. In addition, precision muon measurement and other robust features will be maintained at ultra-high luminosities ($\mathcal{L} \geq 10^{34}\,\mathrm{cm}^{-2}\,\mathrm{s}^{-1}$).

Table 2-2 shows that our basic design goals define a detector whose performance characteristics are truly complementary to SDC: significantly better than SDC in the areas of muon momentum measurement at nominal and high luminosities and electromagnetic energy measurement; comparable to SDC in hadronic energy measurement and heavy flavor identification, and having useful tracking capability.

Table 2-2 Complementarity of This Detector and SDC†

Subsystem / Feature	This Detector vs. SDC
Muon System	better
$\mu^{\pm}$ sign	better
$\mathcal{L} > 10^{33}$	better
EM Calorimeter	better
Hadron Calorimeter	comparable
Compensation	comparable
$\not{E}_T$	comparable
Central Tracking	worse
b, t - tagging	comparable
τ – tagging	comparable
$e^{\pm}$ sign	worse
Jet Fragmentation	worse

† Comparisons between SDC and this detector are based on the SDC LOI and the design parameters of Section I, and always assume the most conservative option we are considering.

These design goals must be justified on physics discovery grounds. Although, our inability to forecast the new physics makes this task difficult, it is precisely this uncertainty that is the prime justification for two detectors with complementary areas of strength, overlap and weakness. From Tables 2-1 and 2-2, then, we list a few of the obvious search processes where our detector will have capabilities superior to SDC.

- Neutral Higgs-like scalars ($\rightarrow \gamma\gamma, ZZ^*$) for $M_H < 2M_Z$.
- $Z' \rightarrow e^+e^-, \mu^+\mu^-$ mass and width.

- $Z' \rightarrow \mu^+\mu^-$ asymmetry.
- ρ_T or $\omega_T \rightarrow \gamma\pi_T$; $\pi_T \rightarrow f\bar{f}$ where f, f' = heavy flavors.
- $\tilde{G}\tilde{G} \rightarrow$ like-sign $\mu^\pm\mu^\pm + X$.
- quark/lepton substructure ($\rightarrow e^+e^-$, $\mu^+\mu^-$) energy scale Λ.
- quark/lepton substructure ($\rightarrow \mu^+\mu^-$) asymmetry.

The detector's undiminished muon measurement at ultra-high luminosity gives it a considerably greater reach in Z' and quark/lepton substructure mass scales than SDC will have.

Together, our proposed detector and SDC ensure that the entire range of 1 TeV physics will be well covered. Whatever the origin of electroweak symmetry breaking, at least one of these detectors will discover it. Together, both detectors should be able to map out all its aspects. Together, both detectors will discover or sharply limit the origin of flavor symmetry breaking. And, together, both detectors will discover all other new physics possibilities that may be lurking in the 1 TeV energy region. To illustrate this, we turn now to a discussion of our detector's capabilities. We discuss its expected performance for a range of physics both within and beyond the standard model.

2.2 Selected Physics Processes

The design of our detector emphasizes superb measurements both of electromagnetic energy in a high-resolution calorimeter and of muon momentum in a large magnetic volume with $B \simeq 1$ Tesla. It also has good measurement of hadronic energy for $|\eta| \leq 3$ and as yet unspecified calorimetry for $3 < |\eta| \lesssim 5$ to measure missing transverse energy E_T. There is adequate central tracking to distinguish high-p_T particles. The calculations presented the following sections assume subsystem measurement precisions and coverages as follows:

- The electromagnetic energy resolution is taken to be

$$\frac{\Delta E}{E} = \frac{(2.0\% \text{ or } 7.5\%)}{\sqrt{E}} \oplus 0.5\%$$

  with segmentation $\Delta\phi \times \Delta\eta = 0.04 \times 0.04$, for $|\eta| \leq 2.5$. The smaller sampling term corresponds to the total absorption options (BaF_2/LXe/LKr), and the larger one to the sampling options (LAr/SPACAL).

- The jet energy resolution is assumed to be

$$\frac{\Delta E}{E} = \frac{50\%}{\sqrt{E}} \oplus 2\%,$$

with segmentation $\Delta\phi \times \Delta\eta = 0.05 \times 0.05$, $|\eta| \leq 3$. In many cases, however, the jet resolution is limited more by clustering effects than by the intrinsic calorimeter resolution.

- The central tracker covers the pseudorapidity range $|\eta| \leq 3$ and has the resolution

$$\frac{\Delta p}{p} = 50\%, \quad \text{for } p = 350 \text{ GeV at } 90°.$$

A silicon vertex detector identifies secondary vertices and contributes to the resolution.

- The muon system covers $|\eta| \leq 2.7$ and has the resolution

$$\frac{\Delta p}{p} = 5\%, \quad \text{for } p = 500 \text{ GeV at } 90°.$$

Since muons are measured outside the calorimeter, the muon system is robust at high luminosity.

We have considered the reach of such a detector for several physics processes taken from those requested by the PAC:

- Search for the standard model Higgs boson, H^0, over the entire mass range $M_H = 80$ GeV to 800 GeV.
- Search for a heavy top-quark with $m_t = 250$ GeV. We assume that t has either the standard-model decay, $t \to W^+b$, or the nonstandard decay $t \to H^+b$ where the charged scalar $H^+ \to c\bar{s}$ or $\tau^+\nu$.
- Search for a heavy Z' gauge boson with $M_{Z'} = 4$ TeV and $\Gamma_{Z'} \simeq .01\, M_{Z'}$. We assume 1000 events of $Z' \to l^+l^-$ where $l = e, \mu, \tau$ and discuss the measurement of its mass, width and decay asymmetry.

In addition we briefly discuss our detector's capability for three signatures of major extensions of the standard model:

- Search for gluino pair production ($\tilde{G}\tilde{G}$) in all-lepton final states.

- Search for a color-octet technirho (ρ_T) in its decay to a pair of decay technipions (π_T) which decay in turn to a heavy quark-antiquark pair or to a heavy quark plus heavy lepton.
- Search for quark and lepton substructure in the production of high invariant mass dijets and dileptons.

Most of our calculations are based on the ISAJET 6.36 and PYTHIA 5.5 event generators and appropriate detector simulation. Unless stated otherwise, the top-quark mass is assumed to be 140 GeV. One standard SSC year corresponds to $\int \mathcal{L} dt = 10^{40}$ cm^2. Details of event selection and background rejection for the searches may be found in the EOIs [1], responses to the PAC [2], and LOIs [3] submitted by the L*, EMPACT, TEXAS and EMPACT/TEXAS Collaborations.

2.3 Search for the Standard Higgs Boson

Experiments at the SSC must be able to discover or exclude the standard model Higgs boson, H^0, in the mass range M_H = 80 – 800 GeV. LEP experiments should should be able to cover the range below 80 GeV, while a Higgs heavier than about 800 GeV is so broad that it may not be recognizable as a resonance. Theoretical studies indicate that new, unspecified physics must occur if $M_H \gtrsim$ 650 – 1000 GeV. In any case, special experimental techniques and extended running at high luminosity will be required to search for a very heavy Higgs boson. This detector will rely on its excellent measurement of photons, electrons, muons and jets to ensure that the mass range 80 – 800 GeV is well-covered.

80 GeV $\lesssim M_H \lesssim$ 180 GeV

All studies of the H^0 search for $M_H < 2M_Z$ agree that the only modes in which it may be found are the rare decays $H^0 \rightarrow \gamma\gamma$ and $H^0 \rightarrow ZZ^* \rightarrow l_1^+ l_1^- l_2^+ l_2^-$ where $l = e, \mu$. The power of our electromagnetic and muon systems are well-matched to searching for these modes.

$H^0 \rightarrow \gamma\gamma$

Two large sources of background to the $\gamma\gamma$ signal must be severely reduced. The first is the irreducible background from $q\bar{q} \rightarrow \gamma\gamma$ and $\mathcal{G}\mathcal{G} \rightarrow \gamma\gamma$. The second background comes from copious QCD production of π^0s and single photons. The irreducible background is suppressed with the following rapidity, energy and angular cuts:

$$\eta_\gamma < 2.5, \quad \eta_{\gamma\gamma} < 3.0$$

$$E_{T\,\gamma} > 20\ \text{GeV}, \quad |\cos\theta^*_\gamma| < 0.8.$$

Since the Higgs is very narrow, the signal is then observable provided that the $\gamma\gamma$ mass resolution $\Delta M/M \lesssim 1\%$. This requires not only the precision measurement of the photon energies provided by the EM calorimeter, but also spatial resolutions of $\lesssim$ 1mm on the photon vertex and the shower positions. Sufficient energy resolution can be achieved, for example, with the BaF_2, LXe or LKr calorimeters [1,2,3] assuming that the 0.5% constant term can be achieved. Indeed, the need to achieve high resolution in EM energy measurements such as these is the strong motivation for this calorimetry. Sufficient energy resolution may also be achievable for a sampling calorimeter with $7.5\% / \sqrt{E} \oplus 0.5\%$, and we are studying the feasibility of this. This 1mm vertex resolution is achievable by measuring charged tracks associated with the $H^0 \rightarrow \gamma\gamma$ event.

Suppressing the π^0 background from jets requires a γ/jet rejection of somewhat better than 10^4. This can be achieved through isolation cuts on the photons. A particle P ($P = \gamma$, e, μ) is said to be isolated if

$$\sum_R E_T - E_{T,P} < E_c + 0.1\, E_{T,P}$$

where the sum is over the transverse energy, E_T, found in the calorimeter in a cone of size $R = \sqrt{(\Delta\eta)^2 + (\Delta\phi)^2}$; $E_{T,P}$ is the transverse energy of particle P; and E_c is the energy cut. In our isolation requirements for photons, we use $R = 0.6$ and $E_c = 5$ GeV. This analysis was done for the BaF_2 calorimeter option. Suppression of the jet background would be enhanced by the ability to separate $\pi^0 \rightarrow \gamma\gamma$ from single γ's. We are currently investigating techniques to do this.

The signal and irreducible $\gamma\gamma$ background are shown in Fig. 2-1 for the two EM energy resolutions under consideration and for Higgs boson masses of 80, 100, 120 and 150 GeV. The signals correspond to 4.6, 8.6, 14 and 13 (3.2, 6.3, 11 and 10) standard deviations for $\Delta E / E = 2.0\% \oplus 0.5\%$ ($7.5\% \oplus 0.5\%$) in one standard SSC year. The corresponding background-subtracted signals are also shown in Fig. 2-1. Note that there are hundreds of signal events per SSC year in this channel. The EM calorimeter and photon position resolutions are essential for the extraction of these signals.

One might also be able to observe $H^0 \rightarrow \gamma\gamma$ in the associated production channels $q\bar{q} \rightarrow HW$ and $gg \rightarrow Ht\bar{t}$. The rates are small, about 20 events produced per

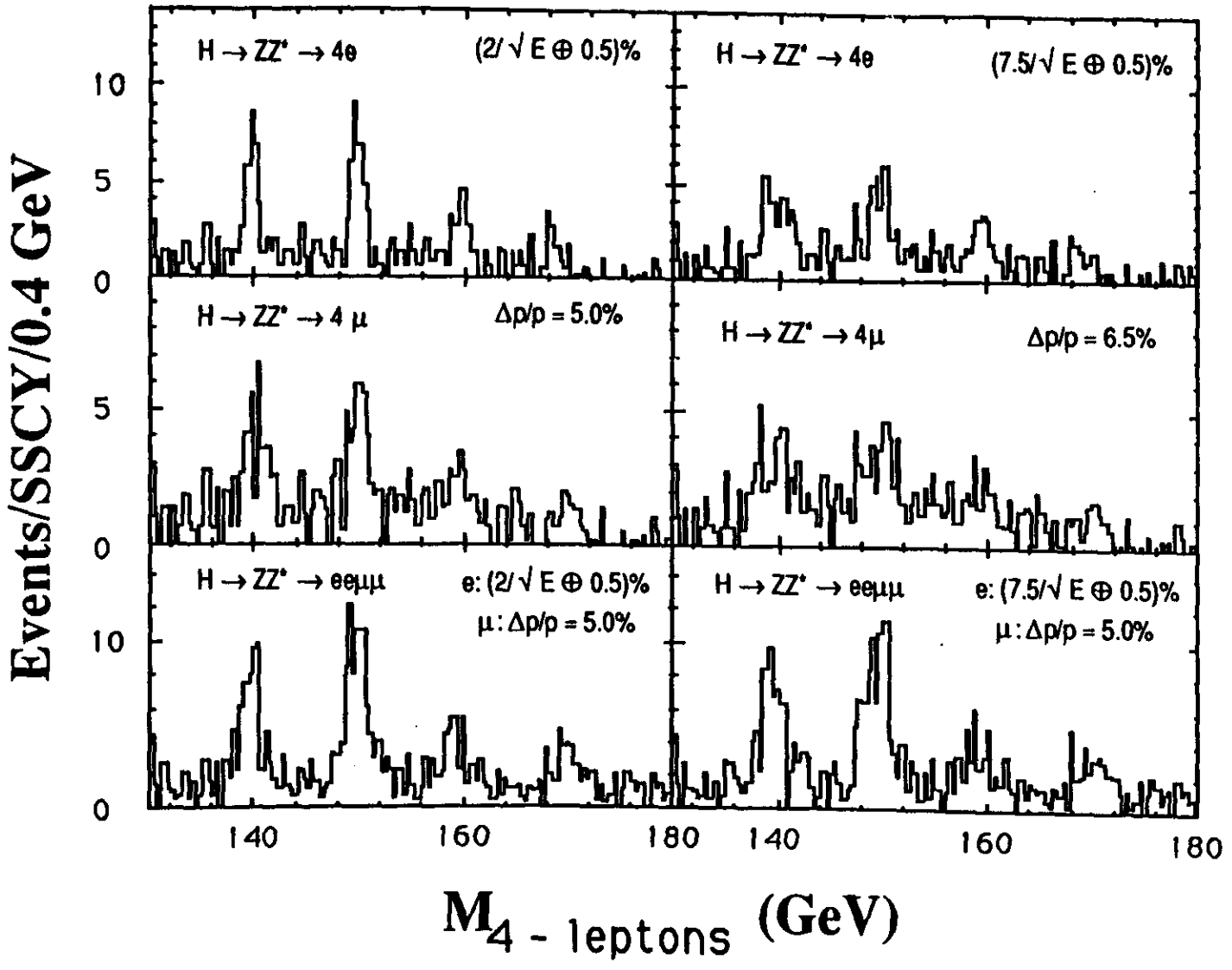

Figure 2-2 Higgs mass spectra obtained in one SSC year, with backgrounds for four Higgs masses and two resolutions

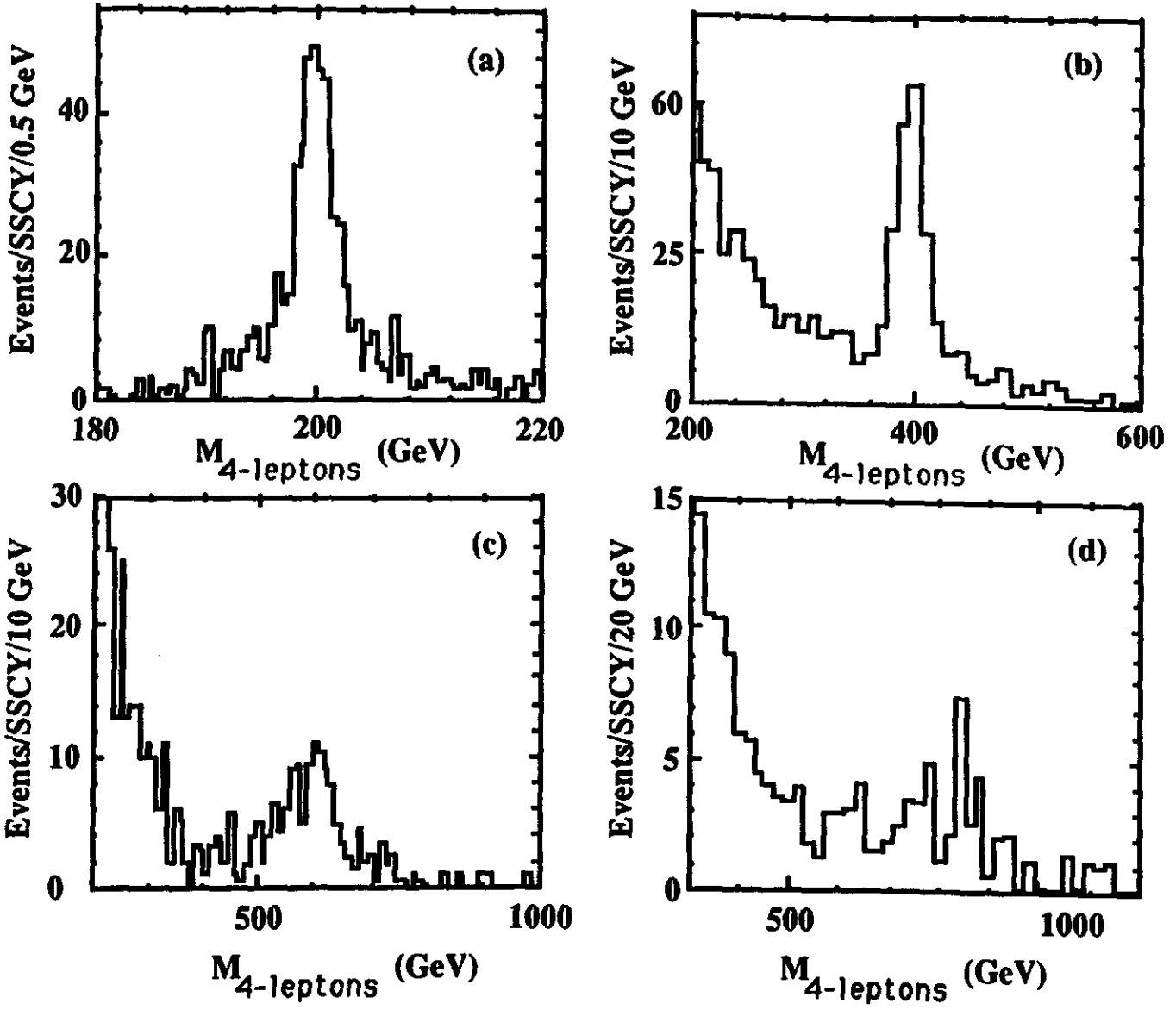

Figure 2-3 Higgs mass spectra to four leptons for four Higgs masses

$M_H \simeq 800$ GeV

For the upper end of the Higgs mass range, and more generally for the study of WW interactions at the TeV scale, the rates are very small. Thus, in this case, it is especially important to be able to exploit several different modes.

The cleanest mode remains $H^0 \rightarrow Z^0 Z^0 \rightarrow l_1^+ l_1^- l_2^+ l_2^-$. The same cuts are used as for $M_H = 400$ and 600 GeV. The signal and background in the sum of the four-lepton channels is shown in Fig. 2-3d. The background is entirely due to the irreducible Z^0Z^0 production process. In the Higgs region, 600 to 1000 GeV, there are 40 events in the signal above 13 background events.

The number of events is potentially doubled if the mode $H^0 \rightarrow Z^0Z^0 \rightarrow l^+l^-\tau^+\tau^-$ is added. According to the E/T LOI, the background from a high-p_T Z^0 with recoil jets faking $\tau^+\tau^-$ appears to be very small even with limited tracking [3]. Positive identification of one or both τ–leptons with the vertex detector would reduce the background even more.

A much larger signal is observable in the mode $H^0 \rightarrow Z^0Z^0 \rightarrow l^+l^-$ + jet jet, where $l = e, \mu$. The width of an 800 GeV Higgs boson is 250 GeV, so resolution on the Higgs mass is not an issue. But, hadronic resolution is needed to reconstruct the $Z^0 \rightarrow$ jets mode and to reject the very large background from Z^0 + jets. The L* analysis made cuts $|M_{l^+l^-} - M_Z| < 5$ GeV and $|M_{jj} - M_Z| < 7$ GeV. A detailed description of the other cuts is given in [2]. The dijet mass distribution in the Z^0 region from the signal and background processes is shown in Fig. 2-4a. The $H^0 \rightarrow Z^0Z^0 \rightarrow l^+l^-$ + jet jet signal and background yields in one SSC year are shown in Fig. 2-4b. There are 155 events in the signal and 460 events in the background – which comes almost entirely from Z^0 + jets.

Part of the Higgs signal comes from WW fusion and produces jets at large η with $p_T \sim m_W$. An E/T analysis found an improvement in signal-to-noise of 1.25 while retaining 36% of the signal. This might help confirm the nature of the signal, but the improvement is modest enough that it will not be a major constraint on the forward calorimetry.

Finally, one can look for $H^0 \rightarrow Z^0Z^0 \rightarrow l^+l^-\nu\bar{\nu}$. Again there is a large background from Z^0 + jets in which the jets are missed by the detector. Observation of this signal requires coverage to at least $\eta \simeq 5$ and avoiding cracks or other non-Gaussian tails in the calorimetry. This appears to be possible, but a detailed engineering design of the entire calorimeter is necessary. There is also a background from the Z^0Z^0 continuum, which must

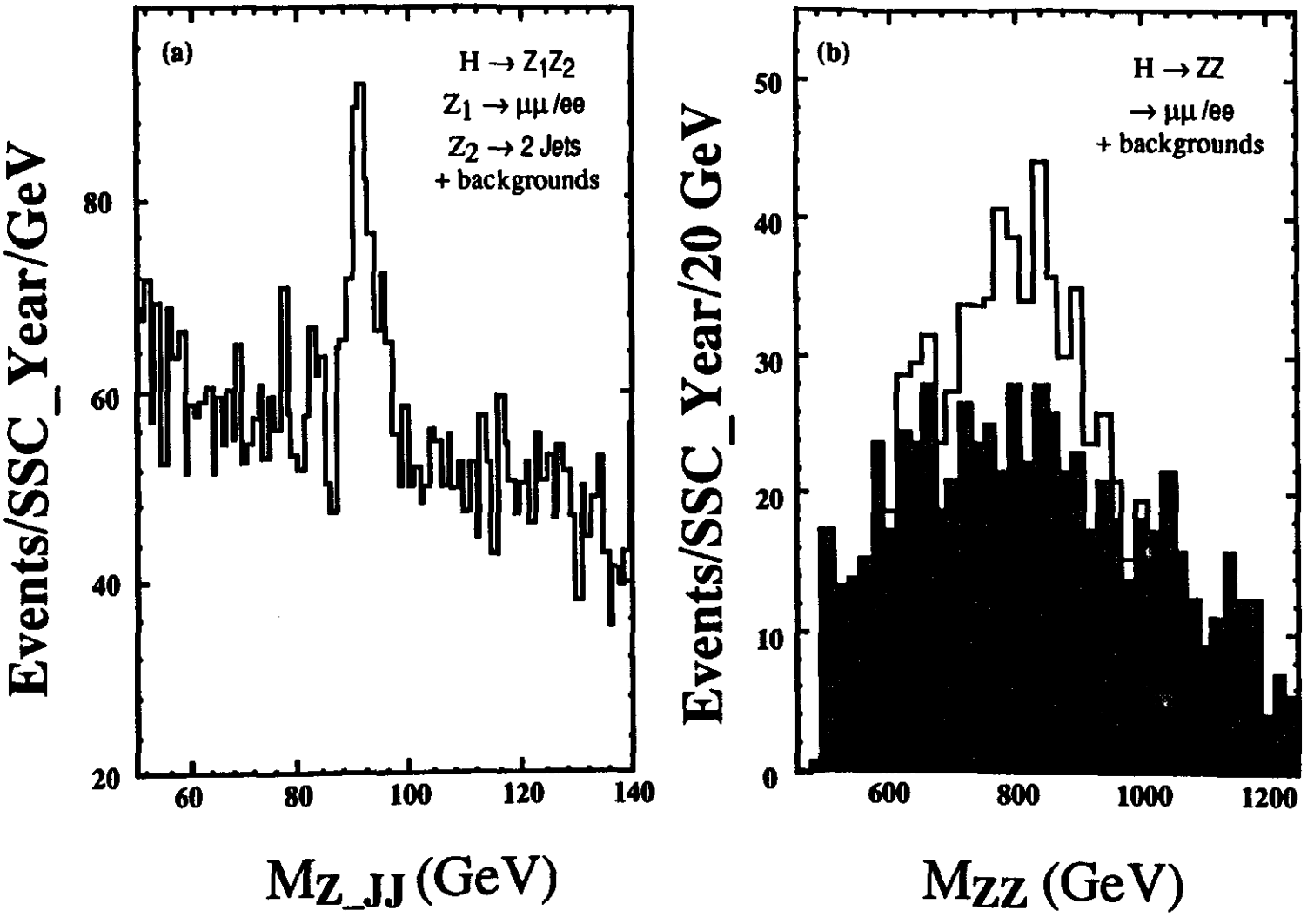

Figure 2-4 (a) Dijet mass distribution in the Z^0 region from signal and background (b) $H^0 \rightarrow Z^0Z^0 \rightarrow l^+l^- +$ jet jet signal and background for one SSC year.

be known to be about 30%. In any case, while this mode provides a useful confirmation for the signal, the four-lepton and lepton-jet modes are better ways to discover the Higgs.

2.4 Search for a Heavy Top Quark

The precision lepton and jet measurement systems of the detector we propose give it the ability to discover rapidly and to study a 250 GeV top quark in both standard ($t \rightarrow W^+b$) and nonstandard ($t \rightarrow H^+b, H^+ \rightarrow c\,\bar{s}, \tau^+\nu$) decay modes. The background rejection techniques described here rely on identifying isolated electrons and muons as well as muons inside jets. This search for the top quark also provides a good example of the reconstruction of high-p_T W-bosons in their dijet decay modes. The detector's ability to discriminate between high-p_T W's and Z's is illustrated by comparing Figs. 2-4a and 2-5b. With suitable modification, the techniques described here should work well for a heavy, fourth-generation quark, Q, produced in the process $\mathcal{G}\mathcal{G} \rightarrow Q\bar{Q}$.

<u>Standard Top Quark: $t \rightarrow W^+b$</u>

The cleanest discovery mode for the standard t-quark is $\mathcal{G}\mathcal{G} \rightarrow t\,\bar{t} \rightarrow e^{\pm}\,\mu^{\mp} + X$ with isolated $e^{\pm}$ and $\mu^{\mp}$ [3]. L* and E/T considered the decay chain

$$t \rightarrow W^+b, \quad W^+ \rightarrow e^+\nu; \quad \bar{t} \rightarrow W^-\,\bar{b}, \quad W^- \rightarrow \mu^-\bar{\nu}$$

To overcome backgrounds, it is necessary to tag at least one of the b-quarks in this process. In our detector b-quarks are tagged by observation of a muon inside the b-jet. Suitable cuts then reduce the backgrounds from W+X, Z+X and $b\,\bar{b}$ production to about 10% of the signal of 2×10^4 events per SSC year. (For L*, e.g., the cuts were $E_c = 5$ GeV in $R = 0.3$ and $p_{Tl} > 30$ GeV.) [3] The $e^{\pm}\,\mu^{\mp}$ mode allows discovery of the 250 GeV t quark in a matter of days. A measurement of the invariant mass of the isolated $e^{\pm}\,\mu^{\mp}$ or of the isolated l and the tagged b-jet gives an accuracy of 5% in one SSC year.

A more direct and precise measurement of m_t uses the decay chain

$$t \rightarrow W^+b, \quad W^+ \rightarrow l^+\nu \; (l = e, \mu), \quad b \rightarrow \mu^-X;$$
$$\bar{t} \rightarrow W^-\,\bar{b}, \quad W^- \rightarrow \text{jet jet}, \quad \bar{b} \rightarrow \text{jet}.$$

Then, m_t is obtained by reconstructing the dijet decay of the W and measuring $M_{jjj} = M_{Wb}$. With the same isolation cuts as above to identify high-p_T leptons from the W, with b-tagging through the inclusive muon, and requiring

$$p_{Tj} > 40 \text{ GeV}, \quad p_{Tjj} > 200 \text{ GeV},$$
$$\Delta R_{jj} < 1.0, \quad |\phi_{jj} - \phi_e| > 100°,$$

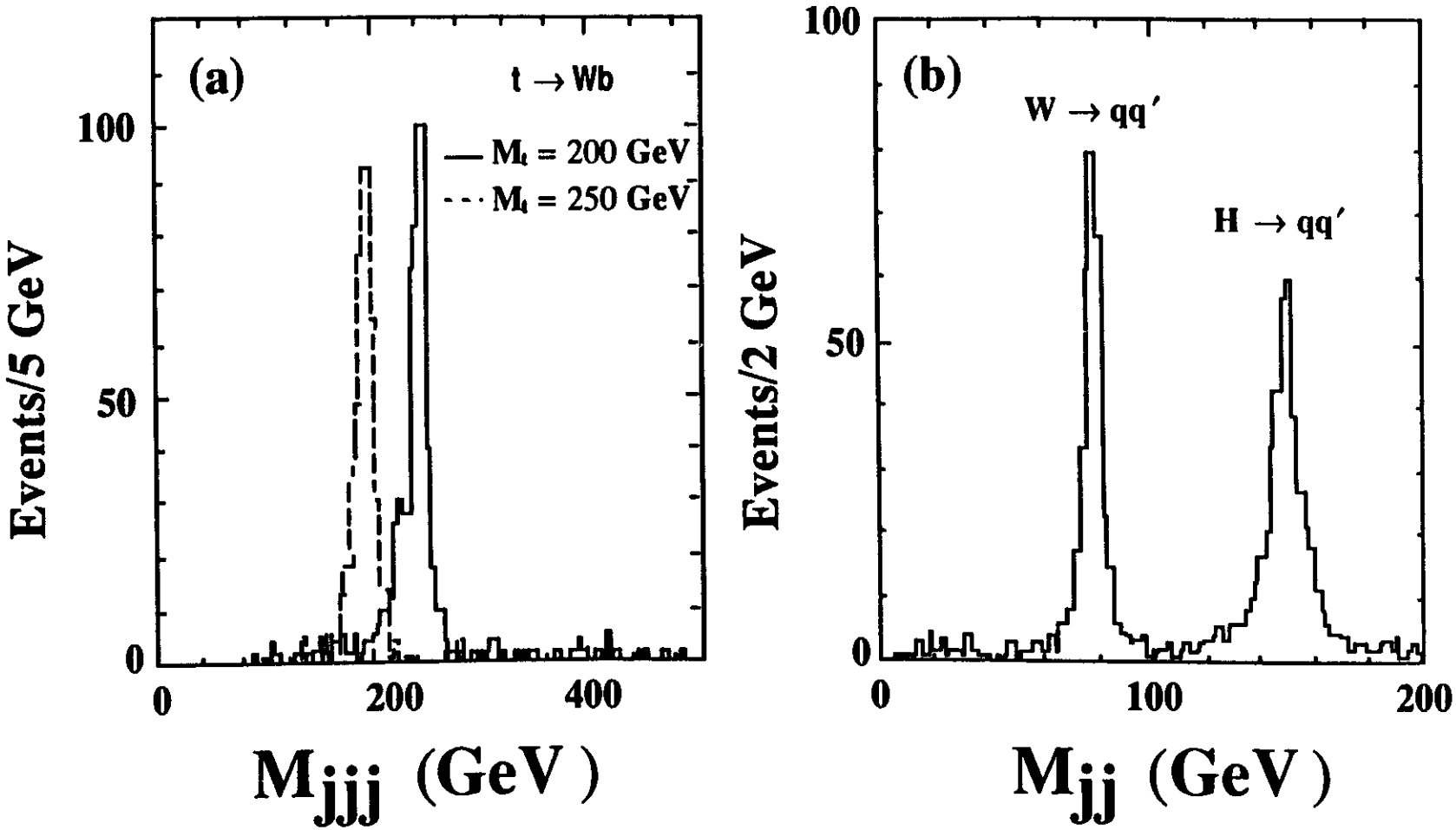

Figure 2-5 (a) t→Wb mass distributions
(b) W and H dijet mass distributions

top quark mass distributions as shown in Fig. 2-5a were obtained by L* [3]. The central value of m_t is determined to about 2%. Since the W is also observed, the systematics of the hadron calorimetry and of the clustering algorithm can be studied using the known W mass.

Non-standard Top Quark: $t \rightarrow W^+b$ and $t \rightarrow H^+b$

If there exists a charged Higgs or technipion lighter than the top quark, then the decay $t \rightarrow H^+b$ can be comparable to the standard mode $t \rightarrow W^+b$. In considering this possibility, we assume that $M_{H^+} = 150$ GeV and that H^+ decays exclusively to $c\bar{s}$ and $\tau^+\nu$. (The decay $H^+ \rightarrow W^+h^0$ would be large if kinematically allowed. The backgrounds would then be different, but the detector requirements are not dissimilar.) The $c\bar{s}$ mode obviously yields a more precise mass measurement of H^+ and t. Using lepton and jet cuts similar to those in the case of standard t-decay and assuming $B(t \rightarrow W^+b) = B(t \rightarrow H^+b) = 50\%$ and $B(H^+ \rightarrow c\bar{s}) = 100\%$, L* obtained the W^+ and H^+ dijet mass spectra shown in Fig. 2-5b. The combinatoric background was eliminated by requiring that the candidate dijets from the W satisfy $|\phi_{j_1} - \phi_{j_2}| < 60°$ and that the W-jets and the b-candidate jet satisfy $|\phi_W - \phi_j| < 100°$. The reconstructed two- and three-jet masses allow M_{H^+} and m_t to be determined to about 2% in one SSC year so long as $B(t \rightarrow H^+b)B(H^+ \rightarrow c\bar{s}) \gtrsim 1\%$.

If $B(H^+ \rightarrow \tau^+\nu) \sim 100\%$, then one must look for a violation of $e/\mu/\tau$ universality by measuring the rates for each, detecting the τ in its hadronic modes. L* selected events by requiring one isolated lepton, one inclusive muon (from $t\,(\bar{t}) \rightarrow Wb$; $b \rightarrow \mu + X$) and a τ-jet (from $\bar{t}\,(t) \rightarrow H^{\mp}b$; $H^{\mp} \rightarrow \tau^{\mp}\nu$). The τ jet was required to have $p_T > 70$ GeV, $|\eta| < 1.7$, more than 30 GeV deposited in the hadron calorimeter, less than four charged tracks inside a cone of $R = 0.3$ around the jet axis, and an acoplanarity angle $\Delta\phi > 100°$ relative to the isolated lepton. The masses are not precisely determined but can be estimated from the kinematic distributions.

To summarize, based on the simulations by the E/T and L* collaborations, we are confident that our detector can discover a heavy top quark in a few days and measure its mass to about 2% in one SSC year. The detector can determine whether t decays are standard or involve a charged scalar and, if they do, measure the charged scalar's mass with comparable precision. This example again demonstrates the detector's power to find physics signals involving isolated leptons and muons within jets and to reconstruct particle masses in multi-jet modes.

2.5 Discovery and Properties of a Heavy Z'

We consider the search for a new heavy neutral gauge boson, Z', with mass $M_{Z'}$ = 4 TeV and width $\Gamma_{Z'} \simeq (.01 - .02)\, M_{Z'}$. We assume 1000 events in each of the three channels e^+e^-, $\mu^+\mu^-$ and $\tau^+\tau^-$. With our projected lepton resolutions, the mass and width are very well determined in the e^+e^- mode and, for a variety of models, the forward-backward asymmetry is well-measured in the muon channel. It is worth noting that, if such a heavy Z' has couplings of $O(e)$ to quarks and leptons, it will take 10 – 30 years at the nominal SSC luminosity to produce 1000 l^+l^- events. Thus, our detector's ability to maintain precision measurement of high energy muons and electrons at $\mathcal{L} \geq 10^{34}\text{cm}^{-2}\,\text{s}^{-1}$ makes these results possible in 1–3 years. Put another way, in one year at $\mathcal{L} \geq 10^{34}\,\text{cm}^{-2}\,\text{s}^{-1}$, our detector can discover a 10 TeV Z' with nominal couplings to quarks and leptons.

The detector acceptance for $Z' \rightarrow e^+e^-$ is about 88% for our rapidity coverage of $|\eta_e| < 2.5$. The Drell-Yan background to $Z' \rightarrow l^+l^-$ at $M_{Z'}$ = 4 TeV is five orders of magnitude below the signal. The cross section for dijets in a 1% mass bin at this mass is about 2pb. These jets typically have $\Delta R \sim 0.7$ and very high multiplicity, so isolation cuts for the electron showers easily eliminate them. Similarly, at these mass scales pile-up is not significant, even at ultra-high luminosity. At such large energies in the e^+e^- mode, only the 0.5% constant term in the energy resolution matters. Figure 2-6 shows the mass spectrum for the Z' as determined by the E/T collaboration. [3] The mass is determined by fitting to a Breit-Wigner plus a smooth continuum. The statistical error on the mass is 0.07%; we estimate that non-linearity effects are about 0.25%. The error on the width is about 3%. Assuming $\int \mathcal{L}dt \geq 10^{41}\,\text{cm}^{-2}$, these precisions are comparable to those obtained at LEP for the Z^0 in about the same running period.

The detector acceptance for $Z' \rightarrow \mu^+\mu^-$ is similar to that for electrons. With $(\Delta p/p)_\mu$ = 5% at p = 500 GeV, taking into account gaps and muon energy loss in the calorimeter, and with the standard isolation cut on the muons, L* found a mass resolution of 16% for the resistive coil option. [3] A similar result should apply for the smaller superconducting coil in this detector. E/T studied the forward-backward asymmetry measurement for a variety of models and found that it can be measured to ±3%, sufficient to help to determine the nature of the Z' [3]. L* concluded that less than 1% of the $Z' \rightarrow \mu^+\mu^-$ had the muon signs incorrectly determined. These capabilities apply, as well, to our detector. The forward muon coverage is improved in the new detector because the aspect ratio of the coil

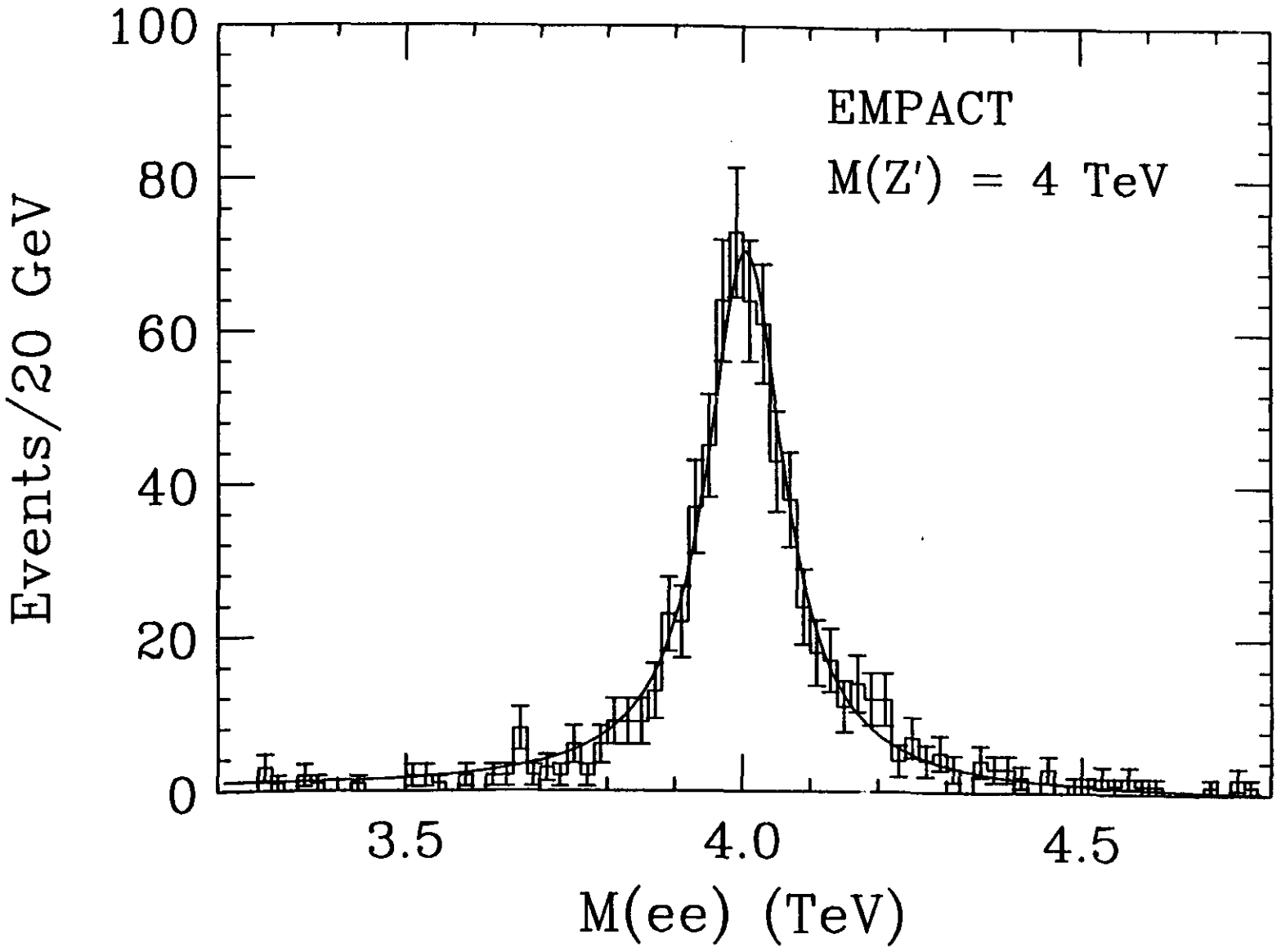

Figure 2-6 Z′ mass distribution

is longer, and we are investigating a variety of ways to improve the resolution in the forward direction to further improve the forward muon performance.

For $Z' \rightarrow \tau^+\tau$ L* required one τ to decay into a muon and the other into hadrons, giving a very narrow jet with less than four resolved tracks. This should work well in our detector and give a sufficient signal above backgrounds to check e-μ-τ universality. At a luminosity of order 10^{34} cm^{-2} sec^{-1} the calorimetric identification of the τ-jet is probably adequate, although this needs more study. Measurement of the τ-jet multiplicity seems possible, but may depend on the technology choices made.

Most detectors would discover a Z' if it were produced at a large rate. Our detector offers significant advantages in that it can discover a 10 TeV Z' in about one year using ultra-high luminosity and, in the same period, measure the mass and width of a 4 TeV Z' with great precision in the e^+e^- channel and its lepton asymmetry in the $\mu^+\mu^-$ channel.

2.6 Supersymmetry

Supersymmetry is a theoretically attractive extension of the standard model because it provides a natural setting for elementary scalars. It is also quite useful for the study of detector design because it provides a scenario with complex signatures. We consider here the minimal supersymmetric extension of the $SU(3) \otimes SU(2) \otimes U(1)$ standard model: two Higgs doublets, supersymmetric partners for all the known particles and the Higgs bosons, an exact R-parity to eliminate unacceptable proton decay, and some plausible unification conditions at the GUT scale. In this scheme, there are four neutralinos, $\tilde{\chi}_i^0$ and two charginos, $\tilde{\chi}_j^\pm$, which are mixtures of the supersymmetric partners of the gauge and Higgs bosons. The conserved R-parity forces all supersymmetric particles to be pair-produced and to decay into the lightest one, $\tilde{\chi}_i^0$, which is absolutely stable and escapes from the detector. Thus, the basic signature for much of minimal supersymmetry is $\not{E}_T$ plus multiple jets.

An E/T analysis of gluino pair production examined the $\not{E}_T$ signature and backgrounds for a variety of masses, including all the predicted decays [2,3]. Events were selected having at least 4 jets with $p_T > 50$ GeV and a sphericity $S_T > 0.2$ in the transverse plane. The dominant backgrounds come from QCD jets containing heavy quarks and from $W^\pm$ and Z^0 production at high p_T. These were calculated including Gaussian detector resolutions obtained from a detailed engineering model of a liquid argon calorimeter taking dead material into account. A signal a few times the QCD and electroweak backgrounds was obtained for all masses; Fig. 2-7 shows typical results for a 750 GeV gluino. The

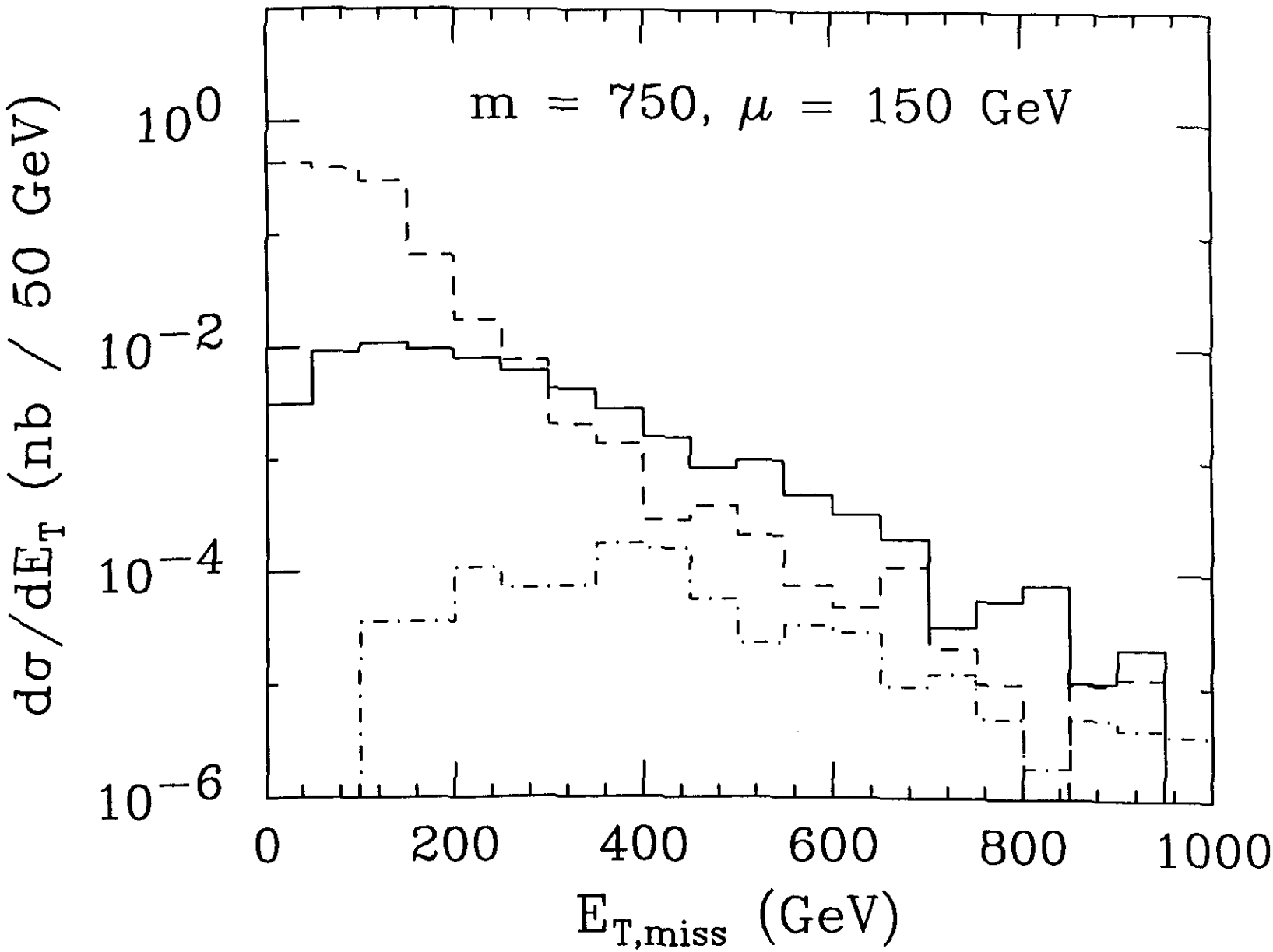

Figure 2.7 Missing E_t distribution from decay of a 750 GeV gluino

effects of the transition at $\eta \approx 3$ between the endcap and forward calorimeters were investigated separately and seem to be acceptable. The lesson of this study is that the contributions to the $\not{E}_T$ cross section from detector effects should be kept less than those from real neutrinos for $\not{E}_T \gtrsim 100$ GeV. This probably requires covering down to $\eta \sim 5$.

If supersymmetry were to be discovered, then the masses and decay modes of all the supersymmetric particles would have to be determined. This is a very complex task, since a single gluino can easily decay through several intermediate $\tilde{\chi}$, giving jets, leptons, $W^{\pm}$ and Z^0 bosons, and even Higgs bosons. Understanding such decays would require studying the events with large $\not{E}_T$ in great detail. It would surely be a multi-year and multi-detector task.

Not all supersymmetry signatures depend on $\not{E}_T$. Since the gluino is a Majorana fermion, it decays equally into l^+X and l^-X, giving isolated like-sign dileptons. The backgrounds for such events seem to be small. Observing this signature requires measurement of lepton signs with momenta that depend on the assumed masses but are typically $p_T \gtrsim 100$ GeV. Our detector would do this mainly in the $\mu^{\pm}\mu^{\pm}$ channel. Since gluinos are strongly produced, the rates are quite large even for masses in the 1 TeV range. An E/T analysis found about 170 like-sign dimuon events with $|\eta_\mu| < 2.5$ for a 1500 GeV gluino with particular choices of the other parameters. Hence, it does not appear essential to measure $e^{\pm}$ signs over the relevant mass range.

2.7. Technicolor

In the technicolor scheme, there are no *elementary* scalar bosons. Rather, electroweak symmetry is broken dynamically through new strong gauge interactions of technifermions. This eliminates the naturalness and hierarchy problems of elementary scalars and is the prime motivation for technicolor. Unlike elementary Higgs models and their supersymmetric extensions, technicolor addresses the flavor question head-on, and this gives rise to its flavor-changing neutral current problem. However, recent developments in technicolor dynamics (known as "walking technicolor") seem to ameliorate this problem and, so, retain technicolor as a viable scenario for solving both the electroweak and flavor symmetry problems.

In minimal technicolor models – those with a single doublet of technifermions – the primary signature at the SSC is the production of charged and neutral technirho vector mesons, ρ_T, of mass 1–2 TeV. These always decay as $\rho_T^0 \to W^+W^-$ and $\rho_T^{\pm} \to W^{\pm} Z^0$. The subprocess cross sections are very small, $O(\alpha^2)$, and it is fairly clear that such a heavy

ρ_T requires $\mathcal{L} \simeq 10^{34}$ cm^{-2} s^{-1} for its discovery[4]. The obvious search mode for $\rho_T^{\pm}$ is $Z^0 \rightarrow l^+l^-$, $W^{\pm} \rightarrow l^{\pm} + \not{E}_T$. These lepton measurements should be possible at ultra-high luminosity in our detector. The $\not{E}_T$ will be ~ 250–500 GeV. Measuring just the charged leptons may be sufficient, but measurement of $\not{E}_T$ at high luminosity will be investigated. The search for both heavy ρ_T in mixed lepton plus dijet modes may also be feasible at $\mathcal{L} \simeq 10^{34}$ cm^{-2} s^{-1}, but this certainly requires much detailed study.

Non-minimal technicolor models – those with several doublets of technifermions – have a rich assortment of signals: several sets of ρ_T vector mesons, each decaying into spinless technipions, π_T. The π_T, in turn, are expected to decay into heavy fermion-antifermion pairs, but this is a technicolor-model-dependent issue. In nonminimal models, the masses of the ρ_T probably are less than 1 TeV. At least some of the technifermions may carry ordinary color, transforming as triplets (like quarks). In that case, there will be color-octet ρ_T produced with large rates ($O(\alpha_s^2)$), roughly comparable to dijet production at the same mass scale. These ρ_T decay into pairs of color-octet and triplet π_T [5], whose signatures we now discuss.

The pair-produced color-octet π_T will be very narrow, decaying into $q\,\bar{q}$ pairs. If the quarks are heavy, the four heavy-flavor signal will be larger than any standard physics background. The detector's heavy-flavor tagging and lepton identification capabilities should allow their discovery. If the flavors are light, there is a potentially large background from four-jet production. Figure 2-8 shows the signal and QCD background at the parton level for $M_{\pi\pi}$ = 200 GeV [5]. The figure shows the dijet mass distribution for jet pairs whose masses are equal to within 25 GeV. Reasonable parton-jet energy resolution of $50\%/\sqrt{E} \oplus 5\%$ and perfect angular resolution were assumed. For this M_{π_T}, all four signal and background jets were required to have $p_{Ti} > 100$ GeV, $|\eta_i| < 2$, $\Delta R_{ij} > 1.0$. We believe that this signal can be seen clearly in our detector, but more detailed simulations will be needed to confirm this.

Color-triplet π_T, "leptoquarks", decay into a quark plus a lepton. If these decays predominantly involve heavy flavors, then the most accessible leptoquark signals will involve pairs of $b\tau$ or $t\tau$. This provides a test of detector performance because reconstruction of the τ-momenta depends on good $\not{E}_T$ resolution, not just on the ability to veto events without large $\not{E}_T$. Thus, this signature is sensitive to the global resolution of the hadron calorimetry.

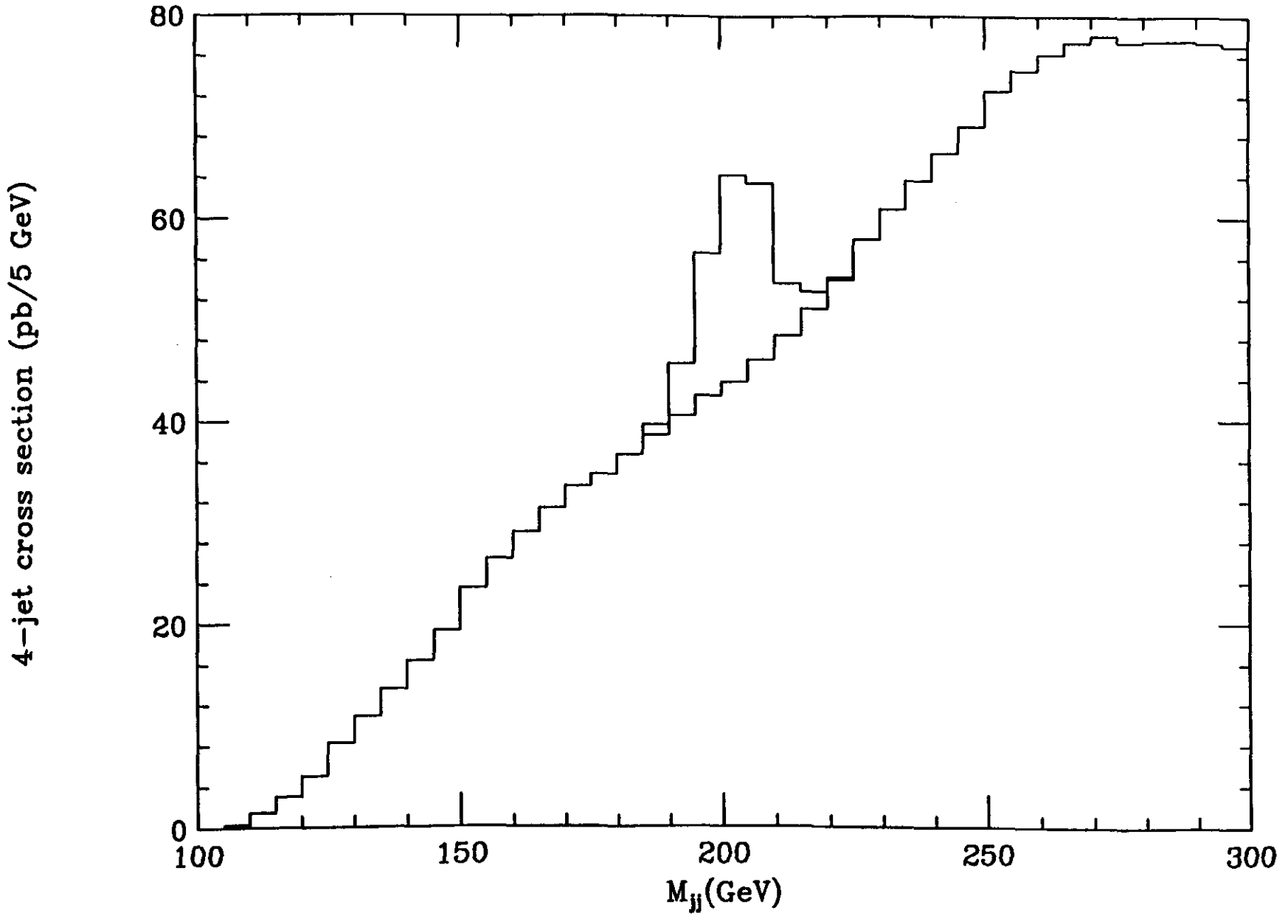

Figure 2.8 Mass distribution from pair-produced π_T into pairs of heavy quarks

2.8. Quark and Lepton Substructure

The profusion of quark and lepton generations and the desire to make sense of the flavor problem long ago led to the hypothesis that quarks and leptons are composite, built out of more fundamental fermions whose characteristic strong-interaction binding scale is Λ. For Λ much larger than the parton subprocess energy, $\sqrt{\hat{s}}$, this substructure shows itself through effective four-fermion "contact" interactions of quarks and leptons with strength of order $4\pi/\Lambda^2$. These contact interactions modify standard model predictions. Specifically, dijet and Drell-Yan cross sections flatten out at large p_T and invariant mass, $M = \sqrt{\hat{s}}$. [5]

Searches for these effects in e^+e^- and $\bar{p}p$ colliders indicate that $\Lambda \gtrsim 1$ TeV. Parton-level calculations, which do not take real detector characteristics into account, indicate that the SSC should be able to reach $\Lambda \simeq 15$ TeV in dijet production and $\Lambda \simeq 25$ TeV in the Drell-Yan process for $\int \mathcal{L}dt = 10^{40}$ cm^{-2}. This expectation has been largely supported by the detector collaborations' more detailed simulations.[2,3,4] Here, again, this detector's robustness at ultra-high luminosity gives it extended reach.

Some of the main experimental problems associated with the search for quark substructure in high-p_T and M have been considered by the detector collaborations [2,3,4] and are summarized here. The jet energy flow into a fixed cone is calculable in perturbative QCD, and CDF has shown that the data follow the perturbative predictions quite well. This means that clustering and fragmentation effects are not important. Thus, the high-p_T measurement is limited only by statistics and by the resolution of the calorimeter. The p_T resolution will also be degraded if $e/h \neq 1$. While it is desirable that e/h be close to one, this may conflict with the design goal of very good electromagnetic resolution. The lack of compensation may be overcome by calibrating at appropriate energies and by weighting the longitudinal samples. Another possibility is that effective compensation may be achieved with a high resolution EM calorimeter followed by a compensating hadron calorimeter. A GEANT simulation of this arrangement for L* gave a constant term of 4.7% in the single charged pion energy resolution and of 2% in the jet energy resolution. The jet energy resolution will be degraded if the calorimeter is not thick enough to contain the shower. These and many other considerations will be carefully studied and weighed in formulating the final design choices for the detector.

Finally, the problems associated with the search for lepton substructure signals in the Drell-Yan process are the same as those encountered for the high-mass Z'. Our detector will be most precise in the e^+e^- mode. But important information on the chiral structure of

the contact interactions may come from measuring the asymmetry in the $\mu^+\mu^-$ channel if a significant excess of high-mass l^+l^- is observed.

* * * * * * * * * * * * *

The design philosophy of our detector emphasizes an open geometry with very precise EM and muon measurements at standard and ultra-high luminosities, as well as quite good determination of hadronic energy and adequate central tracking. These goals and their implementation are very similar to those realized in the L* and E/T designs. Thus, we have been able to use many of their extensive studies of physics signals and backgrounds. We conclude that our detector will discover — or rule out — a very broad range of new physics possibilities that will be within reach of the SSC. In a number of significant areas, our detector will surpass SDC: Our much better electromagnetic resolution allows the search for $H^0 \rightarrow \gamma\gamma$ and more precise measurements of a Z' width and mass—fundamental parameters of a new gauge interaction. Our detector measures muons outside the calorimeter, so it is better able to tag heavy quarks using muons and to measure the heavy flavor content of high-p_T jets. Our detector is less dependant on central tracking and so able to exploit ultra-high luminosities. In many other areas – $H^0 \rightarrow l^+l^-l^+l^-$, $H^0 \rightarrow l^+l^-jj$, and heavy quark physics, to name three — our detector will be at least comparable to SDC. These two detectors, then, provide the complementarity crucial for the broadest possible probes of electroweak and flavor physics at the SSC while maintaining the essential ability to check and to confirm measurements.

REFERENCES

1 Expressions of Interest to the SSC Laboratory by the TEXAS, EMPACT, and L* Collaborations, 1990.

2 Responses to the Program Advisory Committee of the SSC Laboratory by the EMPACT, L* and TEXAS Collaborations, 1990.

3 Letters of Intent to the SSC Laboratory by the EMPACT/TEXAS Collaborations, 1990.

4 E. Eichten, I. Hinchliffe, K. Lane and C. Quigg, Rev. Mod. Phys. 56, 579 (1984).

5 R. S. Chivukula, M. Golden and E. H. Simmons, "Multijet Physics at Hadron Colliders", BUHEP-90-34, to be published in Nuclear Physics B, and private communication.

3.0 DETECTOR SUBSYSTEMS

3.1 Magnet

3.1.1 Introduction

The magnet system consists of a 17.25 meter bore 0.8 Tesla single coil (unshielded) superconducting solenoid oriented parallel to the beam axes. Steel poles cover each end of the solenoid to improve field uniformity. The system includes the cryogenic cooling system of the magnet power supply and related controls and instrumentation.

The general design philosophy, performance characteristics, materials of construction and manufacturing technologies are derived directly from the design presented in the L* LOI Proposal. Key U.S. technical personnel have remained as part of the newly formed collaboration.

Substantial reductions in both cost and manufacturing time have been achieved by removal of the outer shield winding, elimination of approximately 75% of the pole weight and by relaxing to the 5% resolution performance. As mentioned elsewhere in this report, the forward/backward magnets are no longer a part of the detector system.

3.1.2 Design Considerations

The design is driven by the need to achieve substantial cost reduction, the need to achieve reasonable resolution over the angular range of 10°–170° and to provide a minimum of 0.8 Tesla required for the central tracker. The operating parameters also represent a minimum cost for the combined magnet and muon chamber system for a 5% resolution while accommodating the largest expected dimensions for the central detector components. The required schedule for completion and its potential vulnerability to slippage in the experimental hall schedule have also been specifically considered in the design and manufacturing scheme proposed.

The large external fringe fields and related issues of safety and overall system facility and machine operation are discussed in below.

3.1.3 Design Description

The superconducting magnet is shown in Figure 3.1-1; design and operating parameters are shown in Table 3.1-1, and Figure 3.1-2 shows the resolution versus η for the muon system. The magnet will be fabricated into independent halves, thus permitting full assembly and test on the surface prior to installation in the experimental hall.

The unshielded solenoid configuration represents the simplest and most reliable design possible. It saves an enormous amount of money, time and space in the experimental hall. The winding consists of a single layer of niobium titanium cable in conduit superconductor wound on the inside of an aluminum support element.

The unshielded design also permits a very large reduction in the weight and cost of the magnet poles because there is no longer any need for them to carry the total flux in the bore of the magnet.

The poles are thus sized to keep the flux density in the steel low at small radius and thus improve uniformity and low angle bending power. At larger radius where most of the pole mass would be

Table 3.1-1 Superconducting Magnet Parameters

Central induction, B_i (T)	0.823
Mean radius of windings, R_w (m)	8.617
Outer radius, cryostat vessel, R_v,o (m)	9.417
Inner radius, cryostat vessel, R_v,i (m)	8.317
Radius of innermost muon chamber, R_u,i (m)	4.400
Radius of outermost muon chamber, R_u,o (m)	7.847
Inter coil length, L_i (m)	28.00
External coil length, L_e (m)	29.00
Conductor length (km)	23
Total mass of windings, M_w (t)	364
Total mass of cold structure, M_{cs} (t)	258
Total mass of cryostat vessel, M_v (t)	593
Total mass of iron end shields, M_{is} (t)	2.400
Radial pressure on windings, P_r (kPa)	274
Operating current, (kA)	40
Stored Energy (GJ)	1.429
Induction (H)	1.78

In a conventional design, the steel can be driven far beyond saturation without serious effect on overall system performance, as can be seen in the field map of Figure 3.1-3. The field distribution shown is for a uniform current distribution in the winding. The field distribution in the volume near the end of the solenoid winding can be effectively controlled by end compensation in the winding. It is also worth noting that the available bending power at these angles is inherently large and a small loss resulting from less than optimal field distribution would not be serious. The primary purpose of the pole steel at large radius is structural support and can, therefore, easily accommodate substantial access for muon chamber support, alignment, etc.

Both the ALEPH and DELPHI magnet at CERN, and the MFTF-B magnet at the Lawrence Livermore Laboratory, have used the thermosiphon-cooling method, while many other fusion magnets use forced-flow cooling of the conductor. In the present design, both methods are used to combine their respective advantages to offer redundancy for higher reliability. The first cooling system uses the thermosiphon technique to cool the aluminum support cylinders to which the

Fig 3.1-1 Elevation view of the baseline magnet

Fig 3.1-2 Muon Momentum resolution at 500 GeV/c as a function of η

Fig 3.1-3 Field map of the solenoid with a typical pole treatment

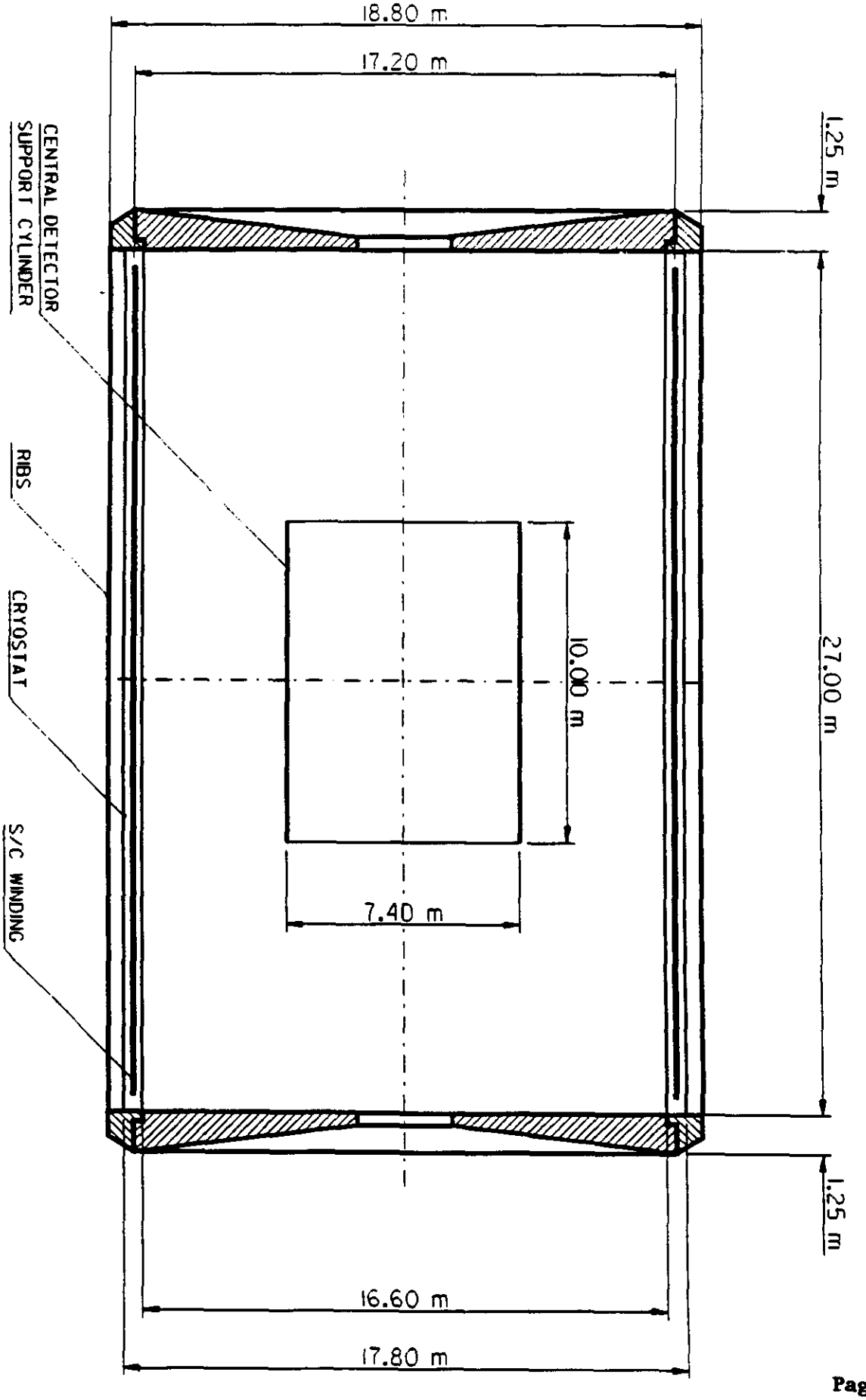
18.80 m
17.20 m
1.25 m
CENTRAL DETECTOR
SUPPORT CYLINDER
RIBS
CRYOSTAT
S/C WINDING
10.00 m
27.00 m
7.40 m
1.25 m
16.60 m
17.80 m

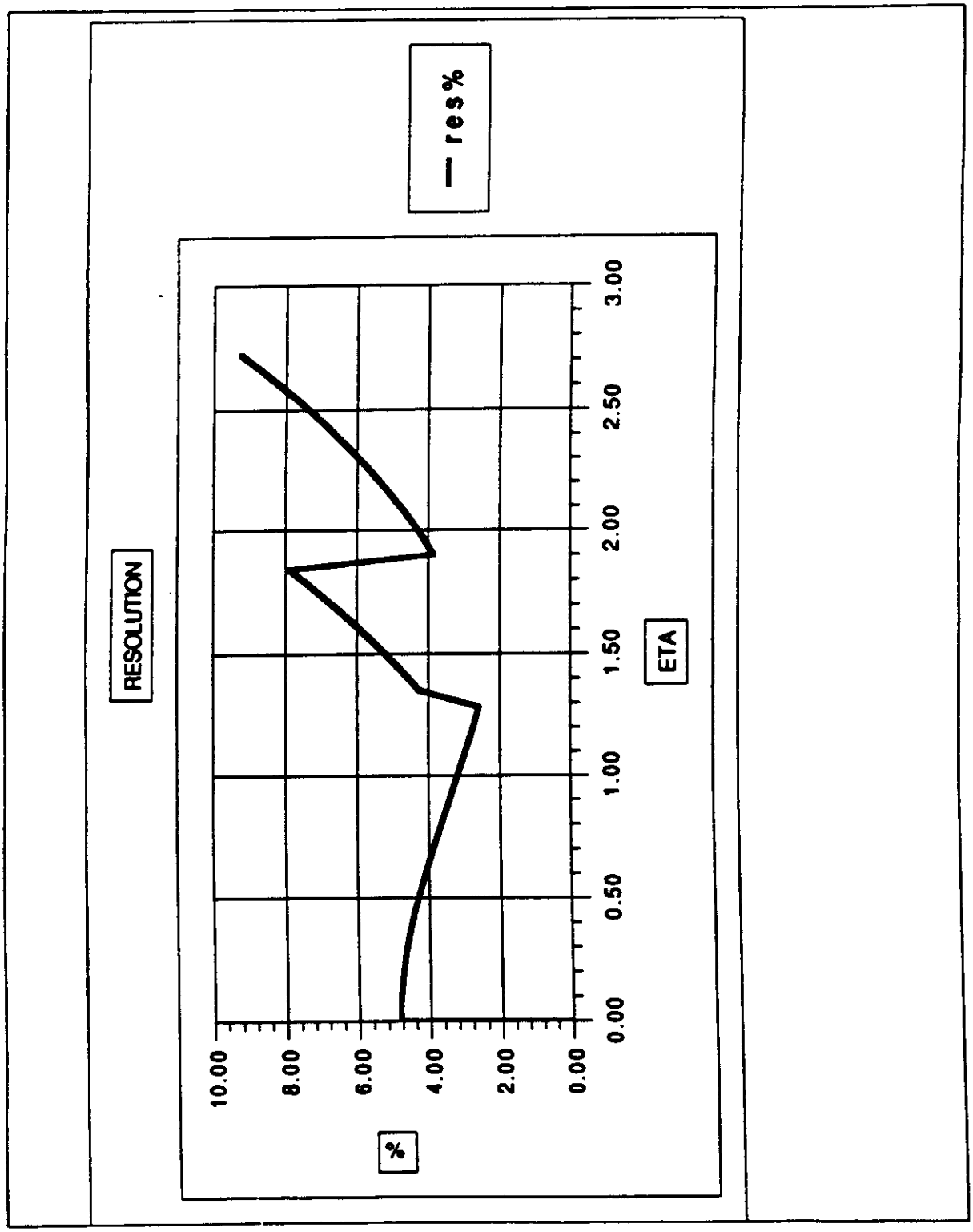
RESOLUTION
%
10.00
8.00
6.00
4.00
2.00
0.00
0.00
0.50
1.00
1.50
2.00
2.50
3.00
ETA
res%

S.C. Coil, Tapered Iron Pole, No Barrel

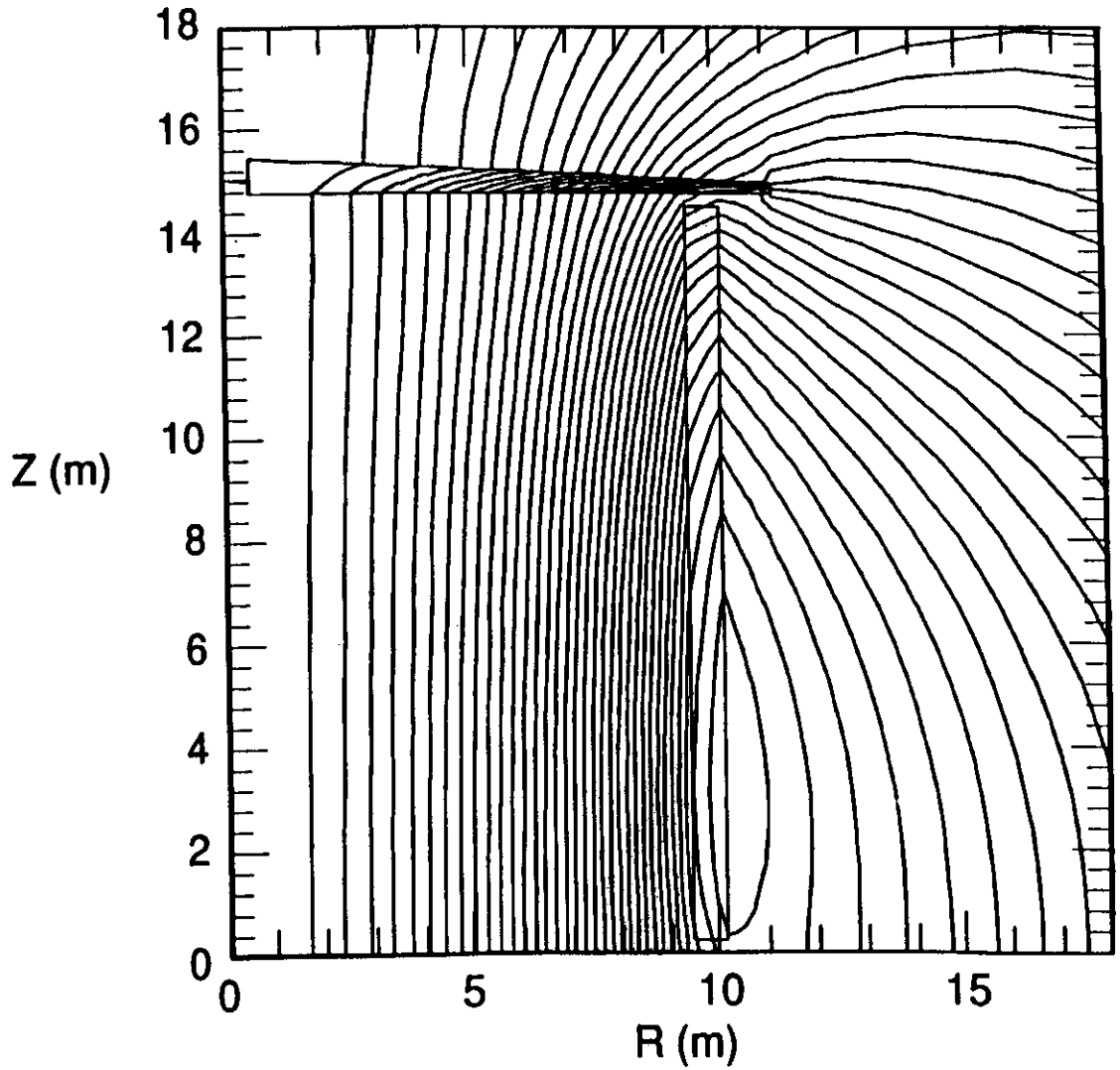

Contours of constant flux

TIP-02054

conductor is bonded. The coil support cylinder has tubing attached to the outside which is connected to headers on the top and bottom to promote free convection. This loop handles all heat loads to the magnet, including thermal radiation, cold mass support conduction, and joint heating. The cooling system is a very reliable passive system that does not rely on pumps or the refrigerator to maintain operation.

The details of the conductor can be seen in Figure 3.1-4. It consists of a standard niobium titanium cable contained inside of a heavy-walled conduit. A small volume of helium, which is in intimate contact with the superconducting cable, flows within the conduit. To greatly increase the thermal capacity adjacent to the current-carrying superconductor, a second circuit from the liquefier uses a straightforward forced flow cooling system that circulates single phase helium. The forced circulation loop is recommended in addition to the natural convection loop for two reasons:

- It provides thermal capacity adjacent to the superconductor. Metals have extremely low thermal capacity at 4.5 K. Without the higher thermal capacity of the helium, the conductor would be extremely sensitive to thermal perturbations associated with conductor motion, and the risk of a quench would be high. The helium in the conductor increases the critical energy margin up to 3.9 Joules per point perturbation.
- The slight flow in the forced flow channel is in direct contact with conductor joints and distributes joint heating over large areas so it can be more readily carried away by the natural convection loop. The forced flow loop eliminates any possibility of hot spots in the conductor, and the natural loop removes all the heat. This design combines all of the benefits of winding and improved thermodynamic stability of cable and conduit conductors, which offer energy margins that are one to two orders of magnitude greater than those associated with the indirectly cooled windings of the above referenced devices.

The heat leak for the superconducting magnet is estimated at approximately 1190 watts which includes the vapor cooled lead flow. The thermosiphon cooling system will function until the liquid helium volume of the storage dewar feeding the system is depleted. This makes the system reliable since it is independent of refrigerator interruptions or shutdowns. A large surface storage Dewar can be used to provide up to forty hours of operation without power which is more than adequate time to make major repairs to the refrigerator.

A 12 × 24 square meter building contains all the cryogenic support equipment and houses the controls for the cryogenic and other detector magnet support systems. The only components in the detector hall are the transfer lines and a small thermal siphon dewar mounted above the detector.

For the refrigerator plant, screw compressors will be installed. They are of proven reliability in helium operation and capable of continuous service over periods up to 8000 hours without maintenance. To prevent air infiltration into the helium gas stream, the suction pressure is kept above atmospheric pressure.

For the cold process, the plant has a cold box placed in the surface building. The refrigerator cold box is equipped with gas bearing turbines. The turbines are appropriate for reliable long term service, with minimum downtime for maintenance. They are readily accessible for maintenance and repair. A surface dewar is in placed strategically to minimize the length of line from the dewar to a local thermal siphon dewar just above the detector in the underground hall. The local thermal siphon dewar subcools the helium before it flows to the superconducting coil and separates the

Fig 3.1-4 Coil end section

COIL END SECTION

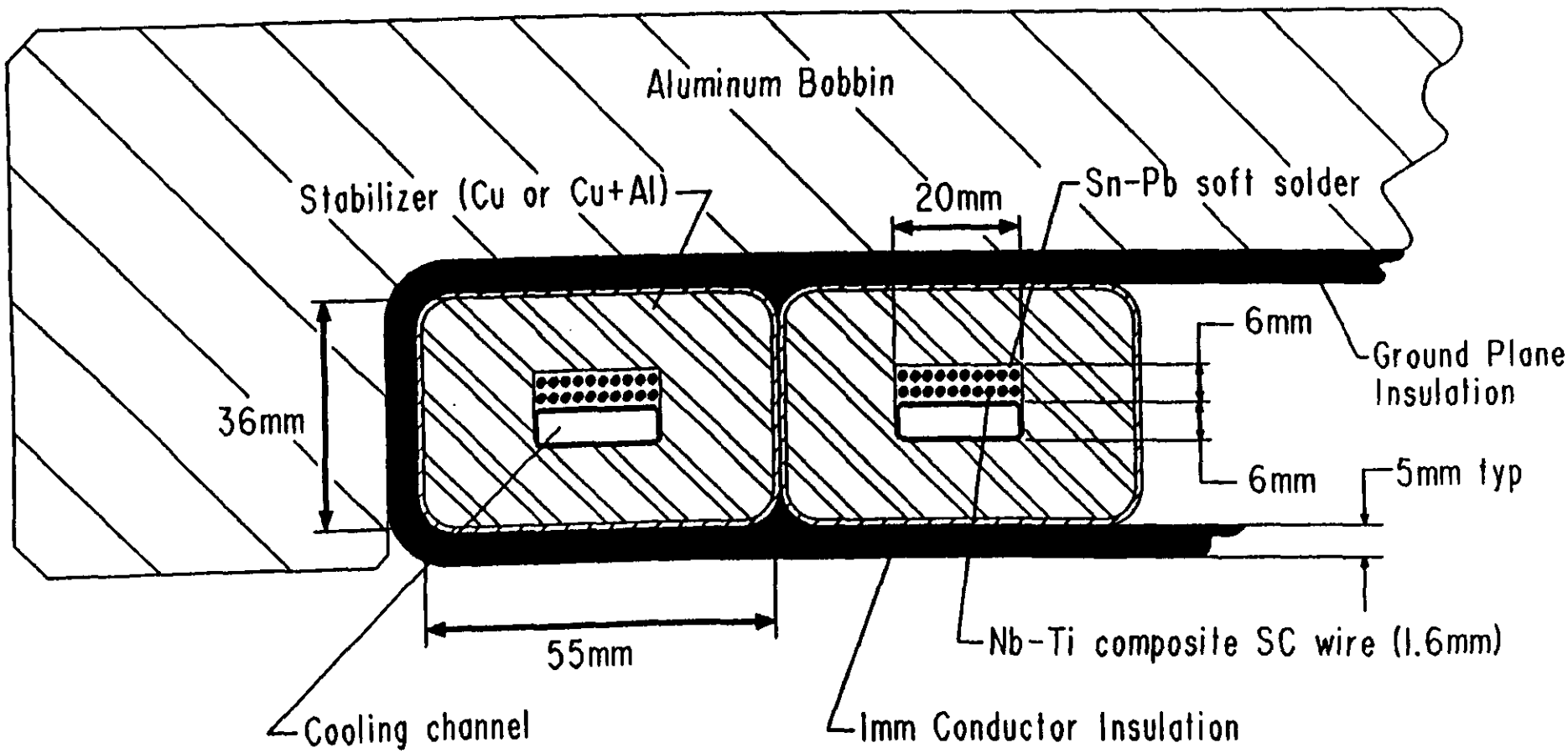

return warm helium and allows only helium gas to return to the surface to the refrigerator low pressure side.

A 40,000 ampere 1.5 megawatt power supply could energize the magnet to full field in approximately 4 to 8 hours, limited only by structural heating. The energy dumping system can discharge the magnet in approximately 10 minutes.

3.1.4 Magnet Manufacturer and Schedule

The major magnet components consist of large, but simple, cylindrical shells. Manufacturing must be on site but is in most respects straightforward. The method of coil winding is shown in Figure 3.1-5. The single layer winding will enable manufacture with simple tooling and a minimum of manufacturing engineering development effort.

The coil will be manufactured into complete independent sections and the force containment and cold mass support structures will be designed to permit testing to full current without the magnet poles.

3.1.5 Fringe Field Effects - Safety and Interface Issues

Stray fields are expected due to the absence of controlled flux return paths. The predicted spread of the field is shown in Figure 3.1-6 and will require a careful survey to ensure that all components in the underground hall and some surface equipment are either suitably shielded or designed to avoid the influence of the field. The magnetic fusion community has a long record of successfully operating large high field u-shielded magnets surrounded by technical components.

It is assumed, at this moment, that an interlock system would ensure that the magnet would be turned off when personnel descend to the underground experimental hall and that there would be patrols before turning the magnet on again to ensure all small, loose magnetic materials (tools, etc.) are removed. There are existing similar environments where cranes, electronic equipment and other actuating components function normally when correctly specified, positioned or shielded.

The surface operations building may be the main concern due to the presence of monitors and computers but, iron shielding or field shaping coils can compensate for this situation and whilst this may induce a cost factor, this cannot be compared to the cost of iron or another large coil to return the flux.

3.1.6 Research and Development

All elements of the design have been demonstrated at adequate scale to reduce the required R&D effort to modest scale verification tests and simulated surface demonstrations. The manufacturing engineering effort will also be quite modest due to the simplicity of the proposed design and manufacturing technique.

Parallel path engineerings studies will continue to explore techniques by which performance at low angles can be improved. Based on existing work, it is reasonable to expect that the low radius field shape can be modified to increase the radial component to achieve 5% resolution (approximately 10 tesla m^2) down to 5°. The methods and costs by which this can be achieved and

Figure 3.1-5 Coil Winding Scheme

Figure 3.1-6 Stray field of the Unshielded Solenoid

COIL WINDING SCHEME

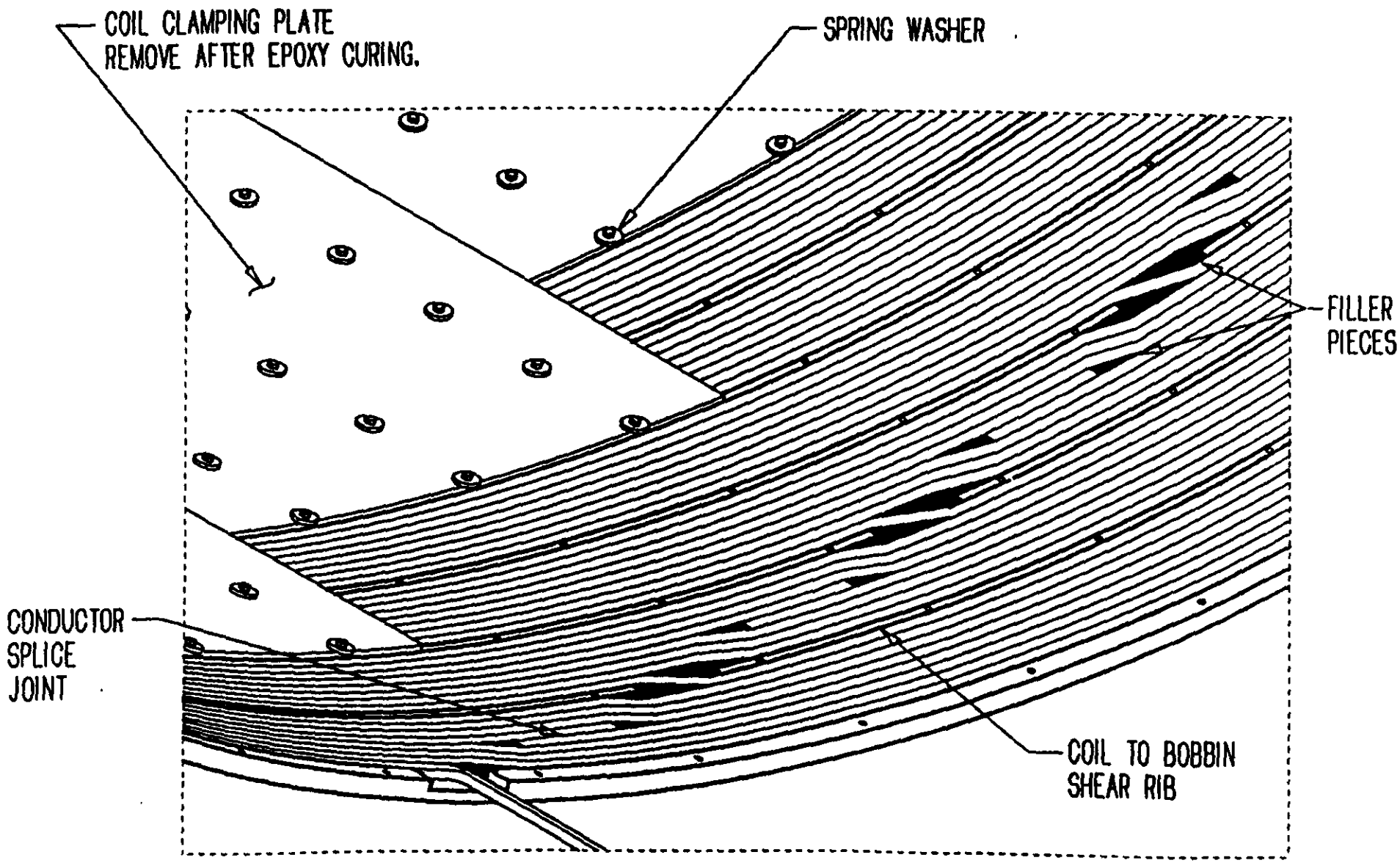

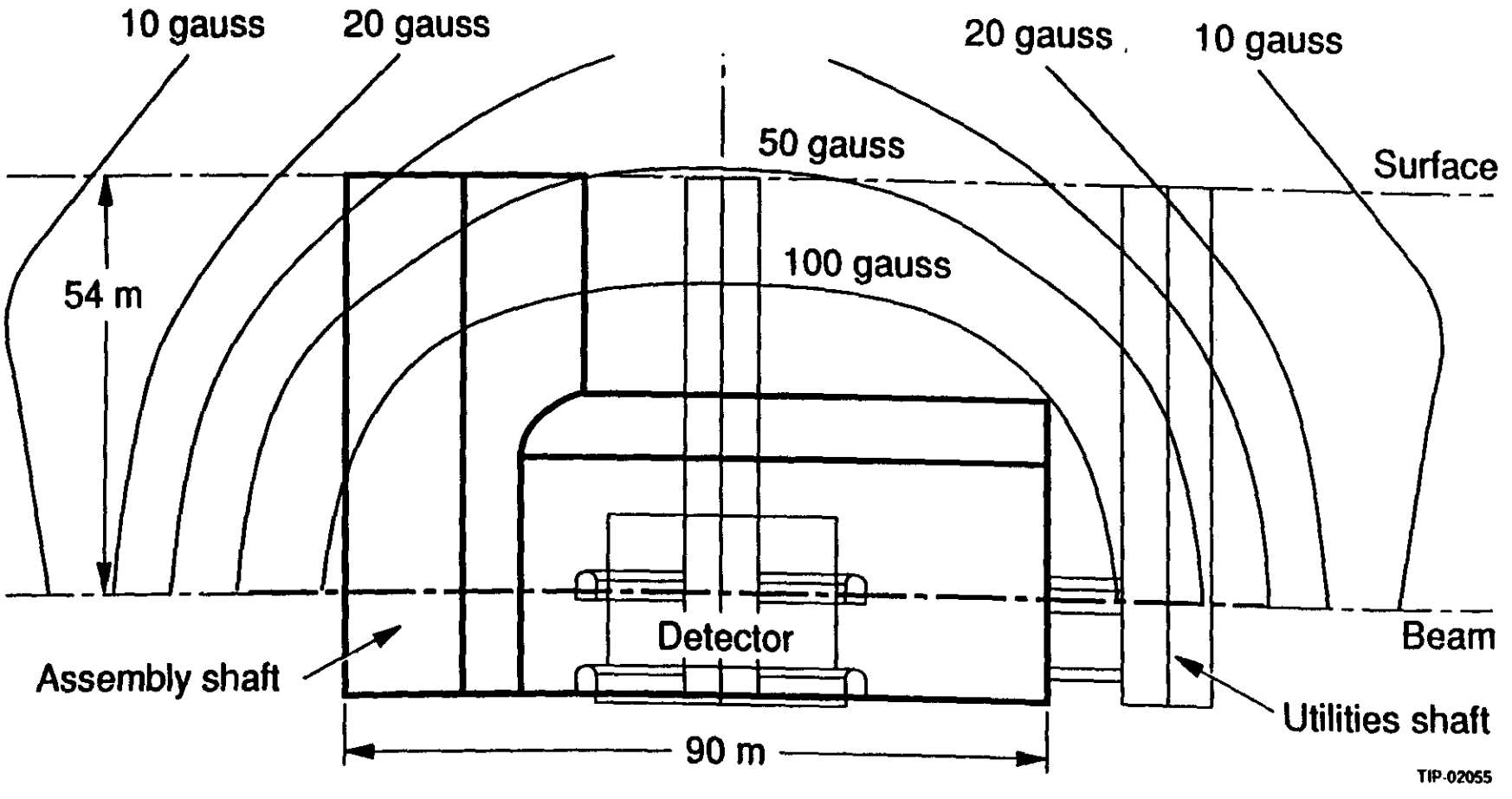
10 gauss
20 gauss
20 gauss
10 gauss
50 gauss
Surface
100 gauss
54 m
Detector
Beam
Assembly shaft
Utilities shaft
90 m
TIP-02055

their impact on calorimetry and the ways in which they might be staged for future upgrade will continue to be studied. The size, simplicity, and extreme conservativism of the proposed baseline will offer considerable flexibility and adaptability for future modification and/or upgrade. This flexibility should be of considerable value.

3.2 Muon System

Precision muon systems for SSC experiments set the scale for size and weight and therefore have a major impact on the overall cost of the experiment. One must therefore carefully specify this system to optimize and balance physics performance of the overall detector. As a complementary experiment to the SDC, this experiment intends to provide a muon system with enhanced capabilities—better resolution, better acceptance in rapidity, and better high luminosity capability. The justification for this comes from consideration of the physics goals and opportunities at the SSC. Precise measurements of muons enhance the discovery potential of this detector. This comes about through the statistical enhancement of the lepton signals, and through the uniquely clean environment for measuring muon momentum with high precision in the low rate environment outside of the calorimeter. At high luminosities, it will be easier to make precision momentum measurements with this muon system, compared to measurements made inside of a calorimeter. Precision muon and electron measurements enable a physics cross-check in these two channels but with different systematic errors. Since muons can be measured in close proximity to jets, measurements of such channels will also be very important for the study of signals of new heavy flavors. And most importantly, precision momentum measurements of muons outside of the calorimeter may very well be the most reliable and robust way of identifying unexpected phenomena at the SSC.

Our intent is to design a system taking advantage of the work done to design the L* experiment. Based on the concepts that have been developed in L3 and other segments of our collaboration, we are confident that an outstanding muon system and magnet can be designed and built for an acceptable cost. One example of such a system is described in Chapter 5.

Our starting point for thinking about the muon system for the second detector is to utilize a magnet such as that shown in Fig 3.1-1 which eliminates the flux return and retains only sufficient iron in the poles to shape and isolate the field from the surroundings. This design, described in the magnet section, is significantly less expensive than a magnet with a flux return. Much engineering effort has been expended on magnet design, on cost parametrizations, and on chamber support and alignment that will be incorporated and retained in the design work for the new experiment.

The muon momentum resolution for this magnet is shown in Fig 3.1-2 which provides a 5% momentum resolution at $\eta = 0$ and 500 GeV/c momentum utilizing high precision drift chambers. The z-coordinates are provided by separate chambers and trigger information is provided by Resistive Plate chambers (RPC).

The muon system group for the second detector consists of over 30 physicists. Supporting this group is a strong engineering team from national laboratories, magnet laboratories and industry. The major engineering efforts are on magnet configurations as well as on detector placement and technology. There is a consensus within the group that improvements in cost effectiveness and performance can be achieved by tuning the design parameters such as the number of tracking layers, the magnetic field, the shape of the magnetic field, the resolution per tracking layer, and the lever arm. There is general agreement that the basic design philosophy, namely that of tracking with precisely aligned muon chambers in a large magnetic volume, should be preserved.

To improve the momentum resolution in the forward regions,we will consider variations of the design by shaping the field with iron poles or additional coils, and will explore the optimum

placement of chambers inside and outside the field regions. Initial studies indicate that redistribution of chambers to take advantage of available external lever arm can provide improved resolution. A more radical departure is the employment of a high field compact solenoid.

Several detector technologies are being considered by this group. We intend to narrow the choices in the near future to husband the limited resources—financial, engineering and intellectual. Selection will be based on performance, viability, cost effectiveness and R&D progress. The system chosen will be affordable, will measure momentum precisely and reliably over a wide η range, will have sufficient pattern recognition and z-coordinate determination capabilities, and will provide a fast trigger which can tag beam crossings reliably.

Representative technologies include the baseline L* system; a system based on high precision drift tubes augmented with streamer tubes; a system utilizing streamer tubes with wire and strip readout; and a system of high precision interpolating pad chamber which provide unambiguous space points.

The baseline system rests on proven technology already developed. Our confidence in this system is based on the experience of costing algorithms, and of performance (both in terms of alignment and resolution per wire).

The hybrid drift tube/streamer tube system builds on extensive experience in drift tubes for high precision measurements. Drift tubes are robust, inexpensive and relatively insensitive to magnetic field strength. Systems employing drift tubes have demonstrated high-resolution performance in both muon and central tracking systems even under the hostile conditions of space and varying magnetic fields. A system is proposed to measure sagittas utilizing 24 layers of pressurized 4 cm diameter stainless steel tubes providing 100 μm resolution per tube layer. The drift tubes would be augmented by Iarocci tubes with wires providing a fast trigger, and stereo strips providing the z-coordinate and resolving ambiguities to enable good pattern recognition.

A slight variation of this system would use only Iarocci tubes. R&D efforts have demonstrated high intrinsic resolution for streamer tubes utilizing either wires or cathode strips. Reading wires and strips in the same gas gap provides strong correlations for sorting multiple hits with either charge or time measurements. These tubes have been produced inexpensively and reliably in large quantities while providing large fast pulses impervious to ambient noise. An SSC supported test beam effort is ready to take data at FNAL now, to study performance with high energy muons.

A different approach proposes using interpolating pad chambers, originally developed for the high multiplicity environment of heavy ion physics. These chambers provide high resolution space points (less than 100 μm), and can also provide fast pickoffs for trigger purposes. They are robust and relatively insensitive to magnetic field, but are sensitive in the wire direction to angle of incidence, which therefore requires a high multiplicity of wire segments in azimuth. The aim of this scheme is to reduce the number of detector planes by providing high resolution and granularity in each plane. The readout lends itself to a high degree of multiplexing.

Independent of the final technology choice, uniform requirements will be imposed for alignment and support of the chamber superlayers and will utilize the extensive work already done. Simulation efforts are now underway to provide an objective comparison between technologies, as

well as between magnet and detector deployment options. Given the limited funding, we expect to prioritize our choices before the beginning of the fiscal year.

In summary, the original design provides a strong base for our muon chamber system that has been demonstrated to meet the necessary physics goals. In light of the strengths available in the new collaboration, we are reevaluating the design considerations. This reevaluation is aimed at providing a lower cost and a technically superior system.

3.3 Calorimetry

The calorimeter is a crucial element of the proposed detector. Calorimetry identifies and measures the energy of photons, electrons, muons, jets, and neutrinos (by missing p_T). The calorimeter also provides fast triggering capability in response to energetic particles. The performance specifications of the calorimeter are driven by the requirement that this detector be complementary to the SDC detector. Consequently, the calorimeter must be hermetic and have excellent energy resolution for electrons and photons, as well as good resolution and linearity for hadrons through either real or effective compensation. The calorimeter must be capable of fast response, have adequate segmentation for good position resolution and for isolation cuts, provide precision over a large dynamic range, determine single-photon vertex, provide two-γ separation to high energy, and be capable of surving in the high radiation environment of the SSC. These requirements are summarized in Table 3.3-1.

The energy resolution of the electromagnetic (EM) portion of the calorimeter is an important issue. Superior resolution is required for the search for the Higgs in the low mass range (80 to 180 GeV) through its $\gamma\gamma$ or ZZ^* decay modes. The resolution is characterized by $\sigma_E = A / \sqrt{E} \oplus B$, where the "$\oplus$" indicates that the terms add in quadrature. For a viable Higgs discovery in a two-year period at $\mathcal{L} = 10^{33}$ cm^{-2} s^{-1}, simulations show that (A) needs to be smaller than 7.5% and (B) about 0.5%. This performance can probably be achieved with fine-sampling calorimeters, but it is near the limit of what can reasonably be expected from these devices. Significantly better energy resolution (A~1.3%) might be possible with total absorption homogeneous calorimeters, such as BaF_2 or liquid xenon. In addition to enhancing the discovery potential for the Higgs, such high resolution may add substantially to our capability to discover unpredicted phenomena e.g. narrow resonances. On the other hand, a homogeneous EM calorimeter combined with a sampling hadron calorimeter may not be sufficiently compensating since the first ~ 1.7 absorption lengths are in the non-compensating EM section. Furthermore, homogeneous calorimeters have been costed to be more expensive than sampling calorimeters.

A high-resolution calorimeter system requires uniformity, precise in situ calibration and monitoring, stability to < 0.5% in a strong magnetic field, and a high degree of resistance to radiation damage. For the physics goals of a high-energy, high-p_T detector, it is the constant term (B) in the energy resolution which dominates the calorimeter performance. This is particularly true for electromagnetic calorimetry for which the desired precision is high and the sampling term is small. To choose between competing calorimeter technologies, demonstration of radiation hardness, calibration, robustness and uniformity with an existing tested system will be very important.

As a high-energy, high-luminosity hadron collider, the SSC places extreme demands on the speed, dynamic range, segmentation, and total depth (absorption lengths) of electromagnetic and hadronic calorimetry. Speed is particularly important for the identification and precise measurement of isolated electrons and muons, which is essential for our physics goals. Speed is also essential for the first-level trigger systems. A dynamic range extending from minimum-ionizing muons through the decay products of multi-Tev Z' bosons is very challenging for calorimeter system response. Lateral and longitudinal segmentation has important consequences for particle identification and precision measurement, and will be optimized as part of the overalldetector design. As with

resolution and calibration, we place a premium on demonstrated system performance in rate capability, dynamic range, particle identification, and limitation of punch-through.

Table 3.3-1 Calorimeter Requirements

Attribute		Physics Requirements	Specification
Survivability		10^{34} cm^{-2} sec^{-1} year^{-1}	
	EM		<10 Mrad
	HAD		<1 Mrad
	Forward		<3 Grad
Dynamic Range			
	EM	Low–50 MeV Shower Tails	10^5
		High–5 TeV Z′	
	HAD	Low–3.5 GeV μ	10^4
		High–15 TeV Jets	
Energy Resolution	EM	$H \rightarrow \gamma\gamma$	$\frac{2\%}{\sqrt{E}} \oplus 0.5\%$ or
			$\frac{7.5\%}{\sqrt{E}} \oplus 0.5\%$
		$\Gamma_{Z'}$	$\frac{15\%}{\sqrt{E}} \oplus 1\%$
	HAD	$Z \rightarrow jj$	$\frac{50\%}{\sqrt{E}} \oplus 2\%$
		Compositeness	$\frac{50\%}{\sqrt{E}} \oplus 2\%$
Time Resolution			
	EM	e, γ, μ	<16 ns
	HAD	jet, μ	<16 ns
Noise			
	EM	e/γ Isolation	$\sum E_T$ <5 GeV in $\Delta R = 0.2$
Depth			
	EM	Resolution	25–30 Xo
	HAD	Punchthrough	12–15 λ
Hermeticity		$H \rightarrow ll\nu\nu$	$\Delta p_T < \nu$ Bkgnd $\eta \rightarrow 5.5$
Segmentation			
	EM	$\Delta x \sim 1$ mm, $\pi \pm/\gamma$ Overlap	$\Delta\eta = \Delta\varphi \leq 0.05$
	HAD	$Z \rightarrow jj$	$\Delta\eta = \Delta\varphi \leq 0.1$
		muon energy correction	

Another important issue is hermeticity. Its specification is set by the magnitude of the missing E_T from neutrinos; the calorimeter must cover out to $|\eta| = 5.5$. Many of the physics signatures relying on ν detection require a hermetic calorimeter throughout this range. While the need for forward calorimetry with $3 < |\eta| < 5.5$ is clear, the forward region presents some formidable rate and radiation problems.

The forward calorimeter has the largest rapidity coverage per unit area and per shower size. It must withstand a radiation dose of ~ 1 Grad/year and measure energies approaching the 20 TeV beam energy. Our calorimetry choice is also guided by the overall requirement to provide fast response time and good energy resolution.

A high resolution preradiator in front of the calorimeter adds considerably to identification and position and angle measurement for electrons and photons. A preradiator determines the point of initiation of an electromagnetic shower within one radiation length in radial position and 0.5 mm in both transverse coordinates. Up to ~ 100 GeV it can discriminate between single γ's and π^0's by observing the origin of both gamma showers from a π^0. This discrimination, calculated to be about a factor of ~ 20 on the basis of beam tests at FNAL, is essential to the trigger for $H \rightarrow \gamma\gamma$ and the elimination of π^0 background. The preradiator measurement of the initiation point of γ induced showers, in conjunction with the shower centroid location from the calorimeter, determines the direction of the γ. This γ "pointing" is essential. (A calorimeter with longitudial segmentation may also provide this "pointing"). A preradiator also unambiguously associates a shower with an interaction point, a feature that is valuable if the calorimeter is slow. By discrimination against charged tracks which deposit very little energy in the preradiator, the π^0 contamination in the electron sample can be reduced by at least a factor of 10 below that achieved by slower-shape or timing cuts in the calorimeter. Contamination of the electron sample by accidental overlap of charged tracks with γ's can be suppressed by detecting the displacement between the charged track and the origin of the shower of the γ. The tagging of b-quark jets by electrons is also enhanced; electron showers are resolvable even when they are comparatively close to the jet axis.

The number of calorimeter technologies for the SSC under development by collaborators on this Expression of Interest is rather large. These technologies, with their main attributes, disadvantages, and R&D programs, are succinctly described in Table 3.3-2. The tabulation displays the breadth of calorimetry experience within the group. No set of technologies immediately emerges as the obvious choice. Therefore we have made no selection in the few weeks since the formation of this collaboration. Nevertheless, a process for narrowing the options to two or three systems by the submission of the LOI has been put into place.

First, an intense review over the next few months will determine whether homogeneous electromagnetic calorimetry is necessary for the physics of this proposal. This decision will drive the R&D program for FY92. The next branch point, completion of the Technical Design Report at the end of FY92, will see the definition of one or two systems for final R&D work in FY93. The primary goal will be the testing of the chosen EM section in front of a hadronic compartment that completely contains a hadronic shower. For the baseline costing exercise in this document, three possible calorimetry configurations have been evaluated. The first consists of a BaF_2 or Liquid Xenon EM section followed by a liquid scintillator hadronic calorimeter read out by wave shifting

fibers. The other two configurations are fully integrated (combined EM and hadronic); one is based on liquid argon and the other on scintillating fiber. Figures 3.3-1, 3.3-2 and 3.3-3 show these systems respectively.

Table 3.3-2 Calorimetry Techniques

TECHNIQUE	ATTRIBUTES	DISADVANTAGES	R&D EFFORTS	REF.
		HOMOGENEOUS ELECTROMAGNETIC		
BaF_2 Crystals	Ultra-high resolution-stochastic term ~ 1.3% Fast – 3 ns peaking tail $<10^{-4}$ after 35 ns	Untested technology Radiation damage unless pure to ppb level Suppression of slow, dominant light-K-Cs-Te Photocathodes necessary Low density high Moliere radius = 2 - 4.7 cm degrades isolation cut Expensive Piping of 220 mm UV light to PM's axial to B-Field Requires external preradiator	Calibration & monitoring Refining materials Photocathodes under development UV prisms	1
Liquid Xenon	3 depth segmentation-angular resolution Very high light production 10^7 γ/GeV Ultra-high resolution-stochastic term ~1% Fast Potential γ/π^0 separation Calibration with α's	Untested technology Expensive Availability- 8 yrs. of U.S. supply Cryogenic dewar Low density high Moliere radius = 2.7-5.6 cm degrades isolation cut VUV Light - 170 nm - reflective wall quality	Large area photodiodes Light attenuation length Wall reflectivity	2

Table 3.3-2 Calorimetry Techniques (cont)

TECHNIQUE	ATTRIBUTES	DISADVANTAGES	R&D EFFORTS	REF.
		EM/HADRONIC		
Silicon	Ultra-high spatial/angular resolution	Very expensive	New production techniques	3
Liquid Argon	Mature technology	Dewar walls, supports etc.-degrade hermeticity	Detailed design	4
	Experience with construction of large systems	Speed/noise tradeoff-isolation cuts		
	Uniform response	Integration time-≥40ns; pileup	Fast shaping preamps	
	10^5 dynamic range	Preamps inside dewar-reliability/maintenance/hardness	Under test	
	Gain = 1	Cryogenic system	Detailed design	
	Simple calibration	Large sampling fraction e/h ~ 1.5	1 mm Pb plate to be tested	
		Positive ion buildup at high luminosity		
EM only:	$7\%/\sqrt{E} \oplus 0.5\%$ resolution for plate geometry	"Accordion" mechanics nontrivial for projective geometry.	Needs detailed design	5
		Large sampling fraction-long Lrad		
Scintillating Fiber	Fast - σ_E and e/π in 16 ns trigger, 32 ns integration time	10 Mrad sensitivity i.e., lives 2 years @ 10^{34} @ η< 3	O_2 influence Rate dependence	6
	Hermetic - no walls/supports/cracks	No intrinsic depth segmentation Short L_{rad} and L_{abs}	Fiber hardening	
	π/e rejection 10^3 via "electronic" segmentation Demonstrated performance		Construction techniques, cost effectiveness	
	Simple construction, modular, inexpensive	Calibration/monitoring	Detailed design	
	Uniform response ~ 0.5% over face			
EM only:	$6\%/\sqrt{E}$ demonstrated (JETSET) resolution for 50% fiber	Compensating 0.5 mm fiber	Under test	7
		Must tilt fibers at 3°		

Table 3.3-2 Calorimetry Techniques (cont)

TECHNIQUE	ATTRIBUTES	DISADVANTAGES	R&D EFFORTS	REF.
		HADRONIC		
Liquid Scintillator- Wavelength-shifting Fiber readout	Fast, 2ns peaking time Easy to replace liquid if radiation damage occurs Fine segmentation 10^5 dynamic range Inexpensive technology Simple modular construction	Leaks Radiation resistance of fibers (> 10 Mrad) New, untested light collection technology	Leak proof design Improves radiation resistance of fibers Demonstration prototypes and beam tests Chemical compatibility of liquid fiber	9
Scintillator Plates Wavelength-shifting Fiber readout	Similar to liquid scintillator, but not replaceable	10-Mrad sensitivity = 2 years @ 10^{34} @ $\eta = 3$ Production technique not yet established Untested light collection technology	Improve radiation resistance of fibers and scintillator Demonstration prototypes and beam tests	8
		FORWARD CALORIMETRY		
Liquid scintillator capillaries	Fast Hermetic Good resolution Inexpensive Uniform response Compensating Small Moliere radius in tungsten version Safe	Circulate and filter for > 10 Mrad dosage Not proven in a large experiment Leaks Readout dynamic range	Rad hardness Liquid monitoring and recycling Engineering of leak-proof design Calibration	10
Liquid Argon	See Liquid Argon entry above Small Moliere radius in tungsten version Rad hard			11

Table 3.3-2 Calorimetry Techniques (cont)

TECHNIQUE	ATTRIBUTES	DISADVANTAGES	R&D EFFORTS	REF.
		FORWARD CALORIMETRY (cont.)		
High Pressure Gas	*Faster than liquid Argon* Rad hard Small Moliere radius Inexpensive Robust	e/π not measured Leaks Not proven in a large experiment Untested technology Safety Long term gain stability	Performance Engineering design	12
Warm Liquid - TMS	*Fast* Rad hard Large dynamic range Small Moliere radius - uranium/tungsten Compensated	Purity maintenance to ppb/materials compatibility Calibration unproven Not proven in a large experiment Expensive Electronics embedded in the detector - rad hard Safety-flammability Radiolysis production of gas and long lived isotopes	Test of a prototype Electronics development Complete engineering workup R&D on radiolysis products	13
		PRERADIATOR		
Scintillating Fiber	*High spatial resolution ~ 0.3 mm - can veto π^0's* Inexpensive Matches tower geometry in one dimension	Stereo - ambiguities Readout undeveloped	Light yield improvement Readout systems	14
Silicon Pads/strips	Pad/strip structure - no ghosts or shadowing Projective in 2-D Spatial resolution < 0.5mm Fast (single bunch response) Only 15k readout channels	Specialized readout (3/-4 bits/ch) to be developed Two track resolution 4.5 mm (π^0 veto for <50 GeV at 1m)	Electronics and detector development and testing Demonstration device with readout	15

TECHNIQUE	ATTRIBUTES	DISADVANTAGES	R&D EFFORTS	REF.
		PRERADIATOR (cont.)		
Silicon Drift	<1 mm precision for excellent γ/π^0 separation at $4X_0$ depth	Readout undeveloped Cost unknown	Demonstration device with readout	16

References for Table 3.3-2:

(1) A Precision BaF_2 Crystal Calorimeter for Superconducting Super Collider," Caltech et al, a subsystem R&D proposal submitted to the SSCL, September 1990;

"Hadron Calorimeter in the L3 detector", O. Adriani et al, CERN PPE-90/158;

(2) M. Chen, MITLNS-163, Proceedings of the SSC Berkeley Workshop, A267, 43, (1988)

M. Chen ECFA Workshop at Barcelone, Spain, et al., Sept., CERN 89-10, 1989;

T. Doke et al., Technical Report KMM-SIPD-3, SCH-PL, July 1990;

T. Doke et al., SCH-PL, October 1990;

M. Chen et al, "Liquid Xenon Detector Engineering", Proceedings of the Third International Industrial Symposium of the SSC, Atlanta, March 1991;

(3) R. B. Gray, "The Effect of Gamma Radiation of JFET and Bipolar Transistors With Applications to the SSC", a thesis for the Master of Science degree, the University of Tennessee (1990);

A. Gola, et al., "Fast Front-End Electronics for Experiments using Silicon Calorimeters at SSC/LHC Colliders:, *Nucl. Inst. and Meth. in Phys. Res.*, A292 (1990) 648-656;

R. A. Todd, "Preamplifier Design for Silicon Calorimetry using Harris Semiconductor Bipolar VHFP Process", presented to Silicon Electromagnetic Calorimetry Collaboration, The University of Tennessee, Knoxville, TN, June 9-10, 1990;

C. L. Britton, Jr., R. A. Todd, M. L. Bauer, E. J. Kennedy and W. M. Bugg, "Bipolar Monolithic Preamplifiers for SSC Silicon Calorimetry", Symposium on SSC Detector Research, Fort Worth, TX, October 15, 1990;

E. J. Kennedy, et al., "Radiation Effects on JFETS, MOSFETS, and Bipolar Transistors as Related to SSC Circuit Design", Presented at 1990 Symposium on Detector Research and Development for the SSC, Fort Worth, TX, Oct. 15-18, 1990;

R. A. Todd, M. L. Bauer, C. L. Britton, Jr., E. J. Kennedy, A. L. Wintenberg, "Bipolar and CMOS ADIC Design for Large Physics Experiments," Conference on Electronics for Future Colliders, Le Croy Corporation, Chestnut Ridge, NY, May 22, 1991;

C. L. Britton, E. J. Kennedy, W. M. Bugg, "A Bipolar Monolithic Preamplifier for High Capacitance SSC SIlicon Calorimetry", *IEEE Trans. Nucl. Sci.*, in publication; Proceedings of "International Workshop on Radiation Damage in Silicon" Oak Ridge National Laboratory, Feb. 19-21, 1991;

S. Berridge, et al "Beam Test of the SLD Silicon-Tungsten Luminosity Monitor" *IEEE Trans. Nuc. Sci.* 37, 1191 (1990);

(4) "Proposal for R&D for a Liquid Argon Calorimeter for the SSC", G.S. Abrams et al., (Subsystem Proposal) 1989, 1990,

"Hadronic and Electromagnetic Liquid Argon LHC Prototype Calorimeter with Pointing Geometry," B. Aubert et al., CERN/DRDC/91-21 (1991);

(5) *Nucl. Instr. and Meth.*, H. Burkhard et al., A268, 116 (1988);

(6) "New results in scintillating fiber calorimetry," Contributed to the Proceedings of the Tucson SSC Workshop, February, 1990. Results of prototype studies for a spaghetti calorimeter, *Nucl. Inst. Meth.* A294, 193, 1990;

Status of scintillating fiber calorimetry, "Contributed to the Proceedings of the Division of Particles and Fields Conference, Houston, TX, January, 1990;

"The High Resolution Spaghetti Hadron Calorimeter," P. Jenni, P. Sonderegger, H.P. Paar, and R. Wigmans, NIKHEF report NIKHEF-H/87-7 (1987);

"Scintillating Fibre Calorimetry at the LHC," D. Acosta et al., CERN report CERN/DRDC/90-23 DRDC/P 1 (1990);}

"A Novel Way of Electron Identification in Calorimeters," R. Desalvo et al., *Nucl. Inst. Meth.* A279, 467 (1989);

"Results of Prototype Studies for a Spaghetti Calorimeter," D. Acosta et al., *Nucl. Inst. Meth.* A294, 193 (1990);

"Electron-Pion Discrimination with a Scintillating Fiber Calorimeter," D. Acosta et al., *Nucl. Inst. Meth.* A302, 36 (1991);

"Localizing Particles Showering in a Spaghetti Calorimeter," D. Acosta et al., CERN preprint CERN-PPE/91-11 (1991); Submitted to *Nucl. Inst. Meth.*

"Electron, Pion, and Multiparticle Detection with a Spaghetti Calorimeter," D. Acosta et al., CERN preprint CERN-PPE/91-85 (1991). Submitted to *Nucl. Inst. Meth*;

"Effects of Radiation Damage on Scintillating Fiber Calorimetry," D. Acosta et al., CERN preprint CERN-PPE/91-45 (1991). Submitted to *Nucl. Inst. Meth*;

"On Muon Production and Other Leakage Aspects of Pion Absorption in a Spaghetti Calorimeter," D. Acosta et al., Submitted to *Nucl. Inst. Meth*;

"Status of Scintillating Fiber Calorimetry," H.P. Paar. Proceedings of the ECFA Study Week on Instrumentation Technology for High-Luminosity Hadron Colliders, p. 207, Barcelona, Spain, 14-21 September 1989, edited by E. Fernandez and G. Jarlskog;

"Beam Tests of Large Lead and Scintillating FiberPrototype Calorimeters," H.P. Paar. Proceedings of the Symposium on Detector Research and Development for the Superconducting Super Collider, Ft. Worth, Texas, October 15-18, 1990;

"Review of Electron Pion Separation Methods Using Scintillating Fiber Calorimetry," M. Sivertz, Proceedings of the International Conference on Calorimetry in High Energy Physics, FNAL, October, 1990;

"A Dichromatic Scintillating Fiber Calorimeter," C. Bromberg et al, Proceedings of the Symposium on Detector R&D for the SSC, Fort Worth, October 1990;

"Cast Lead-Eutectic Solid and Liquid Scintillating Fiber Shower Calorimeters," T. Coan et al, Proceedings of the Symposium on Detector R&D for the SSC, Fort Worth, October 1990;

"The Manufacturing Engineering of a Hermetic Cast Fiber Calorimeter," T. Coan et al, Proceedings of the Symposium on Detector R&D for the SSC, Fort Worth, October 1990;

"Properties of Photodetectors for Scintillating Calorimeters at the SSC," D. Winn et al, Proceedings of the Symposium on Detector R&D for the SSC, Fort Worth, October 1990;

"Search for the Intermediate Mass Higgs," EMPACT/TEXAS Note 340 (1990);

"Beam Tests of a 13 Ton Lead and Scintillating Fiber Calorimeter," Proceedings of the Symposium on Detector R&D for the SSC, Fort Worth, October 1990;

"Scintillating Calorimetry for the SSC: A Progress Report and Request for Funds from the SSCintCal Collaboration," submitted, September 1990;

(7) *Nucl. Inst. and Meth.*, D.W. Hertzog et al., A294,446 (1990);

(8) See L* LOI.

(9) "Expression of Interest to the Superconducting Super Collider Laboratory by the L* Collaboration", May, 1990, pp 52 - 53;

(10) "Liquid Scintillator Calorimetry"- A Research and Development Proposal submitted to the Superconducting Super Collider Laboratory by members of the L* Collaboration, September, 1990 and references therein;

Letter of Intent to the Superconducting Super Collider by the L* Collaboration", November 1990, pp 21 - 24;

"Liquid Scintillator Used as an Active Medium in a Sampling Calorimeter," Yu. Kamyshkov, in Proceedings of the Symposium on Detector Research and Development for the Superconducting Super Collider, Fort Worth, October 15-18, 1990;

"Proposal to Investigate a Liquid Scintillator Alternative to Scintillating Fiber Calorimetry for the SSC," R.C.Webb et al., Generic SSC R &D Proposal submitted to the DOE, September, 1989;

"CAPCAL - Forward Calorimeter for EMPACT," Y. Pischalnikov et al., EMPACT/TEXAS Note 296(1990);

(11) "An Engineering Design of a Hermetic Liquid Argon Calorimeter for the SSC," T. Adams et al., submitted to *Nucl. Inst. and Meth.*(1990);

(12) "Forward Gas Calorimeter for EMPACT/TEXAS", I. Kotov and N. Fediakyn, EMPACT/TEXAS Note 295 (1990);

(13) D. DiBitonto et al., *Nucl. Inst. and Meth.*, A279, 100 (1989).

(14) "Pre-Radiators for Electron Identification," P. Cushman et al., Proceedings of the Symposium on Detector R&D for the SSC, Fort Worth, submitted to *Nucl. Inst. and Meth.*, (1991);

"Results from the Fermilab Pre-Radiator Beam Tests," R. Rusacket al., Proceedings of the Symposium on Detector R&D for the SSC, Fort Worth, October 1990;

(15) D. M. Lee, W. W. Kinnison and W. B. Wilson, LANL internal report, October, 1990;

"Low Cost, Large Area Silicon Diodes for Calorimetry," R. Korde et al., Proceedings of the Symposium on Detector R&D for the SSC, Fort Worth, October 1990:

"Neutron Flux Suppression with Polyethylene Moderation in the EMPACT Silicon EM Calorimeter," K. Furuno et al., Proceedings of the Symposium on Detector R&D for the SSC, Fort Worth, October 1990;

"Beam Test of the SLD Silicon-Tungsten Luminosity Monitor," S.C. Berridge et al., *IEEE Trans. Nucl. Sci.* 37, 1191 (1990);

CERN/DRDC/90-27, D.J. Munday et al., 2 August, 1990;

"Silicon Preconverter for the Barrel Calorimeter of EMPACT/TEXAS," G.Bashindzhagyan, EMPACT/TEXAS Note 298 (1990);

"The Effect of a Pre-radiator on the Electromagnetic Energy Resolution for the EMPACT/TEXAS Liquid Argon Calorimeter," K. Pitts and J. Brau, EMPACT/TEXAS Note 341 (1990);

(16) *Nucl. Inst. and Meth.*, E. Gatti and P. Rehak, A225, 608 (1984);

Nucl. Inst. and Meth., P. Rehak et al., A248 367 (1986);

"SSC Subsystem Proposal to Develop Track and Vertex Detectors Based on Silicon Drift Devices," W. Chen et al., (1989, 1990);

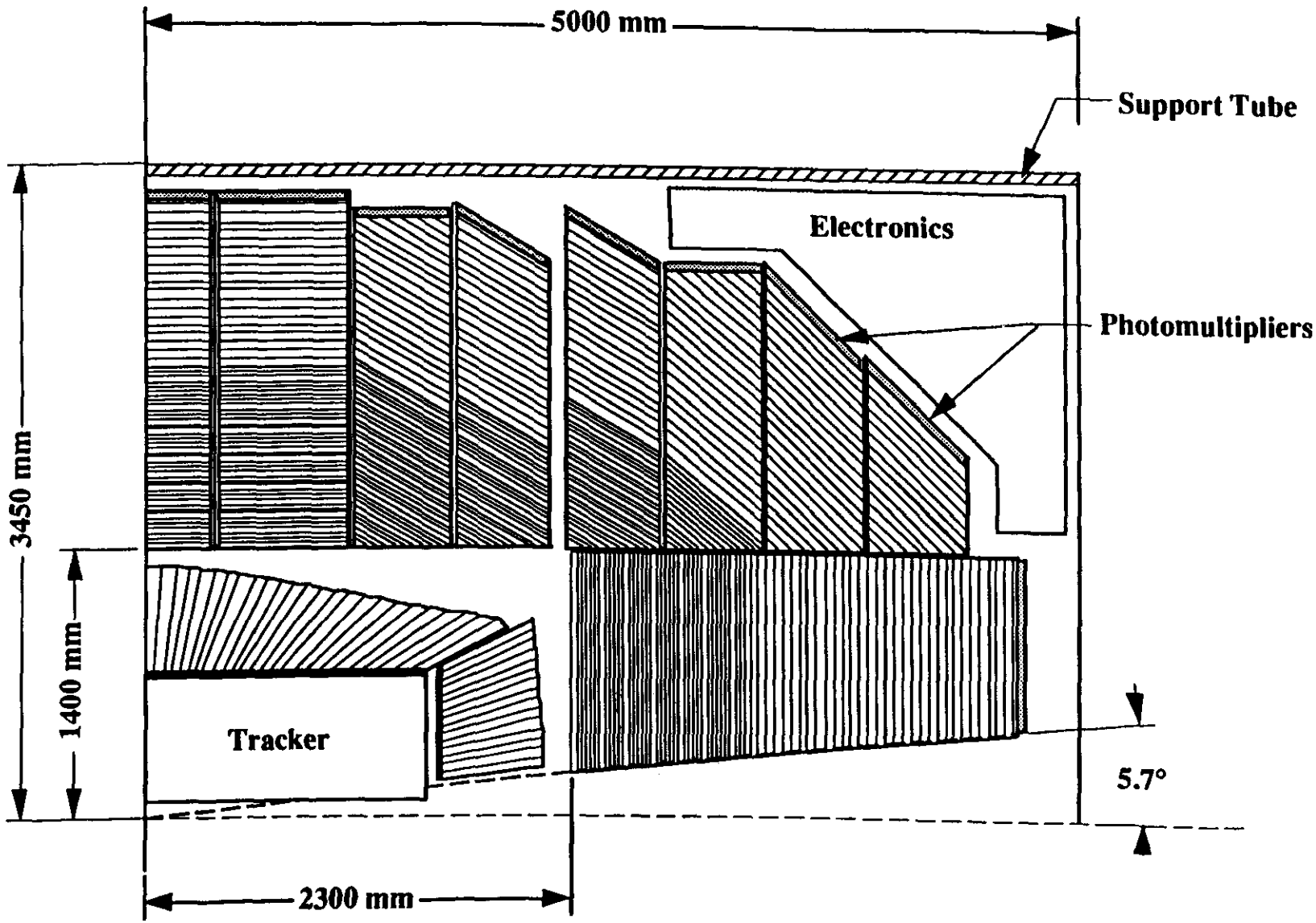

Figure 3.3-1 **Liquid Scintillator Hadron Calorimeter**
Barium Fluoride EM Calorimeter

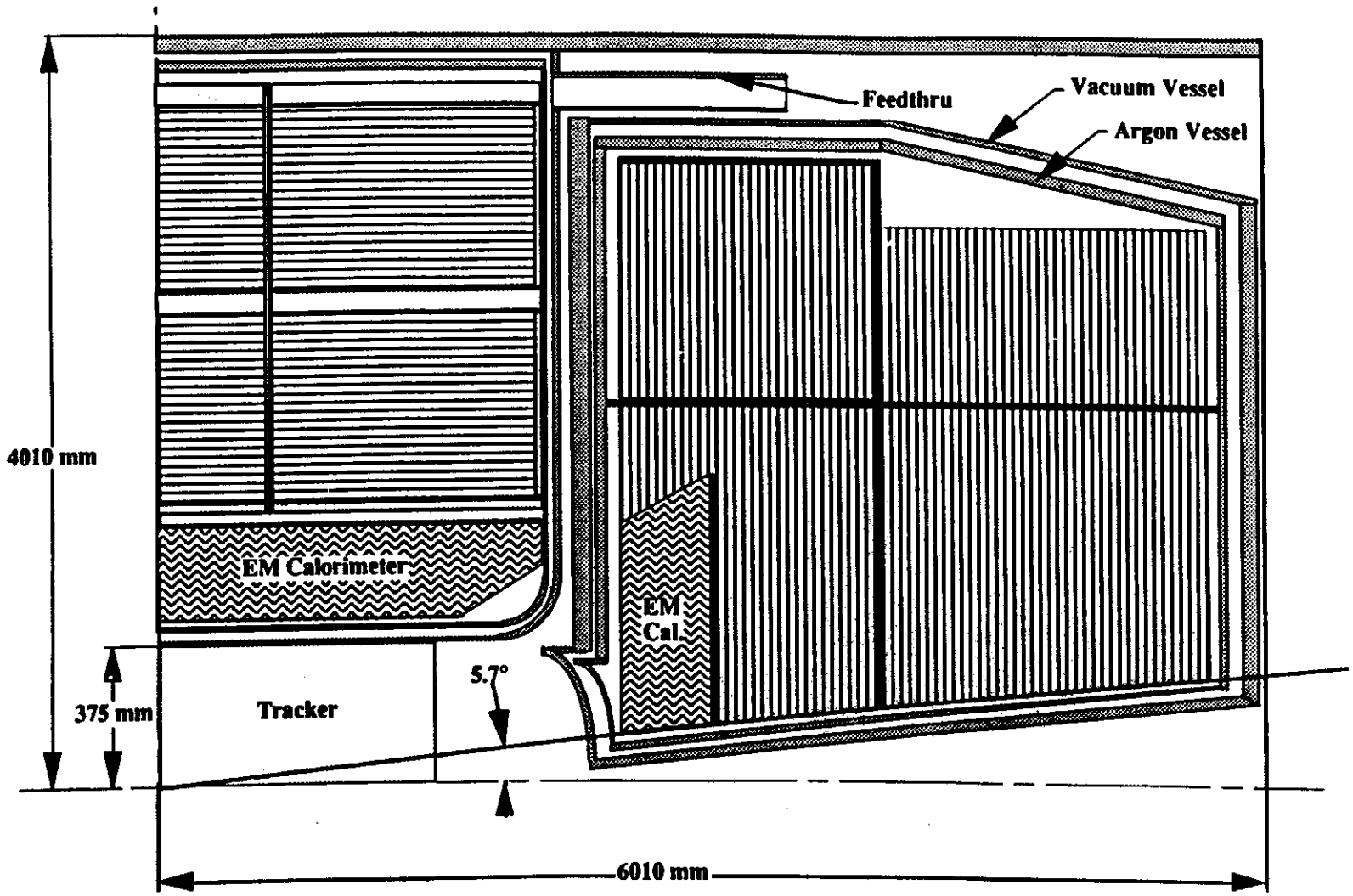

Figure 3.3-2 Liquid Argon Calorimeter

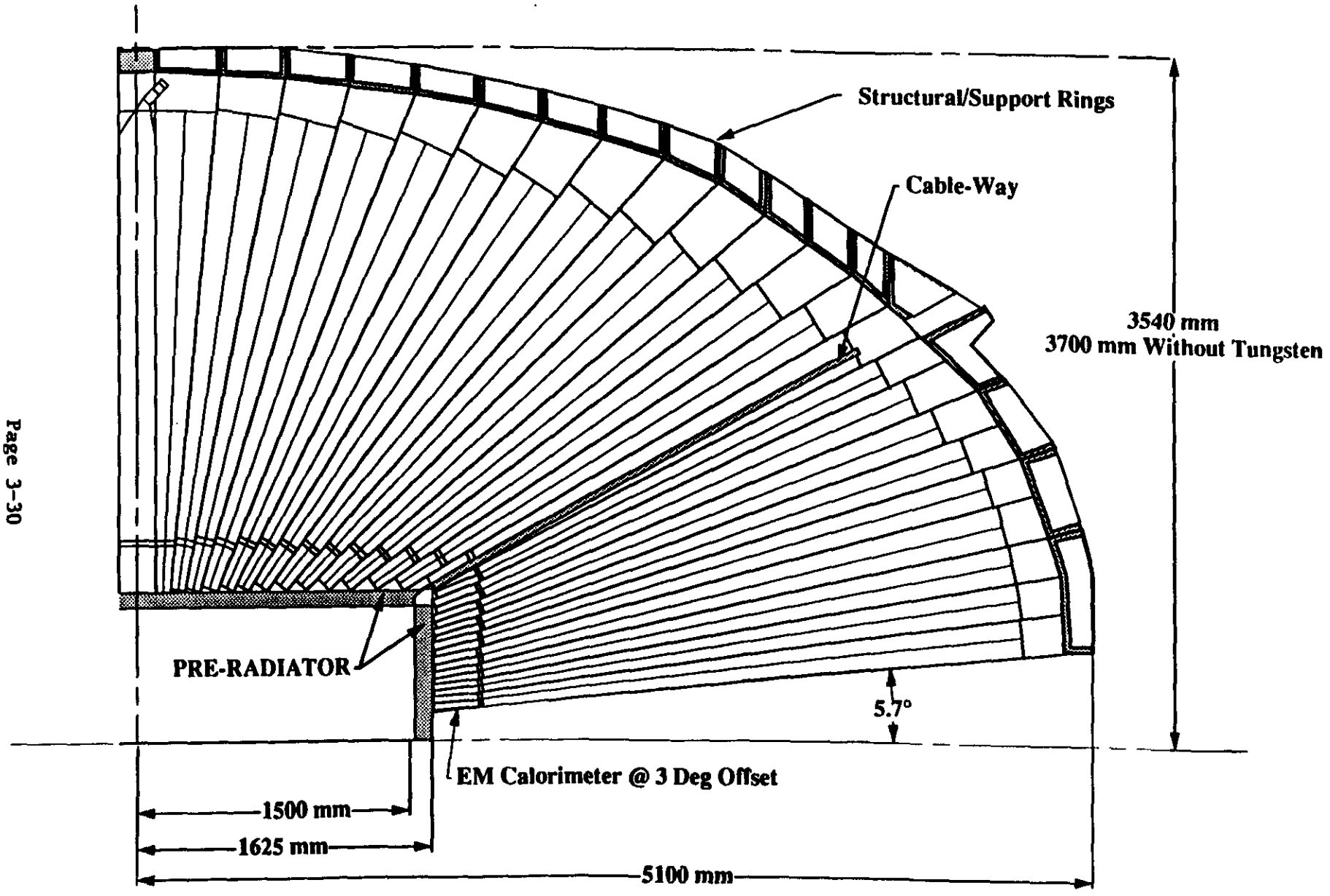

Figure 3.3-3 Spaghetti Calorimeter

3.4 Tracking

The baseline central tracker makes use of an inner silicon microstrip subsystem, and an outer straw tube and scintillating fiber subsystem. Similar to the design of the L* central tracker[1], this baseline has been altered by several significant simplifications. Our goal has been to maintain the basic performance of the L* design, but to take advantage of possible reductions in cost. We are also considering several technologies which have been recently suggested as design options.

Figure 3.4-1 is an elevation view which displays the central tracker layout. Figure 3.4-2 displays the tracker end view. The total radial lever arm for momentum measurements is the same as the L* case, with the innermost silicon detectors at 12.75 cm and the outermost scintillating fibers at 74.5 cm. Thus, the momentum resolution is not significantly changed. The tracker length is nominally the same, as well. However, several significant design simplifications have been made to reduce cost. The primary changes are:

- The outer silicon subsystem diameter has been reduced from 90 cm to 70 cm, maintaining the same number of silicon microstrip layers, but reducing the total area instrumented by silicon.
- The inner radial position of the forward silicon planes has been increased to 12.75 cm, from 10 cm, and the most forward planes have been tapered back to larger inner radii. This change provides more efficient coverage of the detector acceptance, and reflects results of recent simulations of the radiation doses in the forward direction.
- The reduction in the outer silicon subsystem radius, and the tapering of the forward planes permits us to reduce, from two to one, the number of detector wafers required to span the radial thickness of each of the forward planes. This reduces the number of microstrip readout channels sharply, lowering the cost with no significant decrease in performance.
- The three straw tube superlayers have 16 tube layers, reduced from 20 in the L* design. This results in a modest loss of pattern recognition efficiency which is being carefully studied. In previous studies it was found that 12 layers were required to resolve left-right ambiguities, providing confidence that 16 layers is adequate.
- Optoelectronic readout of the straw tube system has been simplified by multiplexing the straws in groups of 8.

3.4.1 Physics Performance

The principal functions of the central tracker are:

- Determination of the event vertex to separate pileup events from real events;
- Separation of photons from electrons;
- Measurement of charged particle multiplicity;
- Identification of secondary vertices of long-lived particles;
- Measurement of charged particle momenta and charge sign to identify leptons, photons and hadronic jets.

The general features and performance of the central tracker, except insofar as noted above, are the same as those presented in the L* LOI (pages 38-39).

3.4.2 Additional Options

The use of silicon pixel detectors, silicon drift detectors, and interpolating resistive pad chambers have been suggested as possible substitute technological options to the baseline design.

Pixels offer the possibility of point measurement, as opposed to projective measurement with silicon microstrips. They have been the subject of an SSCL supported subsystem R&D program, though this technology is less mature than silicon microstrips.

Similarly, silicon drift detectors have been suggested as nonprojective silicon detectors which offer the promise of several micron precision with orders of magnitude fewer readout channels[2]. They provide a signal pipeline several microseconds long within the very volume of the detector. They permit reduced power consumption within the detector volume, mitigating the severe cooling challenge already under study in the silicon microstrip R&D program. Solutions to the precision support of silicon microstrips are only indirectly applicable to the silicon drift detector option, so that the program of mechanical studies should be extended for this option. These devices have never been produced on a commercial scale, nor have they been studied for radiation resistance in an SSC environment. This may increase the vulnerability to signal loss due to radiation induced charge trapping along the drift path. With an aggressive program of radiation damage studies, commercialization of the devices, and development of precision radiation resistant support and cooling technology, these detectors may provide an attractive option for the central tracker inner layers.

Gas proportional chambers with interpolating segmented cathodes[3] may provide a nonprojective solution for robust outer tracker layers. These devices provide a space point measurement of the track position which can significantly simplify the pattern recognition problem and eliminate the need for many layers of straws or fibers. The high degree of segmentation and parallel readout make these chambers attractive for operation in high rate, high multiplicity environments. The information they provide can be used in the on-line trigger. Studies of chamber gases, radiation resistance, precision mechanical design options, and low cost analog readout electronics with radiation resistant components are needed to advance this option to comparable developmental maturity as that reached in the straw tube and scintillating fiber R&D programs.

3.4.3 Baseline R&D Issues

In order to advance upon the achievements of the relevant major subsystems R&D programs for central tracking, studies of the remaining detector specific issues are required. During FY1992, the demonstration of stable mechanical prototypes of single-sided microstrip bridges, bonding of single-sided wafers back-to-back, prototype optoelectronic modulators with sufficient radiation resistance and of extremely compact form are required for the silicon subsystem design to be advanced. Stable mechanical straw and fiber subassemblies must be fabricated and tested. Endplate solutions should be prototyped. Optical mating of the scintillating fibers, light pipe fibers and multichannel photomultipliers should be demonstrated. The photomultipliers produced for this application by industry should be tested. VLPC's must become available for testing and evaluation

as an alternate readout for fibers. Assembly, placement and alignment technologies must be demonstrated.

We propose to carry out the necessary R&D activities for the baseline and alternate technologies so that a downselection can be made in late FY1992 to define our central tracker configuration for a technical design report.

Fig 3.4-1 Elevation view of the baseline central tracker

Fig 3.4-2 End view of the baseline central tracker

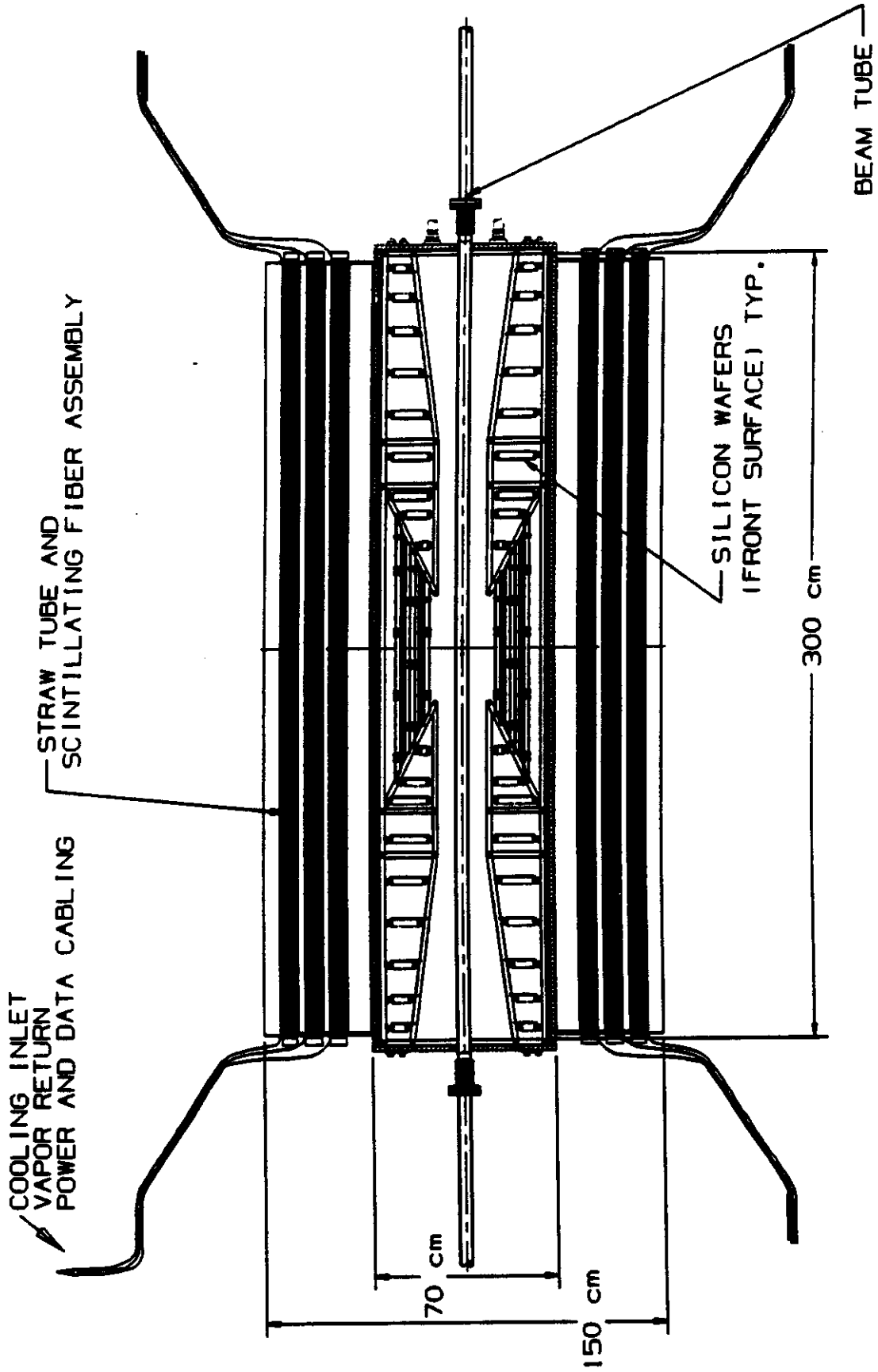
BEAM TUBE
SILICON WAFERS
(FRONT SURFACE) TYP.
300 cm
STRAW TUBE AND
SCINTILLATING FIBER ASSEMBLY
COOLING INLET
VAPOR RETURN
POWER AND DATA CABLING
70 cm
150 cm

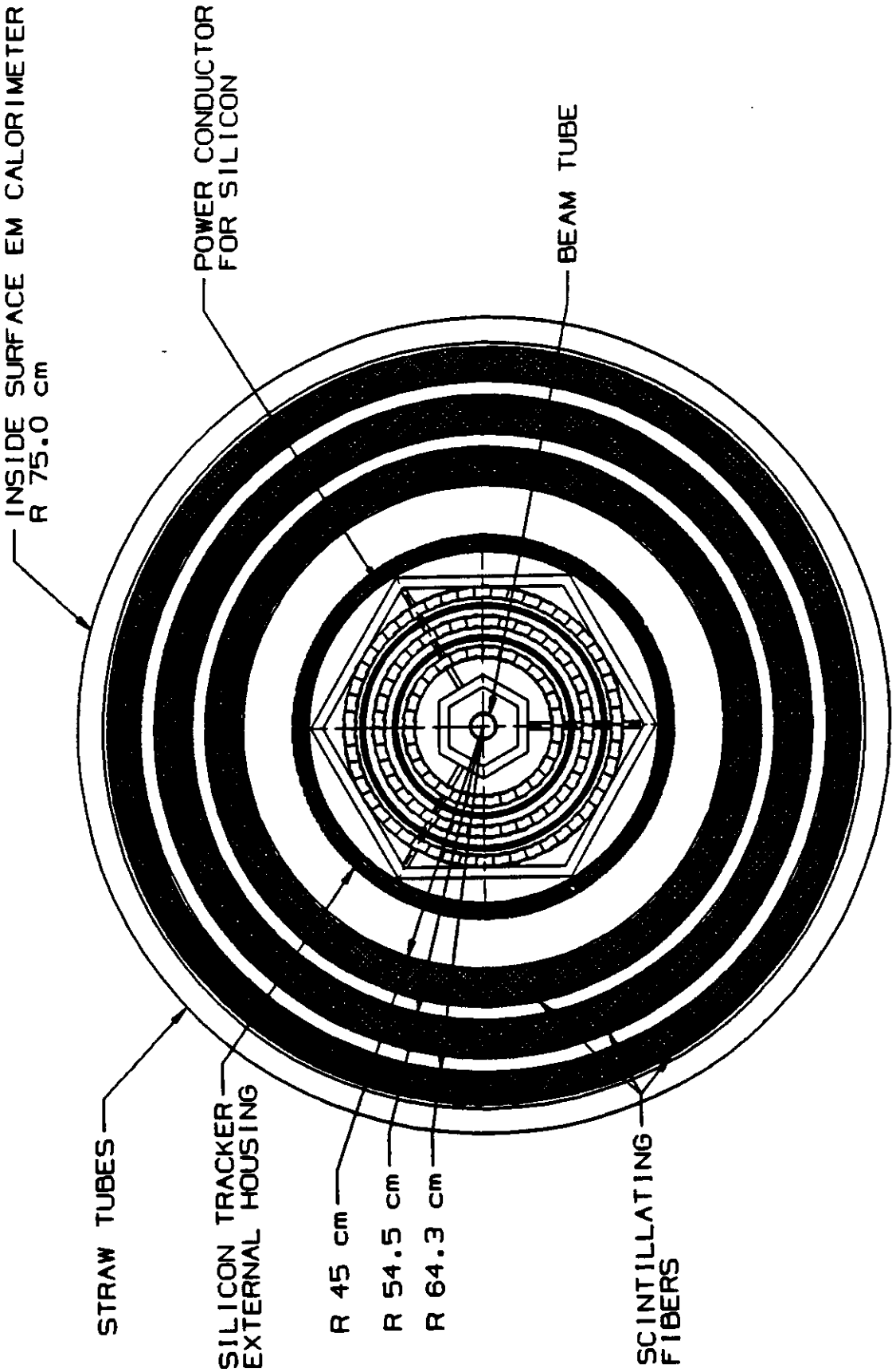
INSIDE SURFACE EM CALORIMETER
R 75.0 cm
POWER CONDUCTOR
FOR SILICON
BEAM TUBE
STRAW TUBES
SILICON TRACKER
EXTERNAL HOUSING
R 45 cm
R 54.5 cm
R 64.3 cm
SCINTILLATING
FIBERS

REFERENCES

[1] L* Letter of Intent

[2] E. Gatti and P. Rehak, *Nucl. Instr. and Meth.*, vol. 225, 608 (1984).

[3] B. Yu et al., *IEEE Transactions in Nuclear Science*, Vol. 38, No. 2, April 1991, Part I, pp 454-460

3.5. Triggering and Data Acquisition

A trigger and data acquisition (DAQ) group met for the first time at the June 11–13 2nd Detector Workshop. Several institutions (BNL, Boston, Columbia, LANL, LLNL, Michigan State, Mississippi, ORNL, Princeton, SSCL, Temple, and Yale) expressed an interest in this aspect of the detector design.

There has not been time to specify a trigger/DAQ design in any detail. Initial studies, however, will assume a conventional three-level trigger [1,2]. In that approach Level 1 is assumed to be synchronous (i.e. a decision occurs a fixed number of bunch crossings after the interaction); Level 2 is asynchronous, but monotonic (decision times vary, but occur in the same order as the events survived Level 1); and Level 3 consists of an event builder plus a massively parallel "processor ranch".

At the workshop we identified a number of issues in need of immediate study. These include:

- Definition of a trigger and DAQ architecture. This work will depend on the results of the studies outlined below.
- Level 1 Monte Carlo studies. We will develop a table of Level 1 trigger rates as a function of p_T and the number of e's, μ's, γs, and/or jets required. The required calculations will be performed using realistic detector geometries and will include as much of the relevant detector-response physics as possible. Where more than one detector option exists, ease-of-triggering considerations will provide input to the selection process.
- Level 1 muon trigger development. This is especially challenging since the typical drift times for muon detectors are too long to permit straightforward tagging of the bunch crossing in the first level trigger. Moreover, unlike calorimeter triggers, where raising the energy threshold provides a solution of last resort, a muon trigger can malfunction in such a way that high p_T (very stiff) tracks and low-to-moderate p_T (fairly stiff) tracks are rendered indistinguishable. One possibility for the muon trigger is the resistive plate chamber[3] (RPC), which offers the possibility of suitable spatial segmentation in combination with good timing resolution. The choice of muon trigger will likely depend on the choice of muon detector; and once again ease-of-triggering will be a criterion in the design of the muon system.
- Level 2 triggers. Study is needed to develop strategies for refined identification of leptons, photons, and jets. The Level 2 electron trigger is of particular importance since it may have an impact on the design of the calorimeter and the central tracker. Whatever the choice of detector, extracting and rapidly processing the relevant signals presents an interesting technical challenge.
- Front-end electronics. Although impressive progress has been made on techniques for the Level 1 pipeline delay[4], the importance of this problem calls for additional effort. We intend to consider fully digital and electro-optic modulator[5,6] schemes as well as switched-capacitor arrays.

- DAQ and simulation. As the design of the trigger and DAQ system evolves, extensive simulation efforts will be needed to detect dataflow bottlenecks and other design flaws at an early stage in the system's development.

We plan to address the above issues through a vigorous R&D effort. To ensure that financial and manpower resources are optimally applied, we will meet as a group in the very near future. At that time we will review the list of tasks and the lines of research proposed by the interested institutions.

REFERENCES

1 C. Blocker et al., "Front End Electronics Development for SSC Detectors", SSC Subsystem R&D progress report & renewal request. November 1990

2 R. Steiner et al., EMPACT Expression of Interest, pgs 5-1 through 5-9, May 1990.

3 R. Santonico and R. Cardarelli, *Nucl. Instr. & Meth.* 187 (1981), 377. M. Bertino et al., *Nucl. Instr. & Meth.* A283 (1989), 654. M. Anelli et al., *Nucl. Instr. and Meth.* A300 (1991), 572.

4 G.W. Foster et al., "Development of a Compensating Scintillator Plate Calorimeter System for the SSC", SSC Subsystem R&D progress report & renewal request, Appendix VI, November 1990.

5 T. Tsang et al., Brookhaven Preprint # 45416, November 1990.

6 E. Ables et al., Lawrence Livermore preprint # UCRL-JC-105645, to be submitted to *Nucl. Instr. & Meth.*, May 1991.

4.0 DETECTOR HALL AND SURFACE FACILITIES

In developing our baseline design and in considering variations, we have paid close attention to the constraints imposed by the design possibilities for the detector hall. The underground hall at IR-1 currently under study by the SSCL, and by the architect/engineer PB/MK[1] appears to be consistent with all currently conceived detector variations. Furthermore, use of the current hall design avoids the schedule delay entailed in any major redesign of the hall.

Figure 4-1 shows the isometric view of the hall concept. Plan, elevation and end views are shown in Figures 4-2 through 4-4 respectively, The architect/engineer proposes use of the caverning technique for the underground construction at IR-1. This alternative is preferred over the cut-and-cover technique due to the local geology. It permits a maximum rock-to rock transverse width of 28m and a finished wall-to-wall clearance of 26.2m. For both the double-coil L* type superconducting magnet, and our baseline single coil design, this clearance is adequate. There may be a modest schedule advantage associated with this construction technique.

The single shaft shown for major installation can accommodate all proposed subsystems and large components. The hall length is adequate for installation and maintenance activities, and provides clearance for opening forward magnet doors, withdrawal of magnet end plugs, placement of forward muon and calorimetry modules, or placement of muon systems external to the magnet. Placement of emergency sumps and cryogenics facilities required for liquid argon calorimeter systems can be included in this design.

Due to the serial nature of the underground construction operations, the design of the hall must proceed in an uninterrupted manner lest the occupancy date be delayed. This would result in a shortening of the time available for detector installation. Design of the hall and detector should be carried out in parallel with continuous and effective communication maintained between the design teams. Indeed, review of the technical design report for the second detector is a major milestone in the underground hall construction schedule.

Figure 4-5 shows the conceptual layout of the surface facilities proposed at IR-1. The large halls are adequate to accommodate construction of the magnet designs under consideration, the muon chambers and modules, and the calorimeters, including the liquid argon option.

REFERENCES

[1] Conceptual Design of Detector Hall Finish Systems Phase B-1, The PB/MK Team, 15 May 1991

Fig 4.1 Isometric view of the second detector hall concept at IR-1

Fig 4.2 Plan view of the hall concept

Fig 4.3 Elevation view of the hall concept

Fig 4.4 End view of the hall concept

Fig 4.5 Layout of the surface facilities at the IR-1 location

ISO VIEW

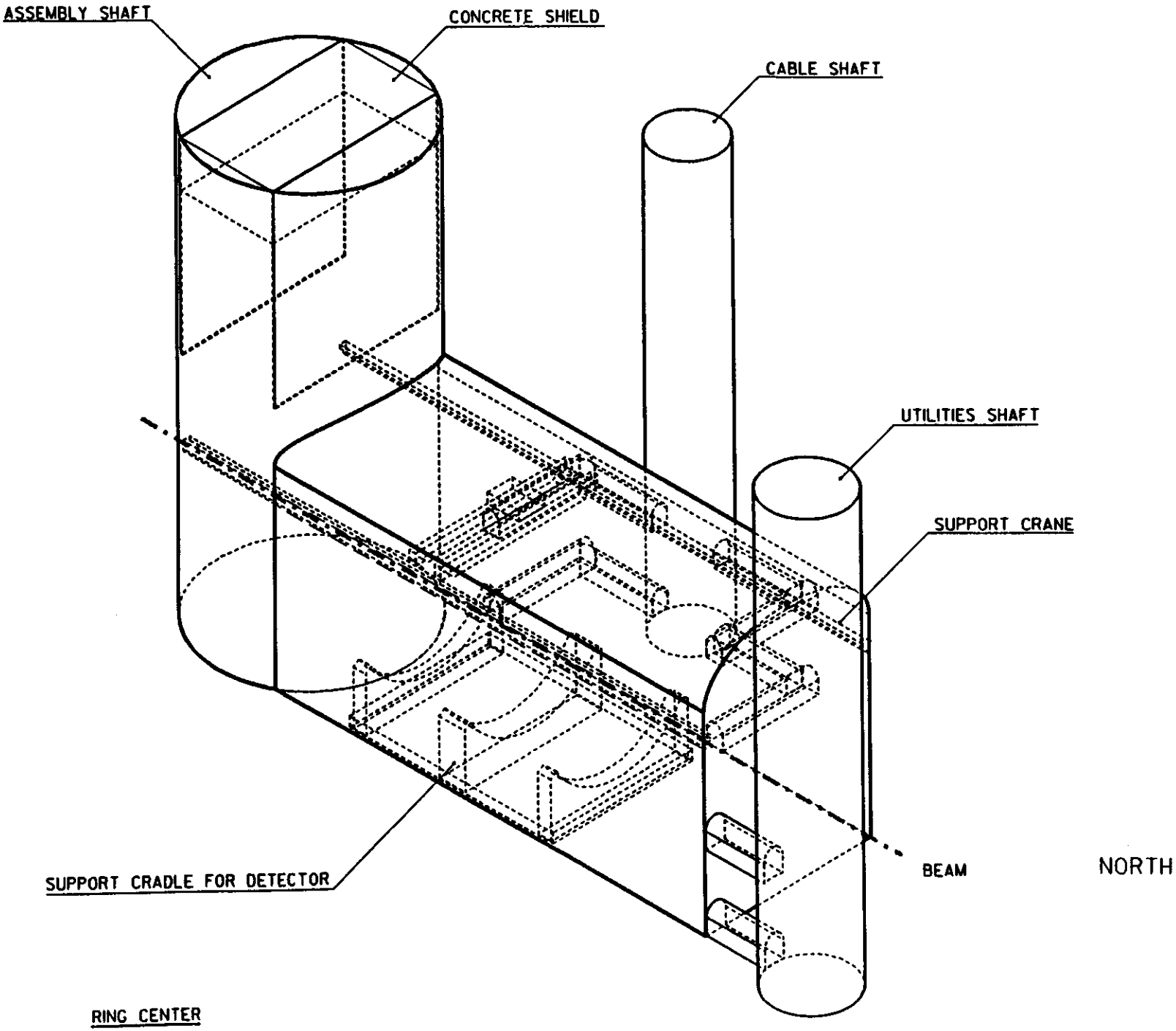
ASSEMBLY SHAFT
CONCRETE SHIELD
CABLE SHAFT
UTILITIES SHAFT
SUPPORT CRANE
SUPPORT CRADLE FOR DETECTOR
BEAM
NORTH
RING CENTER

TOP VIEW

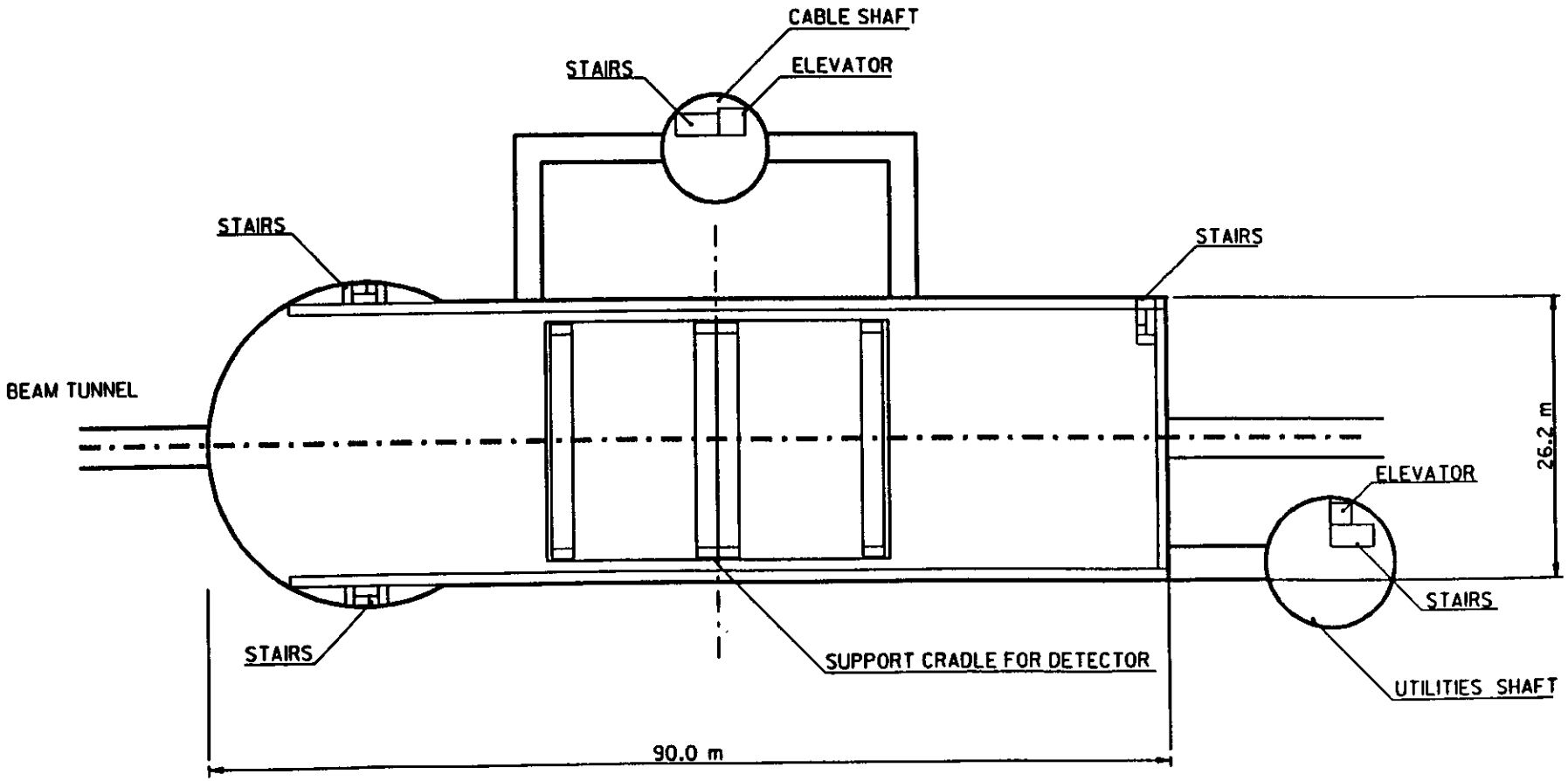

CENTER

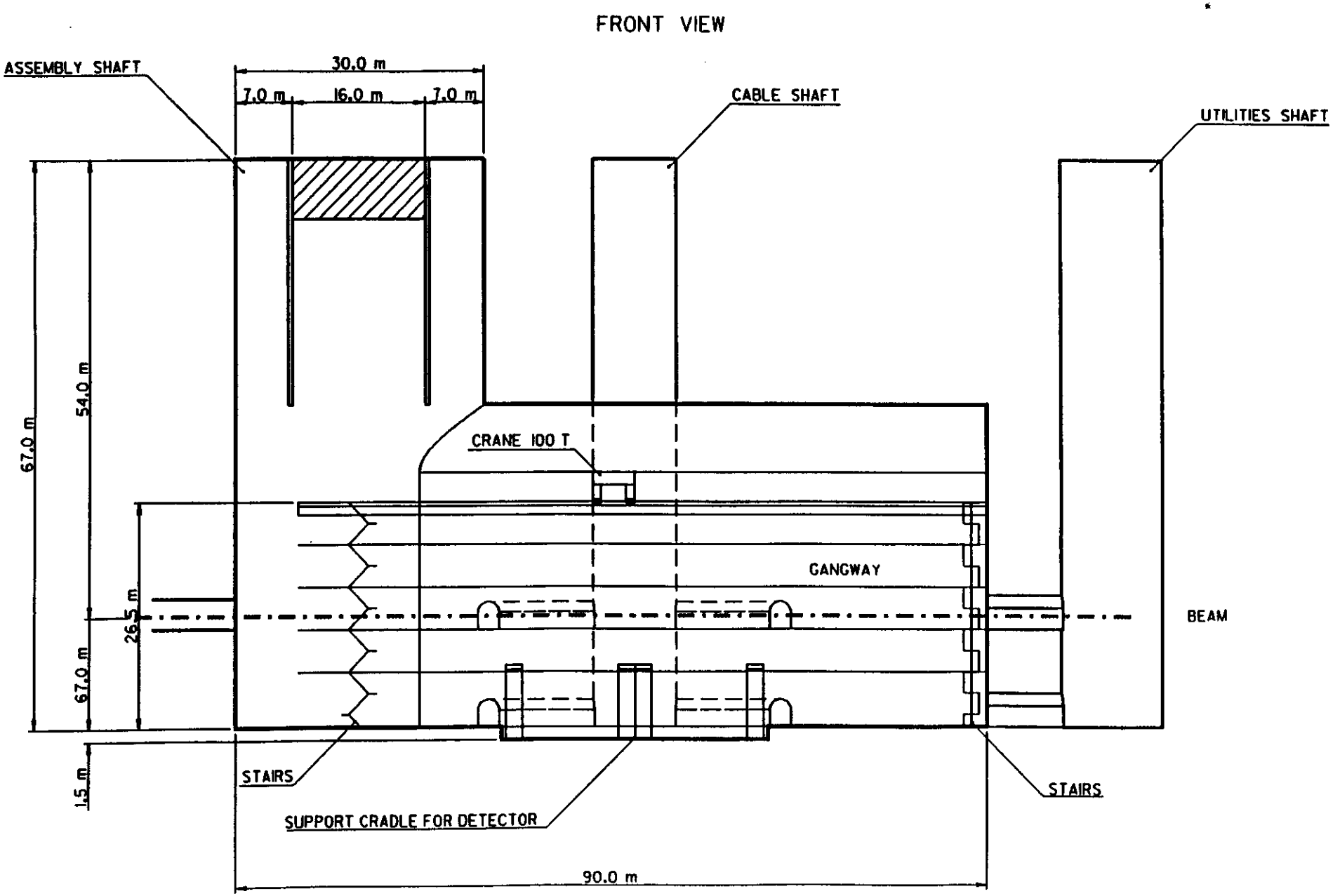
FRONT VIEW
ASSEMBLY SHAFT
30.0 m
7.0 m
16.0 m
7.0 m
CABLE SHAFT
UTILITIES SHAFT
67.0 m
54.0 m
CRANE 100 T
GANGWAY
26.5 m
BEAM
67.0 m
1.5 m
STAIRS
STAIRS
SUPPORT CRADLE FOR DETECTOR
90.0 m

RIGHT VIEW

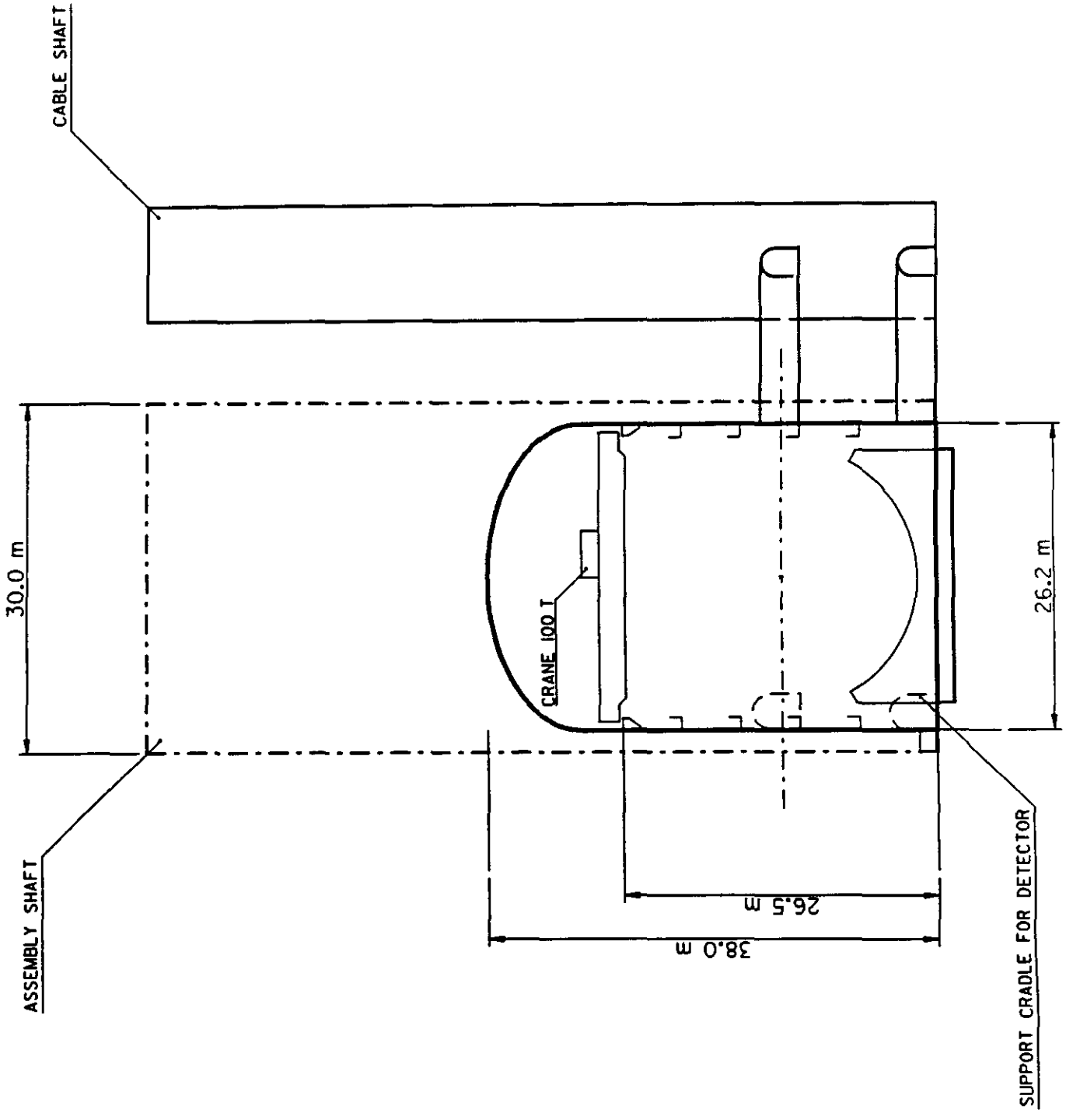
CABLE SHAFT
30.0 m
CRANE 100 T
26.2 m
ASSEMBLY SHAFT
26.5 m
38.0 m
SUPPORT CRADLE FOR DETECTOR

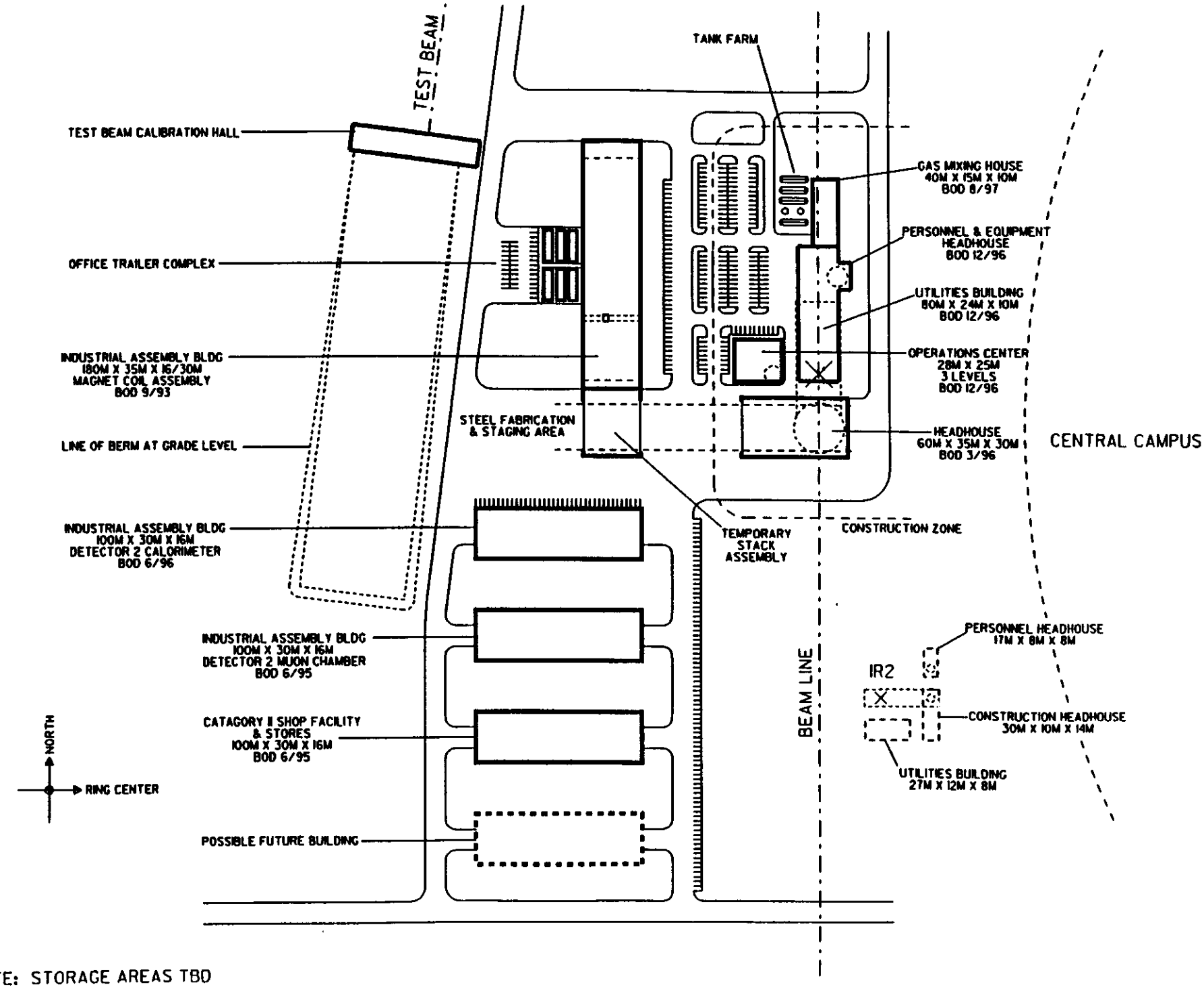

NOTE: STORAGE AREAS TBD

5.0 DESIGNING TO COST AND SCHEDULE

We are committed to achieving our principal physics goals within the cost and schedule constraints. This can be achieved by being selective in our physics goals, paying close attention to staging options, and exercising discipline at every stage of our design process. No option can be pursued without cognizance of the cost and schedule impacts.

We have carried out a study in order to establish the plausibility of a design which meets our physics goals within the cost guidelines previously stated by the Program Advisory Committee, namely, a total cost less than $500 million. This exercise has been carried out over the limited time period during which we formed the new collaboration. The work in progress has been summarized in presentations at the Pasadena (May 16–17) and SSCL (June 11–13) meetings, and it should be viewed as a preliminary study and as a guide to future detailed studies of the many options which are currently being considered by the collaboration.

In order to maintain complementary physics goals to those of a general purpose detector, and to design to cost and schedule, we have made use of the architecture of the L* design, and the design and costing efforts carried out for the L* Letter of Intent and for several EMPACT and TEXAS subdetectors. We have built upon the extensive work of the physics and engineering teams from those collaborations and the work described here has been adapted for this study by the original team members. Thus, our design toolkit is the open solenoidal magnetic geometry of L* and the subdetectors of L*, EMPACT, and TEXAS.

In order to maintain the credibility of the cost estimate, we base all of the costs taken from the L* case upon the full costs described in the Report of the L* Cost Review Panel, D. Theriot, chairman, March 4, 1991[1]. We refer hereafter to this report as the Theriot panel report. For the EMPACT and TEXAS subdetectors which we consider, we have made use of the internal engineering and cost estimates prepared by those collaborations but together with the L* Theriot panel report, several internal SSCL staff cost reviews and the Report of the SDC Cost Review Panel prepared by the Theriot panel as well, we have attempted to upgrade the EMPACT/TEXAS costs in a manner similar to the process that we believe would have taken place had that proposal been subject to the additional review steps. For example, the internal EMPACT cost estimate for the liquid argon calorimeter option has been revised by us to reflect the comments made by the Theriot panel in their review of the SDC liquid argon calorimeter option.

We have not made use of any technological options which were not carefully included in the L* or EMPACT/TEXAS designs, in order to avoid the common cycle in which initial estimates made by physicists incur large cost growth as the designs are detailed and upgraded. This process has already taken place to a large extent in the subsystems which we have considered.

In reducing the scope of some of the systems, we have tried to carry out the cost scaling with some caution in order to maintain the plausibility of the estimate. Thus, some attention has been paid to those components of the costs which do not scale (basic engineering and design, major R&D program elements) and to scale those components which lend themselves to this action (materials, assembly labor, inspection). With additional effort, part of this exercise may result in some changes to the estimate, however, we believe that the costs presented here are plausible and generally consistent with the level of confidence resulting from the Theriot panel reviews.

As explained in our earlier discussion of the experimental hall design, our design exercise must be cognizant of the limitations imposed by the hall and the local geology. The principal constraints are the transverse dimensions of the hall, the hall length, and the construction access, which affect the cost and schedule. As stated earlier, the current hall concept does not limit our design in any significant way. The most significant interaction between our design and cost, and the hall design, is illustrated by Figure 5-1 which is taken from Figure III.6 of the L* Letter of Intent. The curves indicate the strong dependence of the L* double coil superconducting magnet cost on the outside diameter due to the very high magnetic pressures which must be resisted by the coil support structures. The hall clearance at 26m is an acceptable compromise between the civil engineering limits, magnet costs and space requirements for cryostat support. This figure was produced by a parametric cost model of the L* magnet and muon systems developed at Lawrence Livermore National Laboratory and has been used to guide several major steps in the design exercise discussed in this report.

The hall design and the integrated cost model of the L* magnet and muon systems provide the guidance for the three most significant steps in this design to cost and schedule exercise. First, we retain the caverned hall and the surface facilities studied by the SSCL and the architect/engineer firm. Second, we adopt the L* superconducting magnet option as our starting point. This option is superior to the resistive magnet in meeting our physics goals and appears to permit a significantly shorter facility and magnet construction schedule. Third, we choose to relax the muon momentum resolution to 5% for muons at 90 degrees and 500 GeV/c, from that chosen by the L* collaboration. Our choice meets our principal physics goals and makes possible very large reductions in cost.

In order to facilitate the use of the Theriot panel cost results in a rapid turnaround exercise, we have chosen to use the L* base costs published in Table 4 of the Theriot panel report to account for the direct costs of materials and labor. The Theriot panel recommended only a $2 million change in the $507 million resistive option base costs and no change in the superconducting option costs.

We have taken the higher contingency and EDI&A estimates derived by the Theriot panel and spread them evenly over all of the L* subsystems. Thus, from Table 1 of the Theriot report, the total direct costs are $507 million. The contingency and EDI&A applied by the Theriot panel raise the estimate to $714 million. The ratio of these numbers is 1.41. We have used this ratio uniformly for all of the L* subsystems considered. While this raises the apparent total costs of some systems (BaF_2 calorimeter) and slightly lowers other systems (central tracker, forward calorimeter) the cumulative costs for the entire detector are not altered and the individual subsystem errors are within the confidence limits of the conceptual design costs at this stage. The impact of our design changes is properly reflected and that is the aim of this exercise. It should be noted that Table 1 was constructed to summarize the resistive magnet option for L*, an option which we have not included in our design. However, the superconducting option was costed to be only $6 million lower.

To the base costs and the sum reached by applying the Theriot contingency and EDI&A, we add the $50 million identified by Theriot for R&D for the L* design, resulting in a total detector cost of $758 million. This sum is our point of departure for the design to cost exercise. As an additional guide to maintaining the credibility associated with the Theriot panel costs, we note that the EDI&A was 25% of the detector base costs (materials and labor), contingency was similarly 25%, and R&D was 11%. For the SDC estimate, the cost review resulted in fractions for these

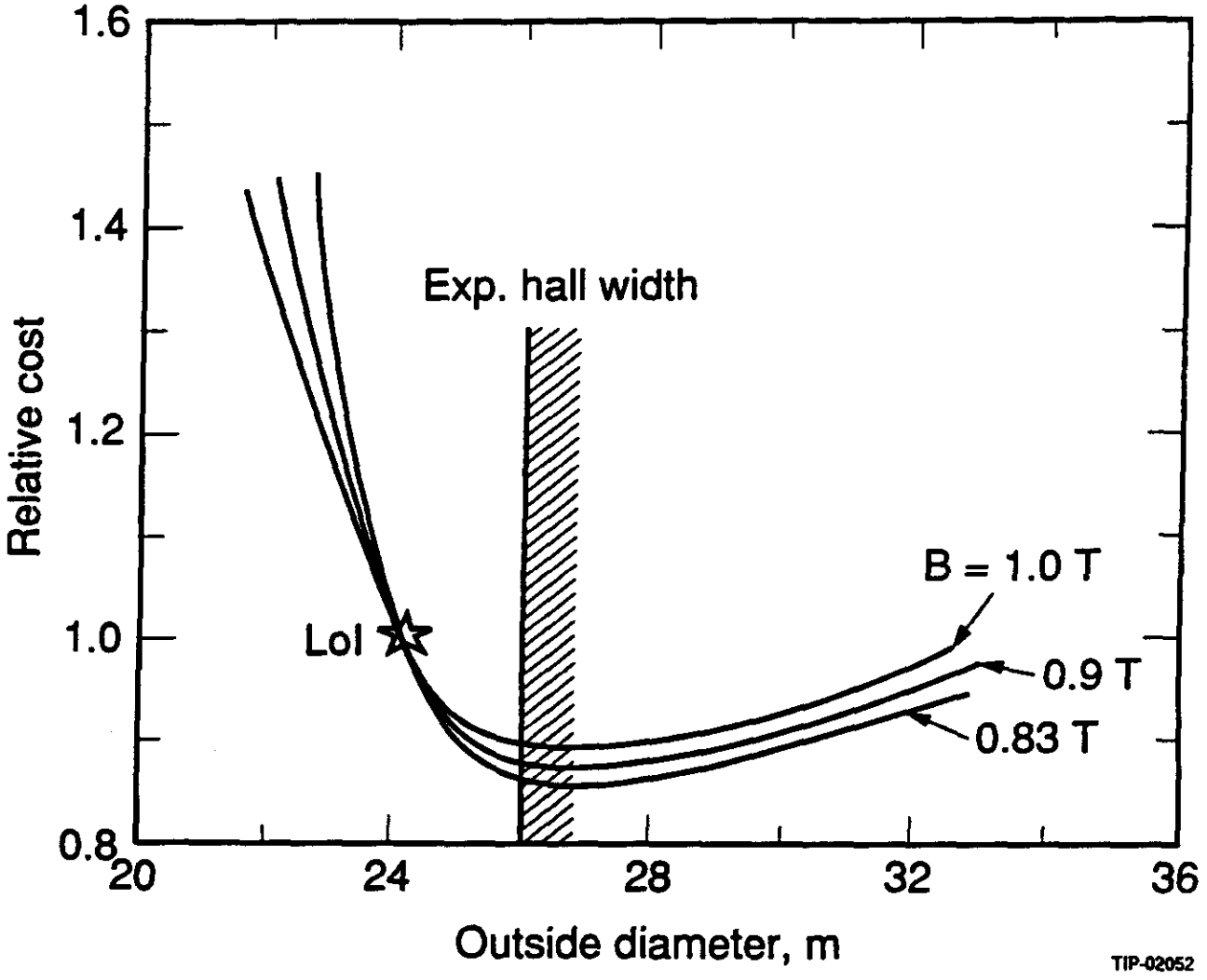

Figure 5-1 Cost versus outside diameter of the L* double coil superconducting magnet option. Numbers at the curves indicate the central field in the detector. The curves indicate the strong dependence of the magnet cost on the outside diameter due to the very high magnetic pressures which must be resisted by the coil support structures. The hall clearance at 26 m is an acceptable compromise between the civil engineering limits and magnet costs.

which were 32%, 37% and 11%, respectively. In reducing the scope of L* subdetectors, our rates fall within ranges consistent with these reviews. For the EMPACT/TEXAS systems, we have explicitly insured the L* or SDC fractions.

We present the results of the design exercise by identifying three stages in the estimate with the goal of defining three price points for the detector with varying capabilities. This provides a basis for estimating the sensitivity of the total detector cost to variations in performance goals and to possible future cost growth or reduction as the design might be modified. In the first stage, the toolkit is taken entirely from L* design elements. In the second stage, a major reduction in the cost and complexity of the solenoidal magnet is considered. In the third stage, two calorimeter options from the EMPACT and TEXAS proposals are included in the design. For each of these stages, the system cost, performance and the confidence in the cost estimate are reduced. However, the cost reductions are large compared to the performance compromises.

For the first stage, the following changes are made to the basic architecture and subsystems used in the L* design. The largest cost variations are made in the combined magnet and muon systems.

- The Theriot panel base costs for the L* double coil superconducting magnet and muon systems are $127 million and $158 million, respectively. This total base cost of $285 million is raised to $402 million with the factor of 1.41 for contingency and EDI&A. **We eliminate the forward/backward magnets and muon systems** reducing the base cost to $252 million, and the total cost to $355 million. The physics impact of this step is the loss of muon physics beyond rapidity of 2.7.

- **We relax the muon resolution to 5% at 90° and 500 GeV/c and we reduce the chamber wires from 32 to 16 planes per chamber.** The base costs are reduced from $252 million to $198 million, or as the figure indicates, the total costs are reduced from $355 million to $279 million.

  This step is supported by Figure 5-2 which is a plot of the combined magnet and muon system costs (with the factor of 1.41 included) for various muon resolution assumptions (3.2% which is our current understanding of the L* Letter of Intent resolution and differs from the 2.8% presented by the L* collaboration, and 5% and 7%), central magnetic fields (0.8 to 1.1 T), and muon chamber designs (32 or 16 wire planes per chamber for L* type muon chambers). The plot was produced by the Livermore integrated cost model. It accounts for such effects as the contribution to resolution due to the number of muon chamber wires offset by the measurement lever arm. The model was based upon several detailed and specific point designs for the two systems which were then used to guide a parameterization. Use of such a model is appropriate for the kind of tradeoff exercise described here, but the final costs must be validated for any specific choice by a detailed point design. The L* Letter of Intent design at 0.83T, 3.2% resolution, and 32 wire planes per chamber is indicated by the large black triangle. This point is the $355 million cost referred to in the previous paragraph.

  The loss of physics performance is modest and is documented in the L* Letter of Intent which considered 5% muon resolution for the resistive coil option. Thus many of the benchmark physics processes and backgrounds have already been simulated and described.

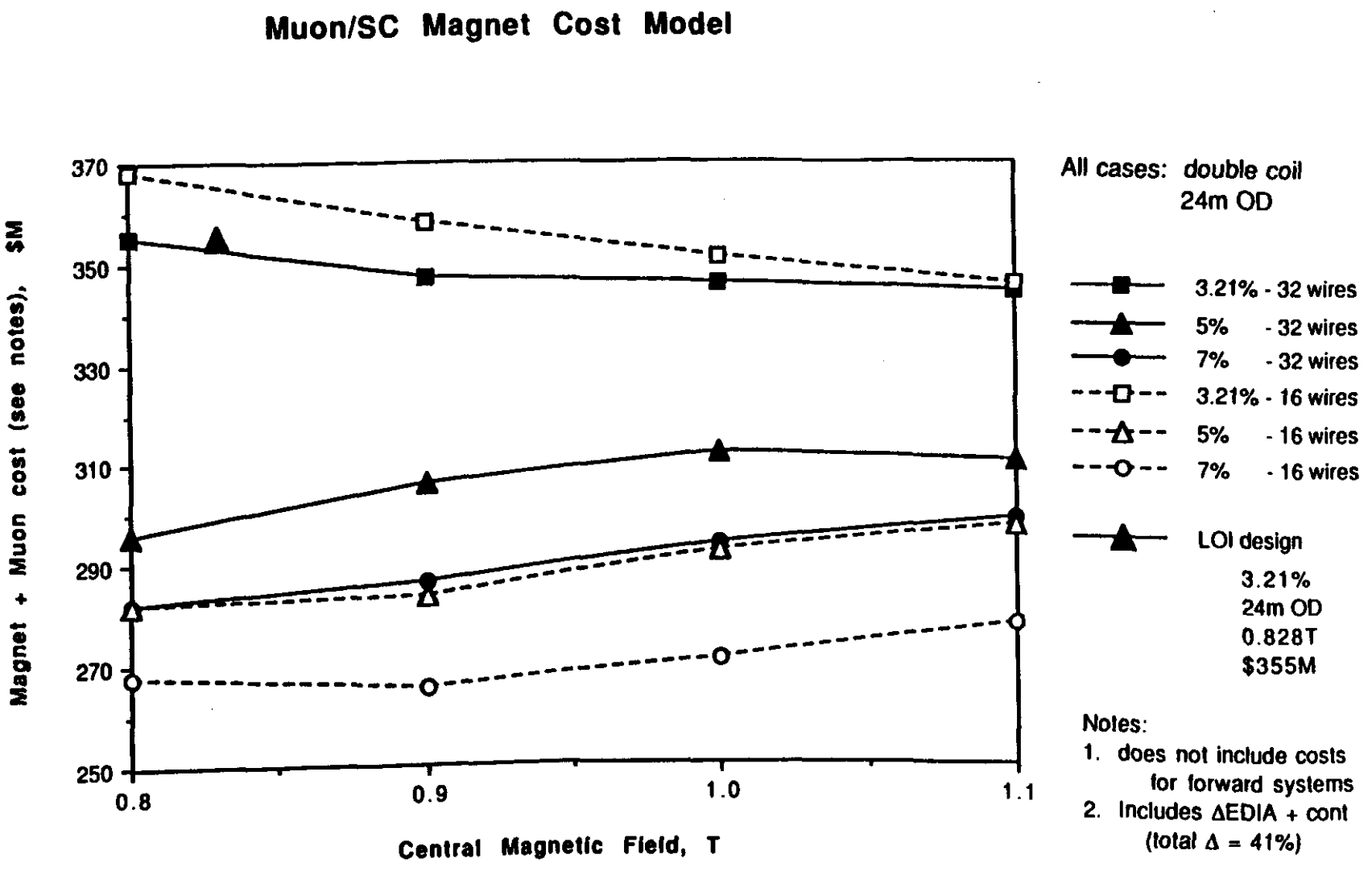

Figure 5-2 Variation in combined central magnet and muon systems cost with resolution, field and chamber construction based upon an integrated parametric cost model. The L* Letter of Intent design point is indicated.

This performance is no worse than that already proposed by L* and is consistent with the core EMPACT/TEXAS physics goals as well.

- The Theriot panel base costs for the L* calorimeters (BaF_2 and scintillator hadronic section) are $72.3 million and $65.3 million, respectively, or $101.9 and $92.1 million total cost. We propose to **reduce the coverage of the electromagnetic calorimeter to rapidity 2.5 from 2.8 and to alter the envelope of the system about the central tracker.** This reduces the base cost by $6.6 million, and the total cost becomes $93 million. We further propose to **reduce the longitudinal segmentation of the hadron calorimeter from 5 to 4 segments.** This lowers the readout costs by 20%, so that the system base cost becomes $61.8 million, and the system total cost becomes $87.1 million.

- The base cost for the L* forward calorimeter was $28.7 million, with a total cost of $40.5 million using the factor 1.41. We propose to **consider a forward calorimeter placed much closer to the interaction point at approximately 5 m.** Careful studies are required to justify the segmentation and to validate the performance at this location, and these studies were not included in the L* design. However, scaling the L* Theriot panel costs to this location reduces the base cost to $8.2 million and the total cost to $11.6 million. We will assume this reduction is plausible, though this step is a significant departure from the confidence level of the other steps we have taken. We note that should further study not support this step, **the forward calorimeter can be most easily postponed to an upgrade stage and we could eliminate this cost item entirely.**

- The base cost of the L* central tracker was $40.1 million, and the application of the factor 1.41 raises this to $56.5 million. We have already noted that the uniform application of this factor slightly lowers some subsystem costs and the central tracker is an example since the uniform treatment does not include all of the 100% contingency applied by the review panel to the advanced technology of this system. This small error does not mischaracterize the impact of the reduction in scope that we consider here, and it is offset by other systems. The central tracker design changes we adopt in this study are described elsewhere in this report as the baseline central tracker design. Briefly, we **reduce the outer silicon subsystem radius to 26 cm, trim the inner boundary of the forward silicon planes, reduce the number of straw tube layers to 16 per superlayer from 20, and multiplex the straw system of optoelectronics by a factor of 8.** The base cost is reduced to $26.5 million and the total cost to $37.4 million.

These steps are the first stage in the design to cost exercise. They are summarized in Table 5-1.

Note that we have maintained the R&D as an approximate constant 11% fraction of the material and labor costs, as both Theriot panel reviews did.

In the second stage of our design to cost study, we consider a major simplification of the superconducting solenoid. The magnet and muon system at this point are estimated to cost $279 million. This system provides 5% muon resolution at our nominal condition, with L* style chambers constructed with 16 wire planes per chamber. The magnet is a double coil solenoid in which the outer coil serves to return the external flux. The outer coil diameter is nominally 24 m and the inner coil diameter is nominally 18 m. We consider two simplifications.

Table 5-1

Item	L* Panel Base Cost ($ millions)	L* Theriot Panel Cost ($ millions)	Stage 1 Design Base Cost ($ millions)	Stage 1 Design Cost with Theriot Panel Additions ($ millions)
Magnet + Muon	285	402	198	279
Hadron Calorimeter	65	92	62	87
EM Calorimeter	72	102	65	93
F/B Calorimeter	29	41	8	12
Central Tracker	40	57	27	37
Computer	14	14	10	10
Total	505	708	370	518
R&D	25	50	37	37
Total with R&D	**530**	**758**	**407**	**555**

- **We eliminate the outer flux return coil and freeze the inner coil diameter at 18 m, retaining the 5% resolution and chamber type.** Figure 5-3 is a parametric plot of the magnet cost with this simplification. Costs have been studied for a variety of single coil diameters as a function of system resolution. For the 5% resolution choice, the system cost is reduced from $279 million to $235 million. Note that relaxing the system resolution would not effectively reduce the cost.

We have taken no credit for the cost savings that reducing the detector hall transverse dimensions might afford. Nor have we added the costs required to mitigate the operational and safety impact of the stray flux. It has been noted earlier in this report that the flux at the earth surface would be approximately 50 gauss, which can be easily shielded for any counting houses at grade. The cost of counting house shielding in the vertical shafts at the 120 gauss point would be about $300K for an average enclosure. The magnetic fusion community has a long record operating large unshielded experimental magnets surrounded by technical components. Given the very large cost reductions promised by removing the flux return of this magnet, we request that the SSCL conduct a thorough study as soon as possible of the technical, safety and operational impacts of this design.

- We have considered one other significant simplification of the magnet. The iron end poles of the solenoid in both the double coil and single coil variants are of quite conservative design. We have carried out a study of the **minimum iron pole volume adequate to control the flux at the magnet apertures.** The cost of the combined magnet and muon system with a minimum pole is reduced by an additional $8.5 million, based upon a specific point design.

Following this second stage in our study, the costs are summarized in Table 5-2.

Table 5-2

Item	L* Panel Base Cost ($ millions)	L* Theriot Panel Cost ($ millions)	Stage 2 Design Base Cost ($ millions)	Stage 2 Design Cost with Theriot Panel Additions ($ millions)
Magnet + Muon	285	402	160	226
Hadron Calorimeter	65	92	62	87
EM Calorimeter	72	102	65	93
F/B Calorimeter	29	41	8	12
Central Tracker	40	57	27	37
Computer	14	14	10	10
Total	505	708	332	465
R&D	25	50	33	33
Total with R&D	**530**	**758**	**365**	**498**

It should be noted that at this stage we are considering a detector design that is consistent with the March, 1991 Program Advisory Committee guidelines. This design is our baseline design for this report. It has physics performance parameters which retain the precision muon, electron and photon goals, and hermetic calorimetry, of both the L* and EMPACT/TEXAS Letters of Intent, and the magnetic tracking of L*. Indeed, the only significant performance compromises that we have made have been the relaxation to 5% of the central muon resolution, and the elimination of the forward and backward muon systems. The basic parameters of our baseline design are described in Table 5-3:

Table 5-3

Item	Rapidity Range	Performance
Muon resolution	0–1.25	5%–4%
(% at 500 GeV)	1.25–2.7	4%–10%
e/γ resolution	0–2.5	$1.5\%/\sqrt{E} \oplus 0.5\%$
Hadron resolution	0–3	$50\%/\sqrt{E} \oplus 2\%$

This set of performance parameters is the basis for the complementarity of our physics goals to those of a general purpose detector. The muon and electron/photon resolutions are very significantly better than those described in the SDC Letter of Intent. The muon performance is achieved without reliance on the central tracking, providing a robust system at even the highest conceivable SSC luminosities.

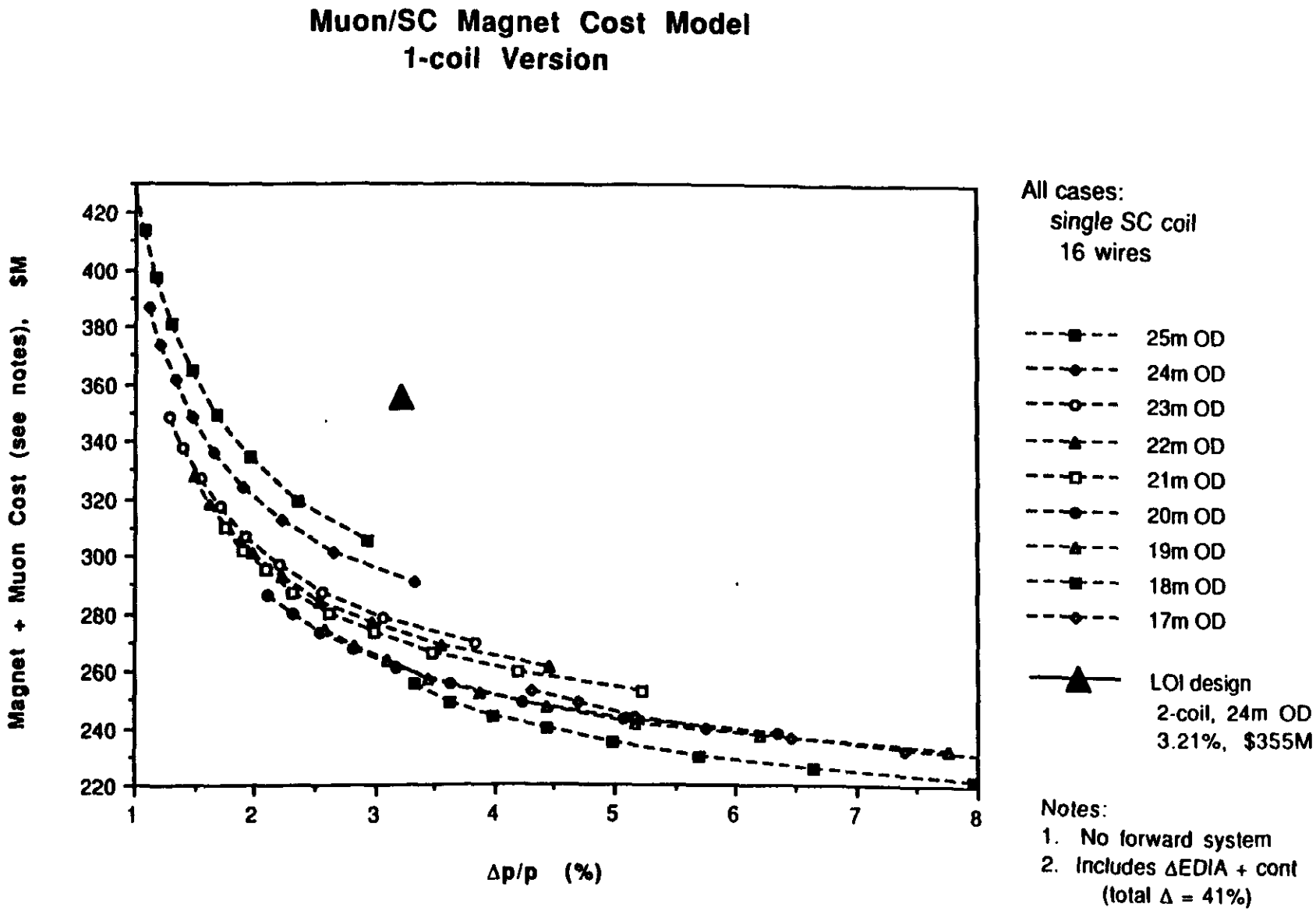

Figure 5-3 Parametric cost plot for the single coil magnet option.

In the third stage of our design to cost study, we have expanded our toolkit to include two calorimeter options considered by the EMPACT and TEXAS collaborations, namely, integrated liquid argon or lead-scintillating fiber electromagnetic and hadronic calorimeters. The primary physics impact of this stage is the relaxation of the resolution of the electromagnetic calorimeter from that promised by the BaF_2 or liquid xenon homogeneous electromagnetic calorimeters to the performance anticipated for the sampling calorimeters such as liquid argon or lead-scintillating fiber. The cost reduction made possible by selecting the sampling option would be possible intrinsic cost reductions particular to the technology (BaF_2 system costs vs. lead-scintillating fiber electromagnetic calorimeter costs) and the cost savings made possible by choosing a single technology (liquid argon or lead-scintillating fiber) for both the electromagnetic and hadronic calorimeter sections. The latter includes reduction in R&D and simplification of structures, services, readout, etc. We have explicitly considered only the technology specific savings, but the savings due to system simplification are partially included by maintaining the constant R&D fraction in our estimate.

Accounting for the costs of the two EMPACT/TEXAS calorimeters is complicated by several factors. First, the EMPACT/TEXAS costs were not subject to review by the Theriot panel. We have attempted to upgrade the EMPACT/TEXAS estimates to include such factors as the Theriot panel contingency rates, assembly labor, subsystem management, etc. Second, the volumes available in the EMPACT/TEXAS and L* designs for the calorimeters were different so that the EMPACT/TEXAS costs must be reduced to unit cost bases and rescaled to the dimensions of our baseline design which uses the L* calorimeter dimensions. Even if the L* dimensions are not used in subsequent design exercises, we must use a common set of dimensions in order to fairly compare the costs.

In order to maintain the 11.7 interaction lengths that the L* calorimeter system had at 90°, the liquid argon or lead-fiber technologies require an additional approximate 40 cm radial thickness. This can be included by increasing the dimensions of the muon and magnet systems (with an approximate \$10–\$15 million cost increase) or by adding up to 10% tungsten powder to the lead absorber plates to decrease the interaction length. The cost of the tungsten powder loading appears to be roughly offset by the reduction in lead costs at the calorimeter outer radius. We choose to adopt this option, but provide the cost of the other option to indicate the sensitivity. For this stage of the study we costed two cases. **Replace the L* BaF_2 and hadron calorimeters with an integrated liquid argon calorimeter that serves both functions following the EMPACT/TEXAS design concept.** Our revision of the EMPACT/TEXAS cost estimate indicates that the combined calorimeter costs are reduced by \$24 million from \$93 + \$87 million = \$180 million to \$156 million. The total detector cost is reduced to \$472 million. We have not added the approximate \$5 million addition to the conventional facilities required to accommodate liquid argon as this appears outside the detector budget.

The other case **makes the calorimeter replacement with an integrated lead—scintillating fiber calorimeter that serves both functions.** We estimate this cost to be lower by \$55 million for a total calorimeter cost \$180 million - \$55 million = \$125 million. The total detector cost is reduced to \$439 million.

We summarize the three stages of the exercise in Table 5-4, which shows three major price points which will guide future design studies. We view the requirement that the total cost of the detector be below \$500 million as a principal constraint in future design exercises. While several

technological options not included in this cost study are discussed elsewhere in this report, cost constraints will be adhered to.

Table 5-4

L* Theriot cost	STAGE 1	STAGE 2	STAGE 3
	double coil 5% muons 16 wires F/B muons out	single coil minimum iron pole	Liquid argon or fiber integrated calorimeter
			$472 million or
$758 million	$555 million	$498 million	$439 million

REFERENCES

---

[1] Report of the L* Cost Review

6.0 COLLABORATION ORGANIZATION

Many institutions have shown great interest in conceiving, designing, building and using a second large detector at the SSCL. These include many groups from L*, EMPACT/TEXAS and others with more expected. In preparation many small and several large meetings/workshops have taken place, at Cal Tech and at the SSCL Lab, to organize and prepare for the many tasks that have to be accomplished for a successful proposal. To this end an interim organization has been set up whose task it is to lead the effort until a permanent organization is agreed to and established. This interim organization consists of a Collaboration Council consisting of members from all the participating institutions. This group has formally met and voted that B. Barish and W. Willis serve as co-leaders for the preparation of the EOI and towards the submission of an LOI and until such time as a permanent organization is approved. These two individuals have been also empowered to form a small steering group to help them in this task, this group also to dissolve with them when a permanent organization is established.

The permanent organization that will design, build and use this large detector has to be such as to assure the success of its mission. As such, it must lend itself to a close and positive relationship with the SSC Lab, its management and staff, attract the best physicists and engineers in the U.S. and abroad, and construct the detector on cost and schedule. Figure 6-1 depicts a draft proposal of such an organizational structure. In effect there are three major bodies—the Steering Committee, the International Committee and the Collaboration Council—all are essential but with different functions.

The Collaboration Council is the representative body, whose membership consists of individuals, approximately one per institution, whose responsibility is to recommend new institutions, concern itself with publications and talks, theses, and any other matters of interest to the whole collaboration. Its chairman, Chair 1, should be elected by this group and serve for a fixed term. The Steering Committee is the scientific, technical and budgetary center of the collaboration. Its chairman, Chair 2, is essentially the spokesman of the group and he/she should choose the members of this committee in consultation with the Collaboration Council. Chair 1, Chair 3 (of the International Committee), and the Project Manager (to be discussed later) should be ex-officio members of this committee. This group would be responsible for the scientific priorities, technical decisions, budget priorities and detector organization and integration, in effect the forum where all the tradeoffs are made. This group should also initiate all ad hoc task forces for gathering input from all the knowledgeable people in the collaboration to address particular issues. Due to the magnitude and complexity of this effort exemplified by the $500M cost, Chair 2 has to have the confidence and respect of the SSC Lab management and as such should be chosen by the SSCL Director, in consultation with the Collaboration Council. It follows that he/she should report directly to the SSCL Director. It is expected that the members of this Steering Committee, numbering ~ 12, will be chosen on the basis of their acknowledged leadership, expertise and reputation in those areas which are deemed important for the successful implementation and operation of this detector.

The International Committee explicitly demonstrates that this is indeed an international endeavor and will have as its responsibility the drafting of institutional and financial agreements and securing international participation. Its membership should comprise of several individuals (with international reputations) from the various geographical regions involved in this collaboration. Again due to its intricate connections with funding agencies and foreign government

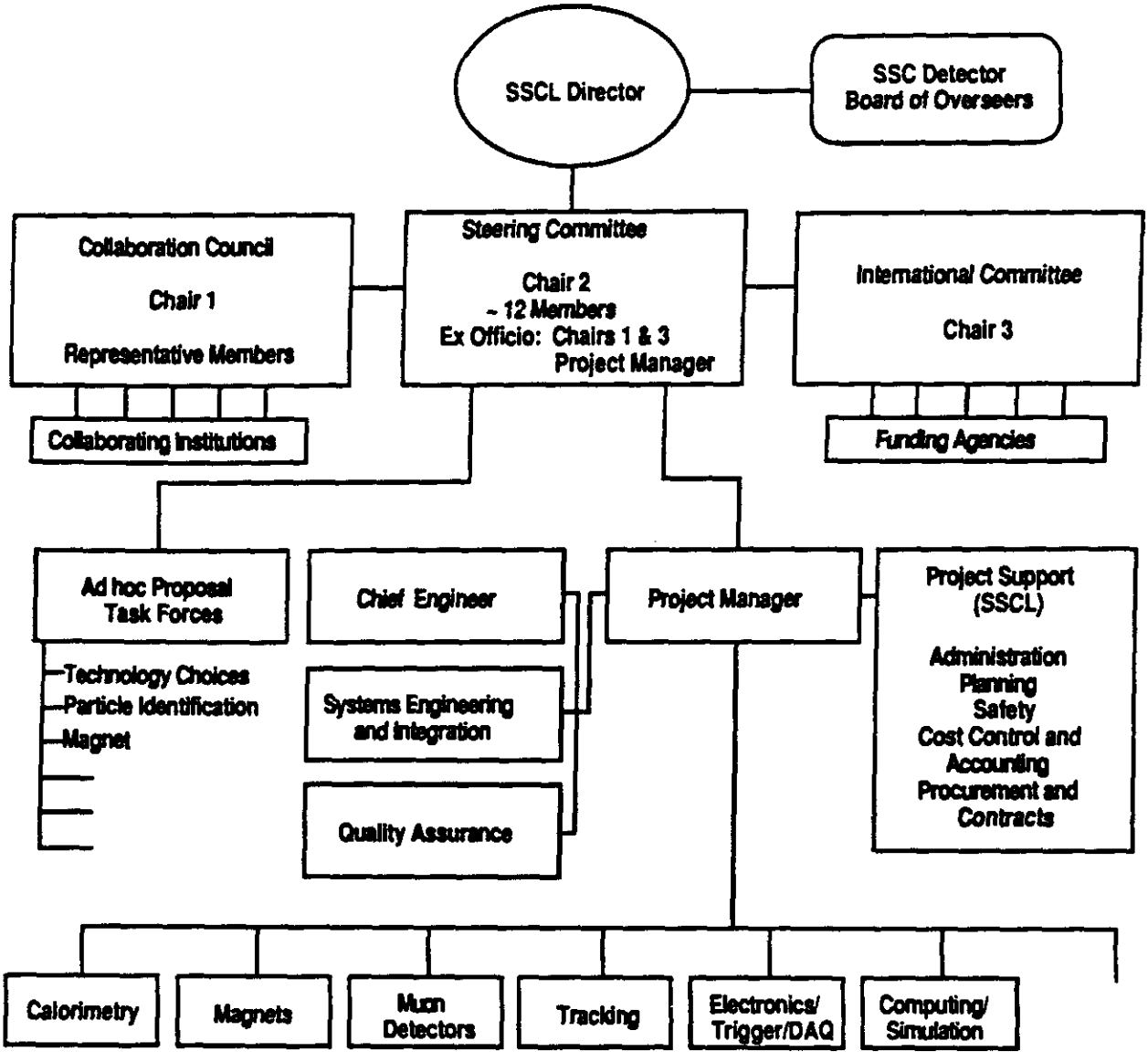

Figure 6-1

Notes for Figure 6-1:

1. SSC Director
   Responsibility
   - Appoint Chair 2 and 3 (in consultation with Collaboration Council)
   - Approve Chair 1

2. Board of Overseers
   - Membership (6–8)
     - Appointed by SSC Director
     - From SPC, PAC ...
   - Responsibility
     - Scientific and Project Oversight
   - Chair
     - Appointed by SSC Director
3. Experimental Steering Committee
   - Membership
     - Chosen by Chair 2
     - Acknowledged Scientific and Technical Expertise (International reputation)
     - Many will be Leaders of the Subsystems
     - *Geographic Diversity*
     - Ex Officio—Chair 1 and 3, Project Manager
   - Responsibility
     - Scientific Priorities
     - Technical Decisions
     - Budget Priorities
     - Detector Optimization/Integration
     - *Initiate Decision Task Forces as needed*
   - Chair
     - Chair 2
4. Collaboration Council
   - Membership
     - Elected by Collaboration—one or more *individuals* per *institution*
     - Geographical Representation
   - Responsibility
     - Scientific Goals
     - Publications and Talks
     - Thesis
     - Recommendation of New Institutions
   - Chair
     - Chair 1
     - Elected by Council
     - Ratified by SSC and Collaboration
5. International Committee
   - Membership
     - 1 or more person per region
   - Responsibility
     - Secure International Participation
     - Draft Financial Agreements
     - Draft Institutional Agreements
   - Chair
     - Chair 3
6. Project Manager
   - Appointed by Chair 2 and Approved by SSC Director
     - Ratified by Collaboration Council
7. Ad hoc Proposal Task Force
   - Membership
     - Open to anyone in Collaboration
   - Responsibility
     - Make recommendations on Specific Scientific and/or Technical Issues, e.g., Calorimeter technology, magnets, Particle Identification
   - Chair
     - Appointed by Experimental Steering Committee
8. Subsystem Leaders
     - Appointed by Chair 2 and Recommendation of Steering Committee

and/or institutions, the chairman of this committee, Chair 3, should be appointed by the SSC Lab Director in consultation with the Collaboration Council.

One of the most important individuals in this organization is the Project Manager. This individual will be responsible for the actual building of the detector. All subsystems, calorimetry, magnets, etc., will report directly to this Manager, and as such, the day by day, detailed responsibility will rest with this individual. The concept, scope, budget allocation for the detector subsystems will be decided by the Steering Committee, but the execution will be the responsibility of the Project Manager–properly audited. It is also through this position that the tight connection is made to the SSCL infrastructure–engineers, contracts, procurement, etc. As such the Project Manager, should report to Chair 2, is expected to be an SSCL employee and must be acceptable to both the SSCL Director and Chair 2. It is suggested that he be appointed by Chair 2 and approved by the SSCL Director, but this delicate issue should be open for discussion. The leader of the subsystems should be appointed by Chair 2 upon recommendation of the Steering Committee in consultation with the Project Manager.

Again because of the importance and magnitude of this effort, we suggest that the SSCL Director appoint an oversight committee, which reports to him, that will apprise him of the progress on all phases of the project. Appended to the draft organization chart as Appendix B are a series of bullets that attempt to summarize the responsibilities and mechanics of implementing this draft organization plan.

7.0 PROPOSED PLAN AND FUNDING REQUESTS

It is our intent, assuming a favorable response to this EOI, to move aggressively toward an Engineering/Design report for this new major SSC experiment. This will be necessary to insure that we will have a powerful detector ready to exploit the SSC at turn-on.

We believe we can produce an LOI by late fall (1991) with the project well enough defined to move from that directly into the engineering design phase. That process will take one year and we will submit the Engineering/Design report in late fall of 1992.

Below we outline the elements of that process as we now see them and, the support for R&D and Engineering that will be necessary to attain our goals.

7.1 Preparing the LOI (July–November 1991)

Over the coming months we will organize the collaboration into working groups toward the LOI. We expect the collaboration to grow significantly during this period, both from within the present set of institutions, plus the addition of new ones. Already the collaboration is quite strong and we are confident that we will be able to do the work necessary to produce a well conceived LOI. We expect to aggressively seek non-U.S. collaborators during this period, but feel we need strong encouragement from the PAC and SSCL management to succeed.

During this period of preparing the LOI, our most important task is to define the detector as well as possible. We are committed to proposing a detector that will cost no more than the $500M PAC guideline. We intend to study options well below that cost, in order to best determine what is really needed and to set the final detector proposed around financial requirements that are realistically attainable.

We will organize the collaboration during this effort, into groups around subsystems, engineering, simulations. Our internal organization during this period will all be considered interim, however we hope to work both inside the collaboration and with the laboratory management toward a smooth evolution into a permanent management.

The most important tasks during this period will be to define the detector to be proposed. Our physics goals are well established and we believe this EOI demonstrates our abilities to conceive of a realistic detector that can address these goals within the PAC guidelines. Now, our aim is to 'design to cost' the best detector we can with the same goals. This will involve many basic decisions. First, we will need to define the magnet which will form the basis of the detector. That magnet will contain an initial array of detectors that must be capable of addressing most early physics goals. At the same time, we must define possible strategies for staging the detector and provide as much flexibility as possible for future upgrades and additions, as a result of the findings of the initial physics program.

We foresee making a number of important decisions before submission of the LOI:

- Magnet. We present in this EOI a baseline magnet at a reasonable cost level. We plan to evolve from this magnet to the final magnet in a process of optimizing the cost-performance of the detector. This will involve determining the dimensions, the operating field, field shaping, etc. We expect to do this in a systematic process over the coming

months. In addition, we have agreed with Kycia and Atiya to investigate their high field alternative, presented by them in the following appendix. These analyses will involve considerable engineering studies over the coming months.

- Muons. We intend to study both the L^* type muon subsystem and alternatives, such as fewer planes of high pressure drift tubes, streamer tubes or pads, all being investigated within our group. We hope to soon define the performance criteria for this system and from that determine which of these possible options to pursue in FY92 toward the engineering design. These studies will be coupled with the magnet optimization. In addition, we will investigate the possibilities of enhancing the performance with measurements outside the magnet.

- Calorimeters. The most important fundamental decision facing us over the coming months involves the calorimetry. We would like to strive for both simplicity and, as much as possible, uniform technologies. However, the physics performance demands much of the calorimeters. For the central calorimeter, there is a fundamental decision to be made as to whether we propose to build a high precision (BaF_2 or Liquid Xenon) separate, homogeneous electromagnetic calorimeter. This will require a large amount of thought and discussion as it involves our basic physics goals. The advantages of this solution will have to be understood, compared to the possible disadvantages from either cost or reduced performance of other elements of the detector. We fully expect to make this decision before the LOI and then to only pursue technologies consistent with that decision. Whether we decide to build the homogeneous electromagnetic calorimeter or not, we expect to pursue R&D on only two or three technologies in FY92. In addition, we will need to define the requirements for the forward calorimeter and how to achieve them. Both the high rates and the desire to keep the costs down may constrain the solutions. For the purpose of this EOI we have included a forward calorimeter in the initial detector. Our final decisions on the forward calorimeter and whether it might be staged or included will depend on our evaluation of the physics, technologies and cost.

- Central Tracker. The tracker as presented in this EOI will be pursued and optimized. In addition, we need to better understand the role of the central tracker in our detector and what is required to meet those goals. We plan to both question whether three technologies are necessary in this tracker and also, to investigate alternate technologies for tracking (e.g. pads). We will determine an R&D and Engineering plan that will enable us to design our tracker for the engineering/design report.

7.2 Preparation of Engineering Design Report (Nov 91 - Nov 92)

We have tried to determine the support that will be necessary during the engineering/design phase. Table 7-1 shows our current request for R&D on the various subsystems being considered during FY92. It is our intent to focus our R&D around systems that we are directly developing toward use in the detector after narrowing the choices.

It is our present estimate that the R&D that will be necessary during FY92 will be approximately $10M. In addition, the engineering needs will be approximately $4M to do the engineering design on both the magnet and detector subsystems.

Lastly, we would like to do everything possible to keep the detector hall on schedule. We will work with the laboratory to make sure all necessary work is done to go into the Title II phase after April 1992. This will be necessary in order to have a completed hall ready for the detector assembly.

Table 7-1 Engineering and R&D Profile for FY92 ($million)

Item	Engineering	R & D
Integration,Coordination,Costing	1.25	
Magnet	1.25	1.5
Muon System	.5	2.0
Calorimetry	.5	3.0
Tracking	.5	2.0
Trigger/ACQ		0.5
Reserve		1.0
Total	4.0	10.0

APPENDIX A
THE HIGH FIELD OPTION

The high field option is an attempt to achieve the physics performance of the November 1990 L* LOI, but at a considerable cost saving. The bending power is kept at least as large as the baseline L* by raising the field and shrinking the radius of the solenoidal magnet. Measurements of the muon momentum can be made both inside the coil and calorimeter by the sagitta method, and outside the coil by the line-point method. The more compact size of the detector allows a reduction of cost and simplicity of design while achieving a larger η acceptance than the baseline L*. We keep all the electromagnetic calorimetry and a significant part of the hadronic calorimetry inside the coil. We will emphasize precision electromagnetic calorimetry. In addition the electron momentum measurement is equal in precision to that of muons. This is a departure from the baseline L* design which allows better electron identification and on-line calibration of the precision electromagnetic calorimetry using physics signals. We also anticipate that this option will offer a flexible and robust approach to SSC physics for a range of luminosities up to 10^{34} cm^2/sec or beyond.

Figure A-1 shows a schematic of one possible implementation of the high field option. A magnetic field of 5T is generated by a solenoidal coil of 3.5m radius and 13m length. The inner tracking volume extends to a radius of 2m for a total bending power of 20 Tm^2. The calorimetry occupies a 1.5m annulus just inside the coil. This allows for a precision electromagnetic calorimeter and an inner hadron calorimeter. The inner calorimetry represents about 6 absorption lengths. We have a coil thickness of 50 cm followed by a hadronic calorimeter "tail catcher" and outer muon measurement stations. An iron flux return of 3m thickness serves the dual purposes of reducing the field outside the detector to a negligible level and providing a muon p_T filter for triggers. Simple muon trigger counters reside outside the iron.

For an initial choice of a tracker we assume three super layers at radii 0.5m, 1.22m, 1.95m. Each super layer has 8 layers of 4mm diameter, 5m long straw tubes. The Z measurement is provided by 1mm scintillating fibers wrapped around each super layer. We have assumed 4 fiber layers per superlayer. Figure A-2 shows the resolution as a function of η for a 0.5 TeV p_T particle. For comparison we plot both the baseline L* and the recently descoped L* resolutions. The larger η coverage of the high field option should provide both a larger acceptance and a better measurement of asymmetries for various physics processes.

As mentioned earlier the inner tracking allows equal muon and electron magnetic measurement. The momentum resolution is a factor of 25 better than the baseline L*. Figure A-3 shows the magnetic and calorimetric resolution for the baseline L* and the high field option at $\eta = 0$. Assuming Liquid Argon-type resolutions, this option has a cross-over point at about 150 GeV/c (versus about 5 GeV/c for the baseline L* design with BaF_2). This significantly extends the electron identification using E/p, allows for sign determination of the electrons into the TeV electron energy region, and provides an on-line calibration of the calorimeter using copious physics signals (e.g., $Z^0 \rightarrow e+ e-$) with electron momenta below 150 GeV/c.

The choice of a sampling electromagnetic calorimeter such as liquid Argon has both drawbacks and advantages. The main drawback is the larger sampling term in the energy resolution (7.5% for LAr vs 1.3% for BaF_2). However the importance of this term diminishes as a function of increasing electron or photon energy. At high energy the dominant contribution is from the

High Resolution Detector (HRD)

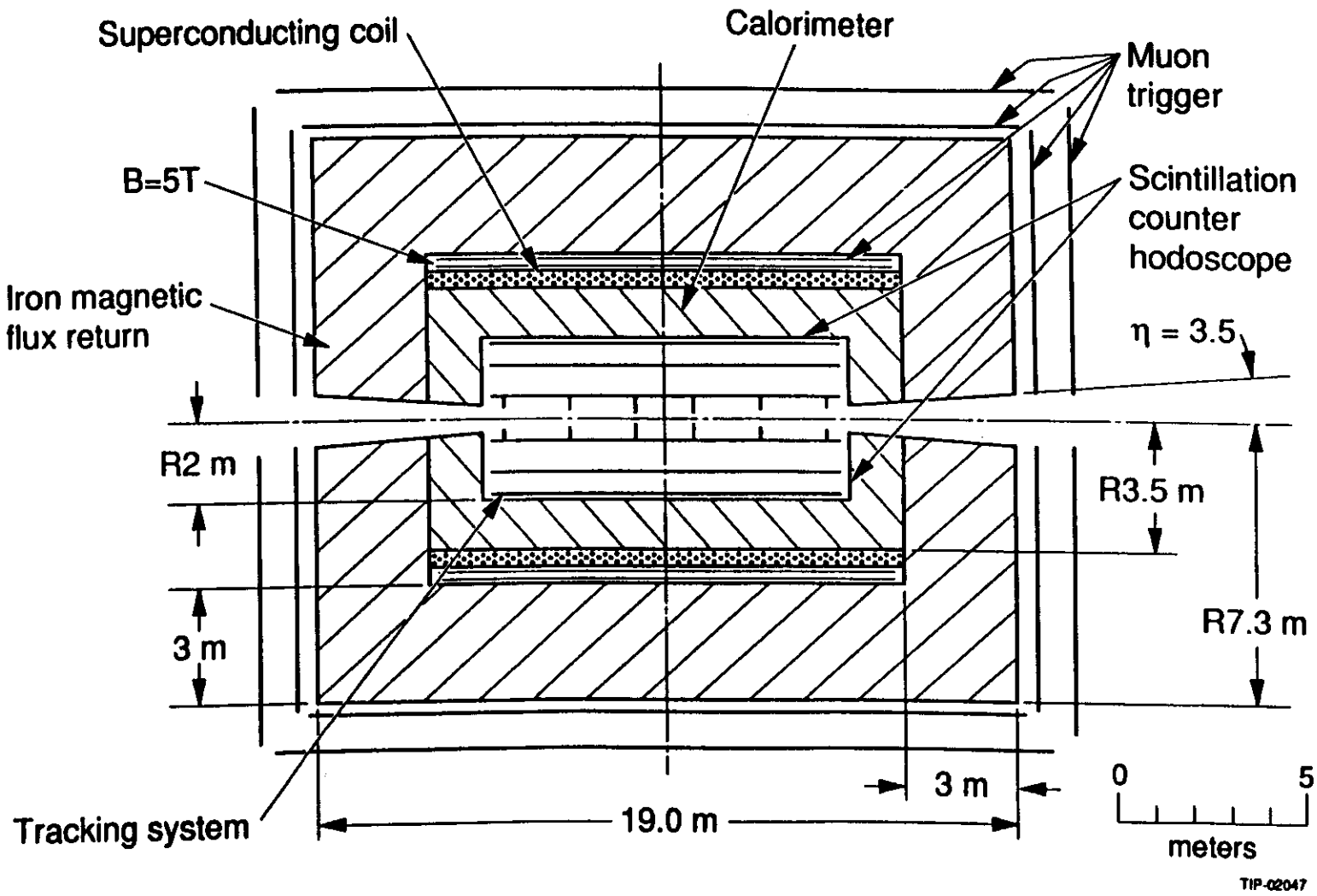

Figure A-1 Schematic of High Field Detector Concept

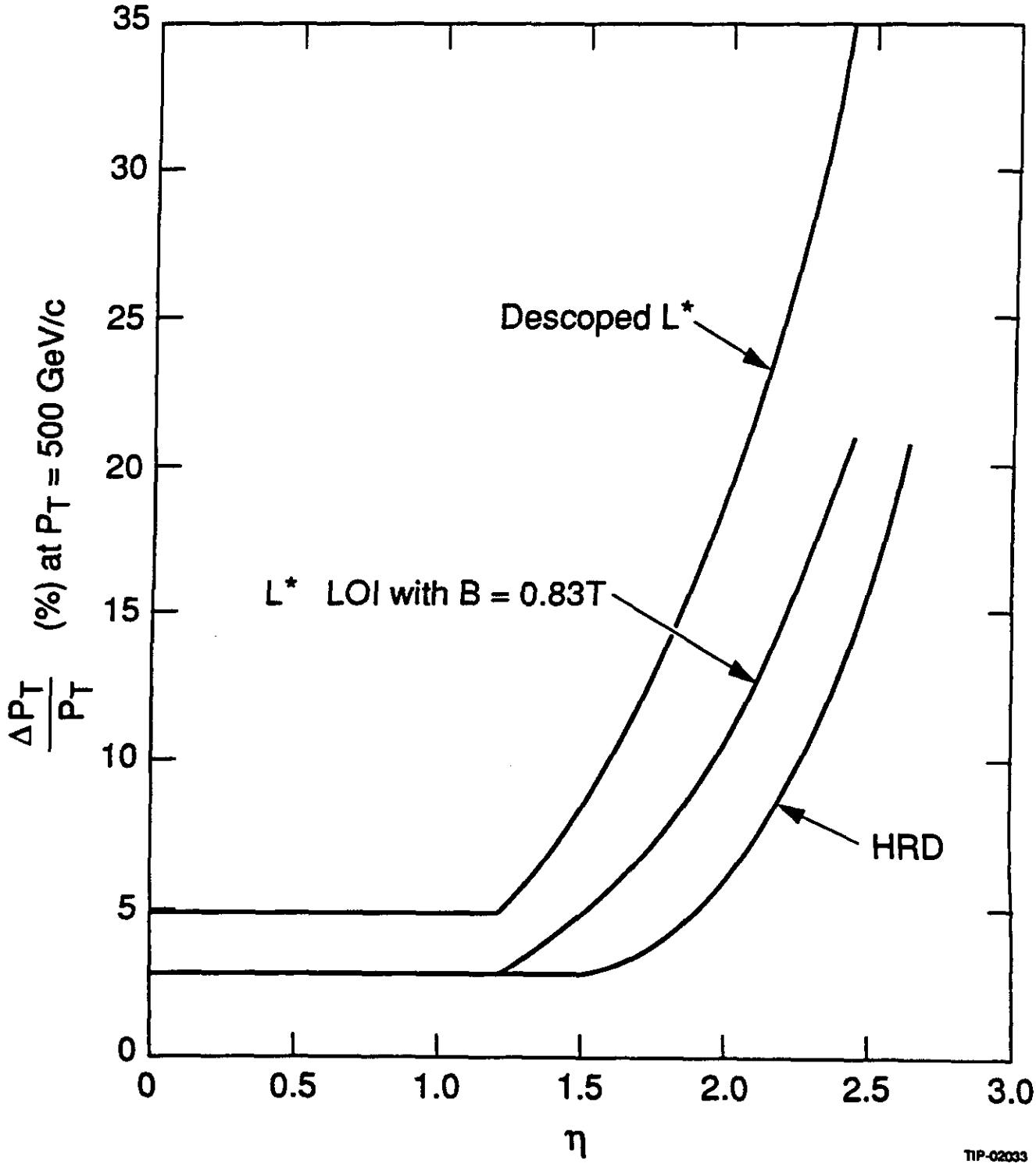

Figure A-2 Tracker Resolution as a Function of η for a 0.5 TeV particle.

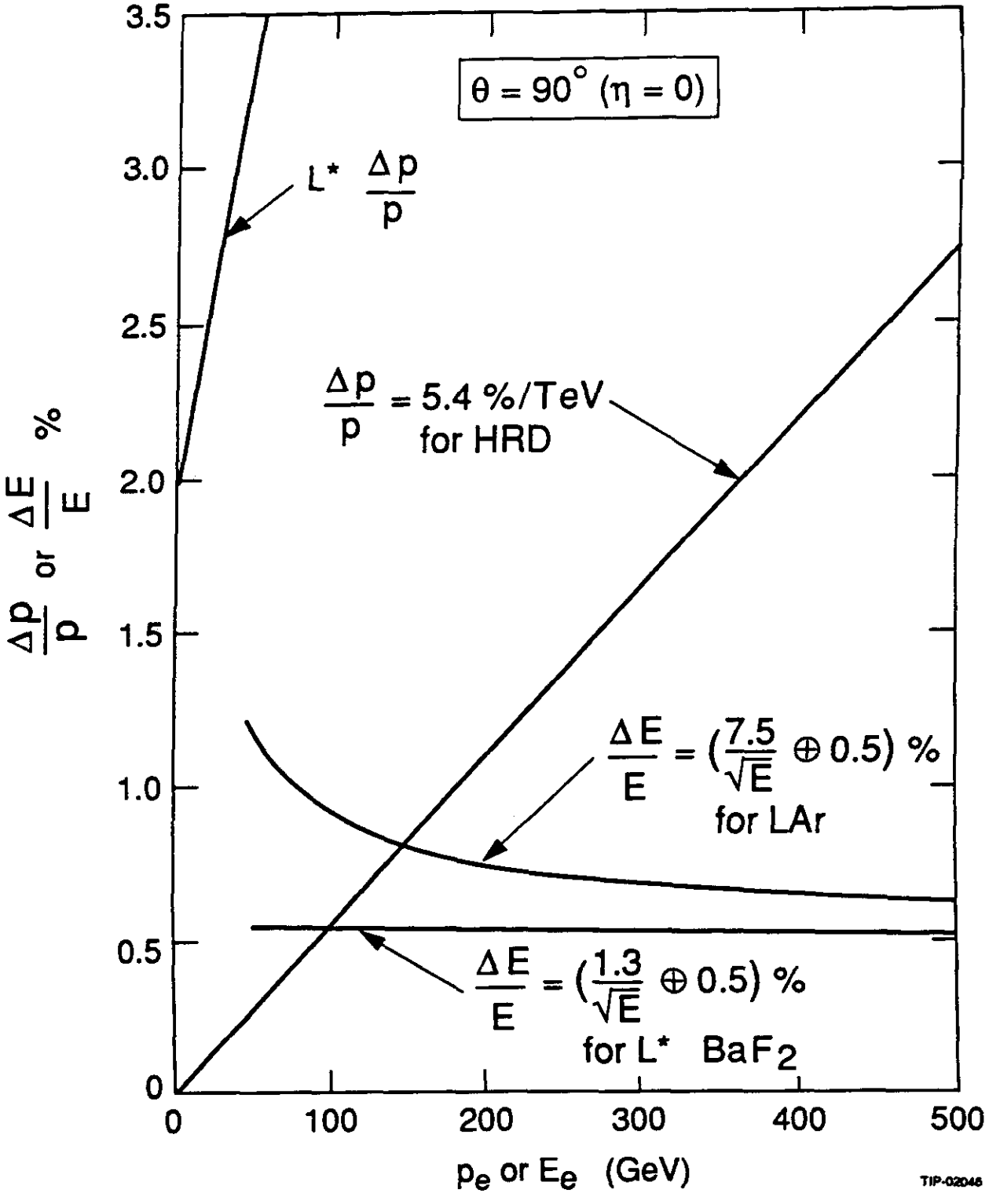

Figure A-3 Magnetic and Calorimetric resolution for the baseline L* and high field option at $\eta = 0$

constant term which depends almost entirely on systematics and calibration. A 0.5% constant term is thought achievable in both technologies with varying degrees of difficulty. In physics processes such as $H \rightarrow \gamma\gamma$, resolution is essential to enhance the signal. However, equally important is the ability to reject the copious π^0 background. In the baseline L* the γ/π^0 discrimination relies entirely on isolation cuts. In the high field option it may be possible to measure the shower widths after a few radiation lengths in the sampling calorimeter. This should give a positive hardware separation of γ/π^0. That the calorimeter is at a larger radius than the baseline L* design (2m vs. 0.75m) should aid in this regard. This option has not been costed.

In the high field option the inner hadronic calorimetry need not serve as a muon filter. The hadron calorimeter is not burdened with the need to measure catastrophic muon energy loss for correction of muon momentum measurement. This allows for an independent cost/performance optimization of both the calorimeter thickness and the number of necessary depth samples. While the issue is still under study, we believe a combined electromagnetic/inner fine-sampling hadronic calorimetry of 6 absorption lengths maybe optimal. To study physics signals with missing energy we will want to implement a coarser "tail catcher" calorimeter outside the coil.

The high field coil will have a roughly 50% higher stored energy than the baseline L* arrangement. However reliable estimates of the cost range from $80 million using scaling from L* design to $90 million using an independent European estimate. It is believed that there are no fundamental technological limits to obtaining fields as high as 5T. In addition the smaller size of the coil reduces many of the mechanical and engineering constraints in comparison to the baseline L* coil. The size of the coil and flux return is significantly smaller than the interaction hall and imposes no additional constraints on its design.

A important consideration is the robustness of the detector at high luminosities ($> 10^{33}$). The high field option allows for a graceful evolution to high luminosity running. The inner tracking volume can be filled with either iron or iron calorimetry. There is enough space to pack sufficient thickness to absorb virtually all hadrons. The penetrating muons can be measured at, at least one point inside the coil and at the outer muon station outside the tail catcher calorimeter and the coil. The effective field in the inner 3.5m is about 7T. Even with the increased multiple scattering the muon resolution should be of order 5-7%, almost independent of p_T up to p_T of about 1.5 TeV. To improve the resolution in the multi-TeV muon momentum region one will need to measure the muons either inside the flux return, or just outside it. This would require a more precise device than the assumed trigger counters outside the iron. A current CERN R&D program (Compact Muon Solenoid) will examine the details of muon measurement in iron at high fields in a test beam.

Various components of this option have been subjected to a serious cost estimate study (Theriot Panel). We will attempt a cost estimate for the high field option with the provision that further and more serious engineering work needs to be done. The cost of the inner tracker can be scaled from SDC to be about $35 million. The cost of the calorimetry can be scaled from EMPACT/TEXAS to be about $135 million. We have assumed the high figure of $90 million for the coil. The cost of the flux return is about $35 million using the standard SSC figure of $2/kg. In addition the trigger systems, data acquisition and computing will probably be similar to the SDC figure of $50 million. The rough total of less than $350 million represents a considerable saving over the baseline L* option.

While the study of the high field option revealed many of its attractive features it also uncovered some important physics and detector questions. Prominent among them are the pattern recognition and reconstruction efficiency for tracks in a high field, the ability to reconstruct jet momentum and direction and the associated missing energy resolution. The thickness of the inner hadronic calorimetry needs to be seriously addressed. We intend to proceed with these studies, along with more substantial engineering designs in the next few months.